sensors

MDPI

Article

Improved Active Disturbance Rejection Control for Trajectory Tracking Control of Lower Limb Robotic Rehabilitation Exoskeleton

Sumit Aole [1], Irraivan Elamvazuthi [2,*], Laxman Waghmare [1], Balasaheb Patre [1] and Fabrice Meriaudeau [3]

1 Department of Instrumentation Engineering, Shri Guru Gobind Singhji Institute of Engineering and Technology, Nanded 431606, Maharashtra, India; sumit.aole@gmail.com (S.A.); lmwaghmare@sggs.ac.in (L.W.); bmpatre@sggs.ac.in (B.P.)

2 Department of Electrical & Electronic Engineering, Universiti Teknologi PETRONAS, Seri Iskandar 32610, Perak Darul Ridzuan, Malaysia

3 ImViA, University of Burgundy, Maison de l'université, 21078 Dijon, Le Creusot, France; fabrice.meriaudeau@u-bourgogne.fr

* Correspondence: irraivan_elamvazuthi@utp.edu.my

Received: 5 April 2020; Accepted: 28 May 2020; Published: 30 June 2020

Abstract: Neurological disorders such as cerebral paralysis, spinal cord injuries, and strokes, result in the impairment of motor control and induce functional difficulties to human beings like walking, standing, etc. Physical injuries due to accidents and muscular weaknesses caused by aging affect people and can cause them to lose their ability to perform daily routine functions. In order to help people recover or improve their dysfunctional activities and quality of life after accidents or strokes, assistive devices like exoskeletons and orthoses are developed. Control strategies for control of exoskeletons are developed with the desired intention of improving the quality of treatment. Amongst recent control strategies used for rehabilitation robots, active disturbance rejection control (ADRC) strategy is a systematic way out from a robust control paradox with possibilities and promises. In this modern era, we always try to find the solution in order to have minimum resources and maximum output, and in robotics-control, to approach the same condition observer-based control strategies is an added advantage where it uses a state estimation method which reduces the requirement of sensors that is used for measuring every state. This paper introduces improved active disturbance rejection control (I-ADRC) controllers as a combination of linear extended state observer (LESO), tracking differentiator (TD), and nonlinear state error feedback (NLSEF). The proposed controllers were evaluated through simulation by investigating the sagittal plane gait trajectory tracking performance of two degrees of freedom, Lower Limb Robotic Rehabilitation Exoskeleton (LLRRE). This multiple input multiple output (MIMO) LLRRE has two joints, one at the hip and other at the knee. In the simulation study, the proposed controllers show reduced trajectory tracking error, elimination of random, constant, and harmonic disturbances, robustness against parameter variations, and under the influence of noise, with improvement in performance indices, indicates its enhanced tracking performance. These promising simulation results would be validated experimentally in the next phase of research.

Keywords: improved active disturbance rejection control (I-ADRC); lower limb robotic rehabilitation exoskeleton (LLRRE); trajectory tracking; linear extended state observer (LESO); tracking differentiator (TD); nonlinear state error feedback (NLSEF)

1. Introduction

1.1. Motivation and Background

Classically, the physiotherapist's job is to assist the patient in performing various rehabilitative tasks, and help them to recover or improve natural strength and movements through a set of objective oriented exercises. Re-iteration of such tasks for a long time results in fatigue of vitality, and it tires both the patient and the therapist [1,2]. In addition, it is difficult for the patient to visit physiotherapy centers for rehabilitation frequently due to physical conditions as well as traveling may affect the safety of the patient. There is no quantitative analysis for the patient's recuperation that can be acquired subsequent to the performance of rehabilitative exercises. Robotic rehabilitation devices can be ameliorated in such cases to overcome the difficulties of therapeutic training [3,4] as they are designed for the purpose of objective oriented tasking and can frequently work on the same trajectory for the duration of time depending on the patient's comfort. The performance tracking after the training through these devices leads to reinforcing the recovery of the patient, where, validation can be established by improvement comparison on the measurement result.

The design of control using a state feedback controller requires the availability of all state variables, but this condition may not always be true; in some cases, due to faulty sensors, these states are unavailable or immeasurable. Hence, observer based technique is utilized in this paper to reconstruct such state variables. Again, utilization of sensors for measuring all parameters is a costly process and adds extra hardware [5].

1.2. Related Research

Different control schemes for the improvement in the area of Lower Limb Robotic Rehabilitation Exoskeleton (LLRRE) for human assistance have been developed. Proportional-Derivative (PD) based control shows good performance in the absence of disturbance [6], but usually suffers when the disturbance occurs in the system [7]. Particle swarm optimization (PSO) based active force rejection control is introduced in [8] for rejecting the disturbance in gait trajectory tracking requires evaluation of a large number of parameters. Computed-torque control (CTC) [9,10] depends on the exact model of the system and may require additional control to compensate for modeling errors. Intelligent control methods [11] require great effort in rule formulation and inference testing. Sensitivity amplification needs an accurate inverse dynamic model and suffers from the introduction of disturbance [12,13]. Radial Basis Functions (RBF) neural network used to compensate for the disturbance but results in large computing costs [14]. Robust control (RC) methods are one of the options in such scenarios, but RC techniques are conservative and consider the worst-case approaches at the cost of relinquishing the transient response. The sliding mode control (SMC) technique can restrain against the uncertainties and parameter fluctuations, but faces chattering due to discontinuous switching [15]. To overcome such modern control difficulties, the active disturbance rejection control (ADRC) method is proposed.

The control theory requires a great effort on system identification, i.e., the mathematical model of the system and obtaining a perfect one is an ideal case. The ADRC controller was firstly proposed by Han [16] and had many advantages. The evolution and rapid use of ADRC in industries in the last three decades prove its popularity in motion control [17–20], flight control [21,22], and process control [23–32] applications and in many fields [33]. The architecture of ADRC is designed to achieve the best performance by actively eliminating the internal and outside uncertainties as a entire disturbance [34]. Its significance is being found out in industries to be a replacement for proportional–integral–derivative (PID). ADRC inherits from PID, but it has improved characteristics. It is based on error-driven rather than model-based control law [35] and does not necessarily depend on full information of the model or system dynamics, i.e., eliminates the necessity of the exact model of the system [36]. ADRC is recognized as a model-free controller, It only requires the order of the system and the approximate value of system parameters [37]. In the category of lower limb rehabilitation,

robotic devices, orthoses, exoskeleton, and prosthesis are developed to assist users mainly for gait rehabilitation and other exercises like sitting, standing, etc. Orthoses and exoskeleton have similar functionality [38]. In recent years, due to popularity and effectiveness, ADRC is used for various robotic rehabilitation devices for tracking applications. A linear extended state observer (LESO) based ADRC has applied on the lower limb exoskeleton for the hip and knee joints in [39] where clinical gait data is used as a reference. Results are compared for PID and ADRC, for the hip and knee trajectories based on error comparison the results show a better performance of ADRC over PID. To keep track of active ankle-foot orthosis (AAFO) [40], a framework similar to [39] is used in which the authors modified the ADRC with the inclusion of Control Lyapunov Function (CLF) instead of PD controller, with Sontag's formula. Stability is checked by input to state (ISS) framework where modification and experiments prove ARDC's effectiveness. In another work [41], ADRC deals with nonlinearities like pressure fluctuation and friction during the control of exoskeleton, a new function is introduced to avoid shaking at inflation point during non-linear state error feedback (NLSEF). A sinusoidal tracking for exoskeleton joint output is compared with ADRC, and for disturbance rejection, it is compared with PID, where ADRC with NLSEF shows better results than ADRC.

There are several control strategies for rehabilitation, such as position tracking, force and impedance control, biosignals based control and adaptive control, etc [42–47]. Position tracking is one of the basic control strategies for robotic rehabilitation devices in which repeatability and position accuracy of motion are improved by the help of the controller for the patient's recovery [3,39,48–50].

1.3. Contribution and Paper Structure

In this paper, more focus is given to position tracking control of predefined sagittal plane gait trajectory. This paper centers around the design of controllers for lower limb robotic rehabilitation exoskeleton (LLRRE) for sagittal plane gait trajectory tracking control based on ADRC combinations. A nonlinear dynamic, multiple-input multiple-output (MIMO) LLRRE with two joints, one at the hip and other at the knee obtained via Euler–Lagrange method, is presented. The proposed controller is a combination of three units, linear extended state observer (LESO), Tracking differentiator (TD), and Nonlinear state error feedback (NLSEF). LESO is used to estimate the states of the system, eliminates disturbance, and control the system by linear or nonlinear gains. NLSEF uses nonlinear gains to take care of the overshoot and speed of response. TD operates on a transient profile of nonlinear input signals by differentiating it, which results in the gradual increasing output instead of sudden changes. The proposed work is verified by performing numerous simulations and on the basis of various performance indices. This new combination of three units results in improved gait trajectory tracking and disturbance rejection performance.

In this paper, Section 2 gives the modeling of the exoskeleton understudy, and Section 3 presents the theory of the proposed control strategy for LLRRE. Section 4 gives the design of the ADRC for the trajectory tracking controller. Section 5 gives the stability of the proposed control method. The results of simulations are highlighted and discussed in Sections 6 and 7. Finally, the conclusion is given in Section 8.

2. Modeling of Lower Limb Robotic Rehabilitation Exoskeleton

An exoskeleton design must be biology-inspired to provide multi-functionality and adaptability to users, a similar approach called clinical gait data analysis is used here for lower limb exoskeleton modeling and design. The model consists of the hip and knee joint movements, which are provided with the help of two electric motors embedded in the structure. The model used in this paper is based on [39]. Figure 1 gives the structure of the exoskeleton and the parameters of exoskeleton are listed in Table 1.

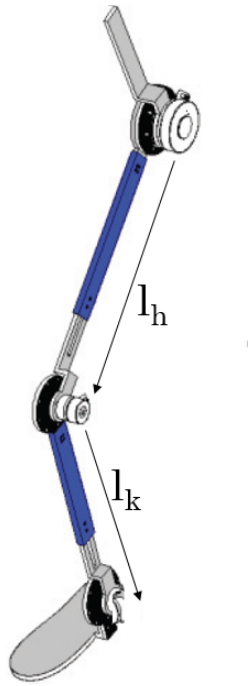

Figure 1. Lower Limb Robotic Rehabilitation Exoskeleton.

Table 1. Parameters of the exoskeleton.

Parameter	Symbol	Numerical Value
Thigh segment	m_h	5 kg
Length of thigh	l_h	435 mm
Length of shank	l_k	475 mm
Shank segment	m_k	2 kg
Gravity constant	g	9.81 m/s^2

The Euler–Lagrange method is used for the mathematical modeling, the swing of the leg is given by

$$\boldsymbol{M}(\boldsymbol{q})\ddot{\boldsymbol{q}} + \boldsymbol{C}(\boldsymbol{q},\dot{\boldsymbol{q}})\dot{\boldsymbol{q}} + \boldsymbol{G}(\boldsymbol{q}) + \boldsymbol{D} = \boldsymbol{T} \tag{1}$$

where,

$\boldsymbol{M}\ (\boldsymbol{q}) \in R^{n\times n}$ is the symmetric definite inertial matrix.
$\boldsymbol{C}\ (\boldsymbol{q},\dot{\boldsymbol{q}}) \in R^{n\times n}$ is the Coriolis and centrifugal force matrix.
$\boldsymbol{G}\ (\boldsymbol{q}) \in R^{nx1}$ is the gravitational force matrix.
$\boldsymbol{T} \in R^{n\times 1}$ is the control input vector.
$\boldsymbol{D} \in R^{n\times 1}$denotes un-modelities and exogenous disturbance.
Properties for dynamic modeling in Equation (1), are as follows :

1. Matrix $\boldsymbol{M}\ (\boldsymbol{q})$ is symmetric and positive definite.
2. Matrix $\dot{\boldsymbol{M}}(\dot{\boldsymbol{q}}) - \boldsymbol{2C}(\boldsymbol{q},\dot{\boldsymbol{q}})$ is a skew-symmetric matrix if $\forall\varepsilon \in R^n, \varepsilon^T(\dot{\boldsymbol{M}}(\dot{\boldsymbol{q}}) - \boldsymbol{2C}(\boldsymbol{q},\dot{\boldsymbol{q}}))\varepsilon = 0$.
3. There exist finite scalars $\delta_i > 0,\ i = 1,..,4$ such that $\|\boldsymbol{M}(\boldsymbol{q})\| \leq \delta_1, \|\boldsymbol{C}(\boldsymbol{q},\dot{\boldsymbol{q}})\| \leq \delta_2, \|\boldsymbol{G}(\boldsymbol{q})\| \leq \delta_3\ and\ \|\boldsymbol{D}\| \leq \delta_4$ which means all items in dynamic model are bounded.

$\boldsymbol{q} = [q_h\ q_k]^T$, where q_h and q_k represent angular position for the hip and knee joints. $\boldsymbol{T} = [\tau_h\ \tau_k]^T$, where τ_h and τ_k represent driving torque for the hip and knee joints.

The equations of matrices are as follows:

$$\begin{aligned}
\boldsymbol{M}(\boldsymbol{q}) &= \begin{bmatrix} m_{11} & m_{12} \\ m_{21} & m_{22} \end{bmatrix} \\
m_{11} &= \frac{1}{3}m_h l_h^2 + m_k l_h^2 + \frac{1}{4}m_k l_k^2 + m_k l_h l_k \cos(q_k) \\
m_{12} &= -\frac{1}{4}m_k l_k^2 - \frac{1}{2}m_k l_h l_k \cos(q_k) \\
m_{21} &= -\frac{1}{4}m_k l_k^2 - \frac{1}{2}m_k l_h l_k \cos(q_k) \\
m_{22} &= \frac{1}{3}m_k l_k^2
\end{aligned} \tag{2}$$

$$\begin{aligned}
\boldsymbol{C}(\boldsymbol{q},\dot{\boldsymbol{q}}) &= \begin{bmatrix} c_{11} & c_{12} \\ c_{21} & c_{22} \end{bmatrix} \\
c_{11} &= -m_k l_h l_k \dot{q}_k \sin(q_k) \\
c_{12} &= \frac{1}{2}m_k l_h l_k \dot{q}_h \sin(q_k) \\
c_{21} &= \frac{1}{2}m_k l_h l_k \dot{q}_h \sin(q_k) + \frac{1}{2}m_k l_h l_k \dot{q}_h \sin(q_k) \\
c_{22} &= \frac{1}{2}m_k l_h l_k \dot{q}_h \sin(q_k)
\end{aligned} \tag{3}$$

$\dot{q}_h$ and $\dot{q}_k$ represent velocities of the hip and knee joints. $\boldsymbol{G}(\boldsymbol{q})$ is expressed as:

$$\begin{aligned}
\boldsymbol{G}(\boldsymbol{q}) &= \begin{bmatrix} g_1 \\ g_2 \end{bmatrix} \\
g_1 &= -\frac{1}{2}m_h l_h g \sin(q_h) - m_k l_h g \sin(q_h) - \frac{1}{2}m_k l_k g \sin(q_h - q_k) \\
g_2 &= \frac{1}{2}m_k l_k g \sin(q_h - q_k)
\end{aligned} \tag{4}$$

for the model of robotic exoskeleton, the error for trajectory tracking is defined as

$$\boldsymbol{e} = \boldsymbol{q}_{\mathbf{d}} - \boldsymbol{q} \tag{5}$$

where, $\boldsymbol{e}$ is the tracking error. $\boldsymbol{q}_{\mathbf{d}}$ and $\boldsymbol{q}$ are desired and actual trajectories, respectively.

In the starting phase of rehabilitation and in passive mode, the exoskeleton allows the patient to move in the well-known predefined trajectory to initialize the joint movements. The objective of the rehabilitation exoskeleton in this paper is to replicate the exact gait pattern with high precision under the influence of noise and disturbances. The trajectories for the hip and knee joints are obtained by using fitting expression using clinical gait analysis data [51]. The period of the cyclical gait is 2 s and

the fitting expression with respect to time is obtained as follows and considering the gait cycle starts at stance phase initially and then repeats.

$$\begin{cases} q_{h,d}(t) = c_0.\cos(0.d.t) + c_1.\cos(1.d.t) + f_1.\sin(1.d.t) \\ \qquad +c_2.\cos(2.d.t) + f_2.\sin(2.d.t) \\ \qquad +c_3.\cos(3.d.t) + f_3.\sin(3.d.t) - 29.1^\circ \\ \\ q_{k,d}(t) = c_4.\cos(0.d_1.t) + c_5.\cos(1.d_1.t) + f_4.\sin(1.d_1.t) \\ \qquad +c_6.\cos(2.d_1.t) + f_5.\sin(2.d_1.t) \\ \qquad +c_7.\cos(3.d_1.t) + f_6.\sin(3.d_1.t) - 26.127^\circ \end{cases} \tag{6}$$

The values of coefficients are shown in Table 2 and Figure 2 shows the respective trajectories for the hip and knee joints.

Table 2. Coefficients for the equation.

Coefficient	Value	Coefficient	Value
c_0	0.208	f_1	−0.103
c_1	0.362	f_2	−0.010
c_2	−0.066	f_3	0.029
c_3	0.001	f_4	−0.342
c_4	0.766	f_5	0.168
c_5	−0.099	f_6	0.084
c_6	−0.219	d	3.142
c_7	0.008	d_1	3.142

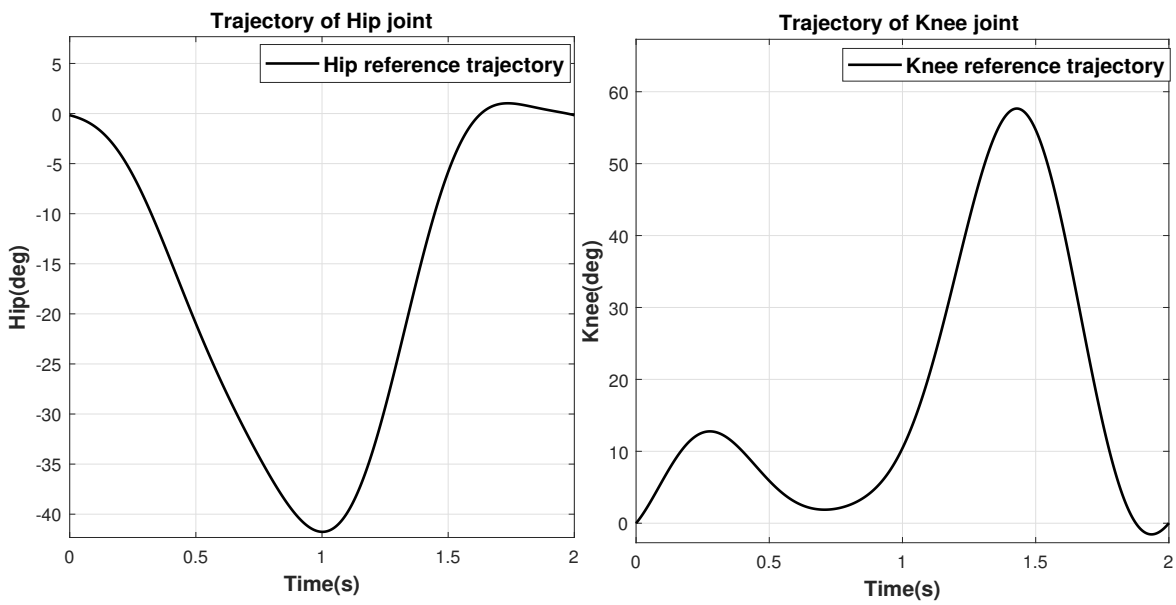

Figure 2. Reference trajectories of the hip and knee joints.

In this paper, the reference trajectories i.e., predefined gait trajectories representing desired angular positions of the hip and knee joints, are obtained using Equation (6) for the analysis of the proposed algorithm. The gait cycle in Equation (6) starts initially at stance phase and continues periodically every 2 s as shown in Figure 2.

3. Active Disturbance Rejection Control for Lower Limb Robotic Rehabilitation Exoskeleton

Figure 3 shows the block diagram of the proposed ADRC applied to the LLRRE. In this paper, the MIMO system is first converted to a single input single output (SISO) by decoupling, for the hip and the knee joint, and then the proposed controller is applied.

The proposed ADRC method as a combination of LESO, TD, and NLSEF eliminates the un-modeled dynamics and uncertainties of the system, improves the dynamic response of the system, and reduces overshoot.

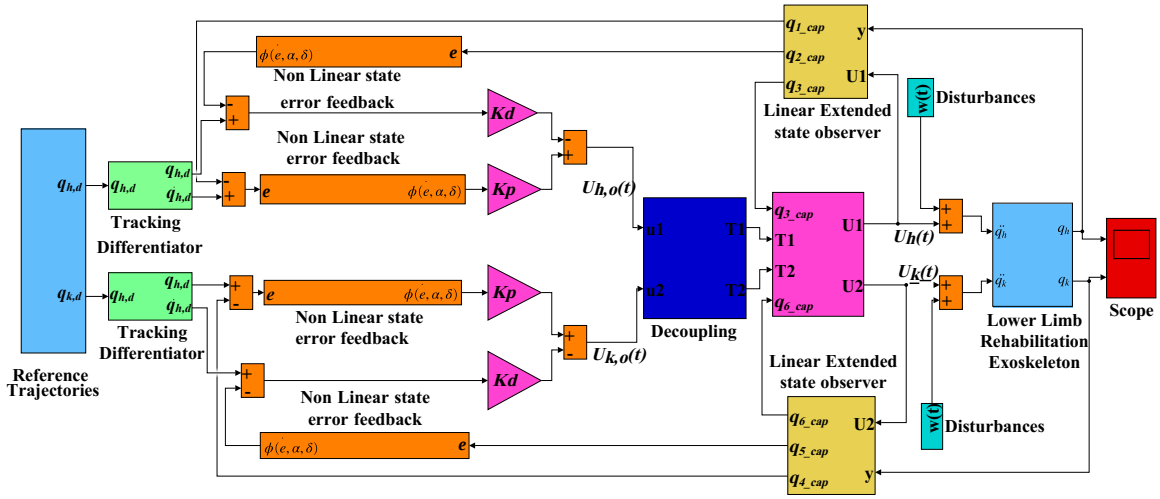

Figure 3. Topology of proposed active disturbance rejection control (ADRC) for lower limb robotic rehabilitation exoskeleton (LLRRE).

Where, $q_{h,d}(t)$ and $q_{k,d}(t)$ are the respective reference trajectories for the hip and knee joints. $\widehat{q}_1(t), \widehat{q}_2(t), \widehat{q}_4(t)$, and $\widehat{q}_5(t)$ are the estimated and $\widehat{q}_3(t), \widehat{q}_6(t)$ are extended states of the LESO for called LESO for the hip joint and LESO for the knee joint, respectively. $U_{h,0}(t)$ and $U_{k,0}(t)$ are the outputs of the NLSEF. $U_h(t)$ and $U_k(t)$ are the outputs of the improved ADRC. $w(t)$ is the exogenous disturbance. $q_h(t)$ *and* $q_k(t)$ denotes the actual angular position respectively for hip and the knee joints.

3.1. Linear Extended State Observer (LESO)

ADRC is an observer-based control strategy that makes use of an LESO [52,53]. LESO is the core in the architecture of ADRC, which makes use of available knowledge for interpretation of the states, online estimates states, and eliminates the caveats like model parameters, exogenous signals, and uncertainties as a total disturbance. The general design of LESO for the SISO system, followed by second-order LESO, is presented in this subsection.

The generalized nth order system (SISO) is presented as follows:

$$y^{(n)}(t) = f(y(t), \dot{y}(t), \ldots, y^{(n-1)}(t), w(t), t) + bu(t) \tag{7}$$

where, *w(t)* is the exogenous disturbance, *u(t)*, input, *y(t)*, output, *b* is the system parameter $f(y(t), \dot{y}(t), \ldots, y^{(n-1)}(t), w(t), t)$ comprising exogenous disturbance and internal modeling uncertainties called as an entire disturbance.

Let, $q_1 = y,\ q_2 = \dot{y},\ q_3 = \ddot{y},\ \ldots, q_n = y^{(n-1)}$, and putting in Equation (7) gives

$$\begin{cases} \dot{q}_1 = q_2, \\ \dot{q}_2 = q_3, \\ . \\ . \\ \dot{q}_{n-1} = q_n, \\ \dot{q}_n = f(q_1, q_2, \ldots, q_n, w(t), t) + bu, \\ y = q_1 \end{cases} \tag{8}$$

The variable q_{n+1} in Equation (9) is augmented and introduced in the architecture of an (LESO) in Equation (8).

$$q_{n+1} = f(q_1, q_2, \ldots, q_n, w(t), t) \tag{9}$$

For linearization of the system in Equation (8). The combination of Equation (8) with Equation (9) gives the extended-state equation, as follows

$$\begin{cases} \dot{q}_1 = q_2, \\ \dot{q}_2 = q_3, \\ . \\ . \\ \dot{q}_{n-1} = q_n, \\ \dot{q}_n = q_{n+1} + bu, \\ \dot{q}_{n+1} = h(t), \\ y = q_1 \end{cases} \tag{10}$$

where, $h(t) = f(q_1, q_2, ..., q_n, w(t), t)$.

For estimation of extended states, a LESO is generally designed as

$$\begin{cases} \dot{\widehat{q}}_1 = \widehat{q}_2 + \beta_1(q_1 - \widehat{q}_1), \\ \dot{\widehat{q}}_2 = \widehat{q}_3 + \beta_2(q_1 - \widehat{q}_1), \\ . \\ . \\ \dot{\widehat{q}}_n = \widehat{q}_{n+1} + \beta_n(q_1 - \widehat{q}_1) + bu, \\ \dot{\widehat{q}}_{n+1} = \beta_{n+1}(q_1 - \widehat{q}_1), \end{cases} \tag{11}$$

where, $\widehat{q}_1, \widehat{q}_2, ..., \widehat{q}_n$, and $\widehat{q}_{n+1}$ are estimates of states $q_1, q_2, ..., q_n$, and q_{n+1}, respectively, and $\beta_1, \beta_2, ..., \beta_{n+1}$ are the observer gains to be designed.

$e_i = q_i - \widehat{q}_i$ $(i = 1, 2, ..., n+1)$ denotes the error for state estimation.

For the second-order system, the LESO can be modeled as

$$\begin{cases} \dot{\widehat{q}}_1 = \widehat{q}_2 + \beta_1(q_1 - \widehat{q}_1), \\ \dot{\widehat{q}}_2 = \widehat{q}_3 + \beta_2(q_1 - \widehat{q}_1) + bu, \\ \dot{\widehat{q}}_3 = \beta_3(q_1 - \widehat{q}_1) \end{cases} \tag{12}$$

Equation (12) can be written in state-space form as

$$\begin{cases} \dot{\hat{Q}} = A\hat{Q} + Bu + \beta e \\ y = C\hat{Q} \end{cases} \tag{13}$$

where,

$$A = \begin{bmatrix} 0 & 1 & 0 \\ 0 & 0 & 1 \\ 0 & 0 & 0 \end{bmatrix}, B = \begin{bmatrix} 0 \\ b \\ 0 \end{bmatrix}, \beta = \begin{bmatrix} \beta_1 \\ \beta_2 \\ \beta_3 \end{bmatrix}, C = \begin{bmatrix} 1 \\ 0 \\ 0 \end{bmatrix} \tag{14}$$

$\boldsymbol{\beta} = \begin{bmatrix} \beta_1, & \beta_2, & \beta_3 \end{bmatrix}^T$ represents observer gain vector. For simplifying tuning, all the observer poles are placed at $-\omega_o$. For determination of observer gains, the following characteristic equation is used [54].

$$\lambda_0\ (s) = s^3 + \beta_1 s^2 + \beta_2 s + \beta_3 = (s + w_0)^3 \tag{15}$$

where, w_o represents bandwidth of observer. For the above characteristic equation, values of gain vector β are expressed by $\beta_1 = 3w_0, \beta_2 = 3w_0^2, \beta_3 = w_0^3$.

The ADRC control law is defined by $u = \frac{u_0 - \hat{f}}{b}$, where b represents system parameter, depends on the system dynamics, $u_0 = K_p(q_d - \hat{q}_1) + K_d(\dot{q}_d - \hat{q}_2) + \ddot{q}_d$ with well-designed ESO, the last term in left-hand side $\ddot{q}$ is very small and the rest of the terms constitute a proportional derivative controller [55]. $k_p = w_c^2$ and $K_d = 2w_c$ are the selected controller gains [56].

3.2. Tracking Differentiator (TD)

The TD is generally implemented to avoid overshoot and optimize the system response [57]. It operates on a transient profile of input signals, differentiated it to avoid abrupt change, which results in the gradual increasing output instead of sudden changes. In this paper TD developed by Zhigao Liu [58] shown in Equation (16), which is easy to implement and superior to the classical nonlinear tracking differentiator, is used to improve trajectory tracking performance.

$$\begin{aligned} \dot{x}_1 &= x_2 \\ \dot{x}_2 &= -R^2 \left(a_1[x_1 - v(t)] - b_1 \frac{x_2(t)}{R} - b_2 \frac{x_2(t)^n}{R^n} \right) \end{aligned} \tag{16}$$

$a_1 > 0, b_1 > 0, b_2 > 0, n > 0,\ n$ is odd.

Here, x_1 is the desired trajectory and x_2 is its derivative. The selection of R depends on application and selected appropriately to adjust the pace of the transient profile. Then, x_2 is denoted as the "tracking differentiator" of *v(t).*

3.3. Non-Linear State Error Feedback (NLSEF)

In this paper a NLSEF based on Equation (17) given by J. Han [16] and Wu Qing Xu [41] in Equation (18) is used. A non-linear state error feedback function *fal(.)* is represented by the form

$$fal(e, \alpha, \delta) = \begin{cases} \dfrac{e}{\delta^{1-\alpha}} & |e| < \delta \\ |e|^{\alpha}.\ sign(e), & |e| > \delta \end{cases} \tag{17}$$

δ and α are the tuning parameter for the exponential function. There exists linear regions for the *fal(.)* and is not a smooth curve which lead to flutter the controller, a new function is used which has a smooth curve is presented in Equation (18).

$$\begin{cases} \phi(e, \alpha, \delta) = newfal(e, \alpha, \delta) = \\ (\alpha - 1)\delta^{\alpha-3}e^3 - (\alpha - 1)\delta^{\alpha-2}e^2 sign(e) & |e| < \delta \\ +\delta^{\alpha-1}e, \\ |e|^{\alpha} sign(e), & |e| > \delta \end{cases} \tag{18}$$

The nonlinear control feedback law non-linearly combines the error between state error feedback and reference, and estimated state.

4. Design of ADRC for Trajectory Tracking Controller

The mathematical model in Equation (1) can be expressed as follows :

$$\begin{cases} m_{11}\ddot{q}_h + m_{12}\ddot{q}_k + c_{11}\dot{q}_h + c_{12}\dot{q}_k + g_1 + D_1 = \tau_1 \\ m_{21}\ddot{q}_h + m_{22}\ddot{q}_k + c_{21}\dot{q}_h + c_{22}\dot{q}_k + g_2 + D_2 = \tau_2 \end{cases} \tag{19}$$

where, $\boldsymbol{D} = \begin{bmatrix} D_1, & D_2 \end{bmatrix}^T$ and $\boldsymbol{T} = \begin{bmatrix} \tau_1, & \tau_2 \end{bmatrix}^T$, D_1 and D_2 are exogenous disturbances and un-modeled dynamics, τ_1 and τ_2 are torques of the hip and knee joints.

Equation (19) in state space is given as:

$$\begin{cases} \ddot{q}_h = \dfrac{1}{(m_{11}m_{22} - m_{21}m_{12})}.(m_{22}\tau_1 - m_{12}\tau_2 - F_1) \\ \ddot{q}_k = \dfrac{1}{(m_{12}m_{21} - m_{11}m_{22})}.(m_{21}\tau_1 - m_{11}\tau_2 - F_2) \end{cases} \tag{20}$$

where,

$$\begin{cases} F_1 = (m_{22}c_{11} - m_{12}c_{21})\dot{q}_h + (m_{22}c_{12} - m_{12}c_{22})\dot{q}_k \\ +m_{22}g_1 - m_{12}g_2 + m_{22}D_1 - m_{12}D_2 \\ F_2 = (-m_{21}c_{11} - m_{11}c_{21})\dot{q}_h - (m_{21}c_{12} - m_{11}c_{22})\dot{q}_k \\ -m_{21}g_1 + m_{11}g_2 - m_{22}D_1 + m_{12}D_2 \end{cases} \tag{21}$$

Equation (21) can be written as :

$$\begin{cases} \ddot{q}_h = C_{f1}.(m_{22}\tau_1 - m_{12}\tau_2) + f_1 \\ \ddot{q}_k = -C_{f1}.(m_{21}\tau_1 - m_{11}\tau_2) + f_2 \end{cases} \tag{22}$$

where, $C_{f1} = \frac{1}{(m_{11}m_{22} - m_{21}m_{12})}$, $f_1 = -F_1C_{f1}, f_2 = F_2C_{f1}$.

The system in Equation (22) is decoupled by matrix D.

$$D = \begin{bmatrix} Cf_1m_{22} & 0 \\ 0 & Cf_1m11 \end{bmatrix} \tag{23}$$

The system Equation (22) can be expressed as

$$\ddot{\boldsymbol{q}} = \boldsymbol{f} + \boldsymbol{U} \tag{24}$$

here, $\ddot{\boldsymbol{q}} = [\ddot{q}_h, \ddot{q}_k]^T$, $\boldsymbol{f} = [f_1, f_2]^T, \boldsymbol{U} = [U_1, U_2]^T = \boldsymbol{D}[\tau_1, \tau_2]^T$ if U is known, the control of input $\boldsymbol{T} = \begin{bmatrix} \tau_1, & \tau_2 \end{bmatrix}^T$ can be obtained as $\boldsymbol{D}_{inv}U$ after the system is decoupled, ADRC can be split into two independent equations for the hip and knee joint.

$$\begin{aligned} \ddot{q}_h &= f_1 + \boldsymbol{D}_{\text{inv}}(1,1).U_1 \\ \ddot{q}_k &= f_2 + \boldsymbol{D}_{\text{inv}}(2,2).U_2 \end{aligned} \tag{25}$$

Based on Equation (12) and Equation (25) the LESO is designed separately for each joint. Two LESOs are

$$\begin{cases} \dot{\hat{q}}_1 = \hat{q}_2 + \beta_1(q_1 - \hat{q}_1\ ), \\ \dot{\hat{q}}_2 = \hat{q}_3 + \beta_2(q_1 - \hat{q}_1\ ) + \boldsymbol{D}_{\text{inv}}(1,1).U_1, \\ \dot{\hat{q}}_3 = \beta_3(q_1 - \hat{q}_1\ ) \\ \\ \dot{\hat{q}}_4 = \hat{q}_5 + \beta_4(q_1 - \hat{q}_1\ ), \\ \dot{\hat{q}}_5 = \hat{q}_6 + \beta_5(q_1 - \hat{q}_1\ ) + \boldsymbol{D}_{\text{inv}}(2,2).U_2, \\ \dot{\hat{q}}_6 = \beta_6(q_1 - \hat{q}_1\ ) \end{cases} \tag{26}$$

where, $\boldsymbol{\beta_{one}} = [\beta_1,\ \beta_2,\ \beta_3]^T$ and $\boldsymbol{\beta_{two}} = [\beta_4,\ \beta_5,\ \beta_6]^T$are the observer gain matrices. In this paper the bandwidth ω_0 for all the LESO observers are of same value. The bandwidth of feedback controller is defined as $w_c = \frac{1}{3}w_0$. $\boldsymbol{K_p} = \begin{bmatrix} w_c^2 & 0 \\ 0 & w_c^2 \end{bmatrix}$, $\boldsymbol{K_d} = \begin{bmatrix} 2w_c & 0 \\ 0 & 2w_c \end{bmatrix}$ are the gain matrices of controller.

The feedback control law for LESO can be written as $\boldsymbol{U_0} = [U_1, U_2]^T = \boldsymbol{K_p e} + \boldsymbol{K_d}\dot{\boldsymbol{e}}$, $\boldsymbol{e}$, and $\dot{\boldsymbol{e}}$ are the state estimation errors for the position and velocity respectively for the hip and knee joints. $\boldsymbol{q_d} = \begin{bmatrix} q_{h,d} & q_{k,d} \end{bmatrix}$ as reference trajectory for the hip and knee joints and $\boldsymbol{e} = \begin{bmatrix} e_1 & e_2 \end{bmatrix}^T = \begin{bmatrix} (q_{h,d} - \hat{q}_1) & (q_{k,d} - \hat{q}_4) \end{bmatrix}^T$, $\dot{\mathbf{e}} = \begin{bmatrix} \dot{e}_1 & \dot{e}_2 \end{bmatrix}^T = \begin{bmatrix} (\dot{q}_{h,d} - \hat{q}_2) & (\dot{q}_{k,d} - \hat{q}_5) \end{bmatrix}$.

The ADRC strategy for standard second order integrator $\boldsymbol{y} = \boldsymbol{U_0}$ can be expressed as $\boldsymbol{U} = [\tau_1, \tau_2]^T = \boldsymbol{D_{inv}}.(\boldsymbol{K_p e} + \boldsymbol{K_d}\dot{\mathbf{e}} - \hat{f})$. $\hat{f} = [\ \hat{f}_1,\ \hat{f}_2]^T$ for the estimated disturbances.

The control law for ADRC designed from Equations (12), (16), (18) and (25) is given in Table 3.

Table 3. The control law for proposed active disturbance rejection control (ADRC) with combinations

Controller	Control Law
ADRC	$\boldsymbol{U} = [\tau_1, \tau_2]^T = \boldsymbol{D}_{inv}(\boldsymbol{K_p e} + \boldsymbol{K_d}\dot{\mathbf{e}} - \hat{f})$ $for\ hip\ joint\ e = (q_{h,d} - \hat{q}_1), \dot{e} = \hat{q}_2;\ \hat{f} = \hat{q}_3,$ $for\ knee\ joint\ e = (q_{k,d} - \hat{q}_4), \dot{e} = \hat{q}_5;\ \hat{f} = \hat{q}_6,$
ADRC-NLSEF	$\boldsymbol{U} = [\tau_1, \tau_2]^T = \boldsymbol{D}_{inv}(\boldsymbol{K_p}\ \phi(\boldsymbol{e}, \alpha, \delta) - \boldsymbol{K_d}\ \phi(\dot{\mathbf{e}}, \alpha, \delta)\ - \hat{f})$ $where,\ for\ hip\ joint\ , e = (q_{h,d} - \phi(\hat{q}_1, \alpha, \delta)), \dot{e} = \phi(\hat{q}_2, \alpha, \delta);\ \hat{f} = \hat{q}_3,$ $for\ knee\ joint\ , e = (q_{k,d} - \phi(\hat{q}_4, \alpha, \delta)), \dot{e} = \phi(\hat{q}_5, \alpha, \delta);\ \hat{f} = \hat{q}_6,$
ADRC-TD	$\boldsymbol{U} = [\tau_1, \tau_2]^T = \boldsymbol{D}_{inv}(\boldsymbol{K_p e} + \boldsymbol{K_d}\dot{\mathbf{e}}\ - \hat{f})$ $where,\ for\ hip\ joint\ e = (q_{k,d} - \hat{q}_1), \dot{e} = (\dot{q}_d - \hat{q}_2),\ \hat{f} = \hat{q}_3,$ $for\ knee\ joint\ e = (q_{h,d} - \hat{q}_4), \dot{e} = (\dot{q}_d - \hat{q}_5),\ \hat{f} = \hat{q}_6,$
ADRC-NLSEF-TD	$\boldsymbol{U} = [\tau_1, \tau_2]^T = \boldsymbol{D}_{inv}(\boldsymbol{K_p}\ \phi(\boldsymbol{e}, \alpha, \delta) + \boldsymbol{K_d}\dot{\mathbf{e}} - \hat{f})$ $where,\ for\ hip\ joint\ e = (q_{h,d} - \hat{q}_1),$ $\dot{e} = (\dot{q}_{h,d} - \phi(\hat{q}_2, \alpha, \delta)),\ \hat{f} = \hat{q}_3,$ $for\ hip\ joint\ e = (q_{k,d} - \hat{q}_4),$ $\dot{e} = (\dot{q}_{k,d} - \phi(\hat{q}_5, \alpha, \delta)),\ \hat{f} = \hat{q}_6,$

The system in Equation (7) finally becomes Equation (27) for well-designed control law as shown in Equation (24)

$$\ddot{\boldsymbol{q}} = \boldsymbol{f} + \boldsymbol{D}_{inv}((\boldsymbol{k_p}\phi(\boldsymbol{e}, \delta, \alpha) + \boldsymbol{k_d}\dot{\boldsymbol{e}}) + \ddot{\boldsymbol{q}}_{\boldsymbol{d}} - \widehat{\boldsymbol{f}}) \tag{27}$$

$\ddot{\boldsymbol{q}} = [\dot{q}_2,\ \dot{q}_4]^T$. In the control laws $\boldsymbol{q_d} = \begin{bmatrix} q_{h,d} & q_{k,d} \end{bmatrix}^T$ is the desired gait trajectory of the joints of exoskeleton. $\ddot{\boldsymbol{q}}_{\boldsymbol{d}} = \begin{bmatrix} \ddot{q}_{h,d} & \ddot{q}_{k,d} \end{bmatrix}^T$ is negligible, $\boldsymbol{f} = \begin{bmatrix} q_3 & q_6 \end{bmatrix}^T$ whereas $\hat{q}_1,\ \hat{q}_2,\ \hat{q}_4,\ \hat{q}_5$ are the estimated states for $q_1,\ q_2,\ q_4,\ q_5$, and $\widehat{\boldsymbol{f}} = [\hat{q}_3,\ \hat{q}_6\ ]^T$ represents the extended state which eliminates the disturbances and uncertainties that occur in the system.

5. Stability Analysis

Assuming $f(q_1, q_2, ...q_n, u, \omega(t), t)$ is globally Lipschitz with respect to q, there exists a constant $w_0 > 0$, $w_c > 0$, such that the closed loop system Equation (27) is asymptotically stable.

Proof. From Table 3 one has

$$\boldsymbol{U} = \boldsymbol{D}_{inv}((\boldsymbol{k_p}\phi(\boldsymbol{e}, \delta, \alpha) + \boldsymbol{k_d}\dot{\boldsymbol{e}}) + \ddot{\boldsymbol{q}}_{\boldsymbol{d}} - \widehat{\boldsymbol{f}}) \tag{28}$$

Assume that the control design objective is to make the output of the plant follow a given, bounded, reference signal $q_{h,d}$, whose derivatives, $\dot{q}_{h,d,1},\ \ddot{q}_{h,d,2}, ..., q_{h,d}^{(n)}$ are also bounded. Let, for the hip joint $[q_{h,d,1},\ q_{h,d,2},\ q_{h,d,3}]^T = [\dot{q}_{h,d},\ \dot{q}_{h,d,1}, \dot{q}_{h,d,2}]^T$. Define $e_i = q_{h,d,i} - q_i,\ i = 1, 2, ...n$ and $\tilde{q}_1 = q_1 - \hat{q}_1,\ \tilde{q}_2 = q_2 - \phi(\hat{q}_2, \alpha, \delta) = q_2 - \hat{q}_2,\ \tilde{q}_3 = q_3 - \hat{q}_3, e_1 = q_{h,d,1} - q_1,\ e_2 = q_{h,d,2} - q_2$. The ADRC control law is given as

$$\begin{aligned} U_1 &= [k_p(q_{h,d,1} - \hat{q}_1) + k_d(q_{h,d,2} - \hat{q}_2) + q_{h,d,3} - \hat{q}_3]/D(1,1) \\ &= \{[k_p[(q_{h,d,1} - (q_1 - \tilde{q}_1)] + [k_d[(q_{h,d,2} - (q_2 - \tilde{q}_2)] + q_{h,d,3} - \hat{q}_3\}/D(1,1) \\ &= [k_p(e_1 + \tilde{q}_1) + k_d[(e_2 + \tilde{q}_2) + q_{d,3} - \hat{q}_3]/D(1,1) \end{aligned} \tag{29}$$

It follows that for the hip joint

$$\begin{aligned} \dot{e}_1 &= \dot{q}_{h,d,1} - \dot{q}_1 = q_{h,d,2} - q_2 = e_2, \\ \dot{e}_2 &= \dot{q}_{h,d,2} - \dot{q}_2 = q_{h,d,3} - (q_3 + D(1,1).U_1) \\ &= q_{h,d,3} - q_3 - [k_p(e_1 + \tilde{q}_1)] - k_d[(e_2 + \tilde{q}_2) - \hat{q}_3 + q_{h,d,3}] \\ &= -k_p(e_1 + \tilde{q}_1) - k_d[(e_2 + \tilde{q}_2) - \tilde{q}_3 \end{aligned} \tag{30}$$

Let $e = [e_1, e_2]^T \in R^n,\ \tilde{q} = [\tilde{q}_1,\ \tilde{q}_2,\ \tilde{q}_3]^T \in R^{n+1}$, then

$$\dot{e}(t) = A_e e(t) + A_{\tilde{q}}\,\tilde{q}(t)$$

$$A_e = \begin{bmatrix} 0 & 1 \\ -k_{p,h} & -k_{d,h} \end{bmatrix} \ and\ A_{\tilde{q}} = \begin{bmatrix} 0 & 0 & 0 \\ 0 & 0 & 0 \\ -k_{p,h} & -k_{d,h} & -1 \end{bmatrix} \tag{31}$$

Similarly, for the knee joint

$$\dot{e}(t) = A_e e(t) + A_{\tilde{q}}\,\tilde{q}(t)$$

$$A_e = \begin{bmatrix} 0 & 1 \\ -k_{p,k} & -k_{d,k} \end{bmatrix} \ and\ A_{\tilde{q}} = \begin{bmatrix} 0 & 0 & 0 \\ 0 & 0 & 0 \\ -k_{p,k} & -k_{d,k} & -1 \end{bmatrix} \tag{32}$$

Since $k_{p,h}$ and $k_{d,h}$ for the hip joint and $k_{p,h}$ and $k_{d,h}$ for the knee joint are selected in such a way that $s^2 + k_d s + k_p$ is Hurwitz, A_e is Hurwitz. For tuning simplicity we just let $s^2 + k_d s + k_p = (s + \omega_c)^2$ where $w_c > 0$. This makes w_c, the controller bandwidth, only tuning parameter to be adjusted for controller.

$\lim_{t\to\infty} ||A_{\widetilde{q}}\, \widetilde{q}(t)|| = 0$ if $h(q, u, w, \dot{w})$ is globally Lipschitz with respect to q [55]. For tuning simplicity $s^2 + k_d s + k_p = (s + w_c)^2$ where, $w_c > 0$. This makes w_c the only tuning parameter such that $\lim_{t\to\infty} e(t) = 0, i = 1, 2, ..., n$ Q.E.D. $\widetilde{q}_1$, $\widetilde{q}_2$ $\widetilde{q}_3$, $\widetilde{q}_4$, $\widetilde{q}_5$, and $\widetilde{q}_6$ are the observer estimation errors, e_1, e_2, e_3, e_4, e_5, and e_6 are the controller errors for hip joint and knee joints, respectively. From the above, it is shown that the closed loop system is asymptotically stable. □

6. Result Analysis and Discussion

The simulation studies for four cases are discussed. Case 1 : without effect of disturbance, Case 2: with addition of random control disturbance, Case 3: with addition of constant control disturbance, and Case 4: with harmonic control disturbance. The parameters were chosen as shown in Table 4, for tracking differentiator design.

Table 4. The parameters selection for tracking differentiator.

Parameters	Variation	Final Selected Values
a_1	*5 to 50*	*30*
b_1 and b_2	*1 to 10*	*5*
R	*10 to 80*	*30*
n	*1, 3, and 5*	*3*

For NLSEF as shown in Table 5, the parameter values are selected. δ is the linear interval width of *fal(·)* [59] and relates to the error range. If it is too small, *fal(·)* will also cause the high-frequency flutter phenomenon.

Table 5. The parameters selection for NLSEF.

Parameters	Variation	Final Selected Values
α	*0.5 to 1*	0.995
δ	*0.001 to 0.5*	0.01

Dr. Gao suggested factors to decide the bandwidth of the observer and controller [56], which has a vital effect on the performance of controller. A large bandwidth leads to noise sensitivity, a choice of which is a trade-off between the LESO performance and noise tolerance. For the designed LESO, the bandwidth of the observer is varied within the range of 400 rad/s to 1200 rad/s and the chosen value was 900 rad/s. The tracking error tends to decrease with the increase in observer bandwidth but it inversely affects the control effort which increases with the increase in bandwidth. The proportional and derivative gains in the ADRC was chosen by relation $k_p = w_c^2$ and $K_d = 2w_c$ [56].

The proposed ADRC on LLRRE was tested by carrying out the simulation. All the simulations were performed with the sampling time 0.001 s and ode4 (Runge–Kutta) solver in MATLAB(*2019b*, *MathWorks*) [60]. In this paper, trajectories of the hip and knee joints are taken as predefined gait trajectory as a reference, external control disturbance of amplitude 5 N.m for constant disturbance and amplitude 5 N.m with frequency 50 Hz for a harmonic disturbance.

The performance indices chosen for comparison are Integral of the absolute magnitude of error (IAE), Integral time absolute error (ITAE), Integral square error (ISE), Integral time square error (ITSE), and Integral square of the control signal (ISU). All these performance indices can be formulated as:

$$\begin{aligned} IAE &: \int_0^t |(r-y)|\,\mathrm{d}\,t \\ ITAE &: \int_0^t t \times |(r-y)|\,\mathrm{d}\,t \\ ITSE &: \int_0^t t \times (r-y)^2\,\mathrm{d}\,t \\ ISE &: \int_0^t (r-y)^2\,\mathrm{d}\,t \\ ISU &: \int_0^t (u)^2\,\mathrm{d}\,t \end{aligned} \tag{33}$$

where, r is the reference input signal, y is output of the system, and $r - y$ denotes the error of the system and u is the control output. IAE, ITAE, ISE, ITSE are known as time-integral criteria which are generic and comprehensive tools to evaluate the performance of a control system, they allow comparing between different controller designs or even different controller structure [61]. In this paper, the minimum value of index suggests best performance [62] and the parameters were chosen on that basis. Whereas ISU relates to denote control effort required for a controller [63]. The simulation results for gait trajectory tracking of LLRRE for the hip and knee joints, for various controllers, are compared. The comparison of conventional LESO based ADRC with proposed combinations ADRC-NLSEF, ADRC-TD, and ADRC-NLSEF-TD is carried out based performance parameters such as IAE, ITE, ITAE, ISTE, and ISU.

6.1. Effect of Disturbance

Case 1: No Disturbance

In Case 1, the performance of the ADRC is compared with the proposed controllers without external disturbance. Figures 4 and 5 show the trajectory tracking performance of mentioned controllers for the hip and knee joints. Figures 6 and 7 show the control signal required, and Figures 8 and 9 show trajectory tracking error for ADRC, ADRC-NLSEF, ADRC-TD, and ADRC-NLSEF-TD for the hip and knee joints.

Figures 4 and 5 show the trajectory tracking performance of the controllers in the no disturbance case. The trajectory tracked by ADRC-NLSEF-TD has best reference tracking followed by ADRC-TD, ADRC-NLSEF, and ADRC in the no disturbance case which can be seen from the minimized plot (a) in both the figures.

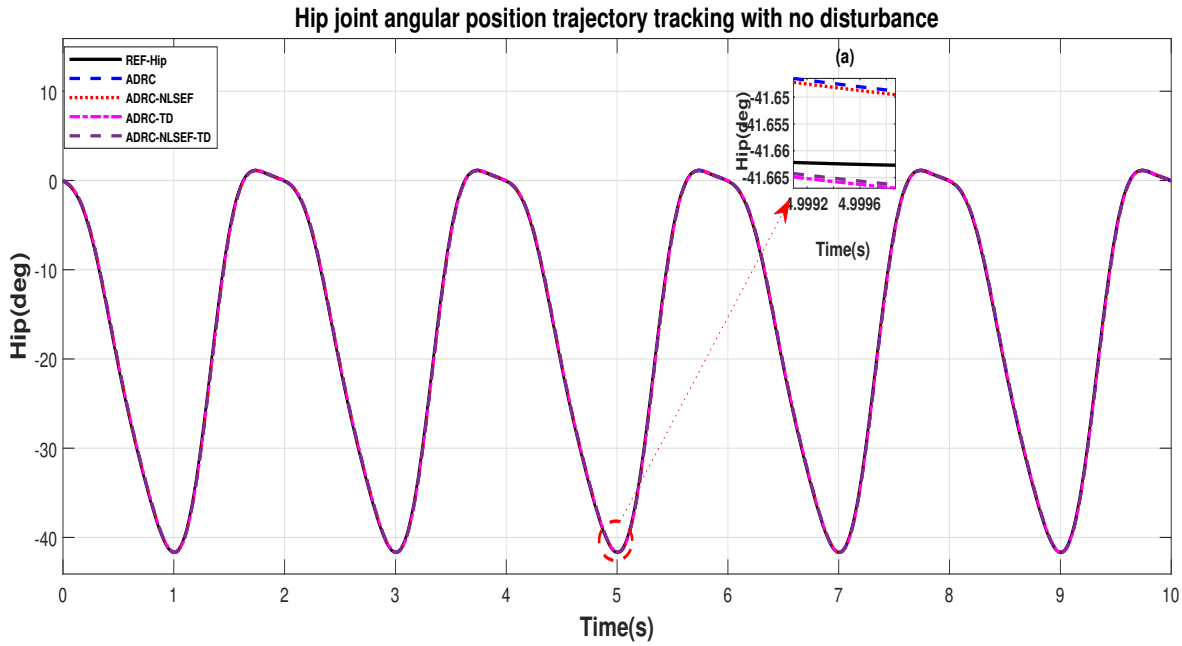

Figure 4. Gait trajectory tracking comparison of ADRC, ADRC-NLSEF, ADRC-TD, and ADRC-NLSEF-TD for the hip joint with a reference without disturbance.

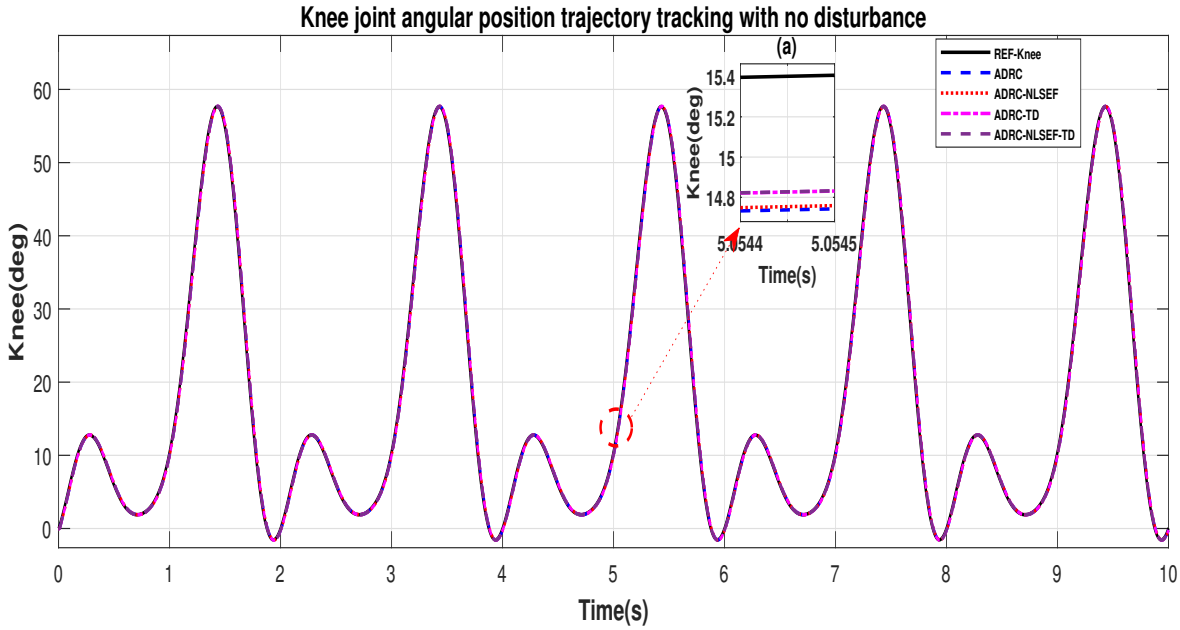

Figure 5. Gait trajectory tracking comparison of ADRC, ADRC-NLSEF, ADRC-TD, and ADRC-NLSEF-TD for the knee joint with a reference without disturbance.

The initial response of the control signal is shown in the minimized plot (a) and control signal in blown up in the minimized plot (b) shown in Figures 6 and 7, gives us the idea of control signal required by the controllers and no chattering in the control signal was observed in plot (b).

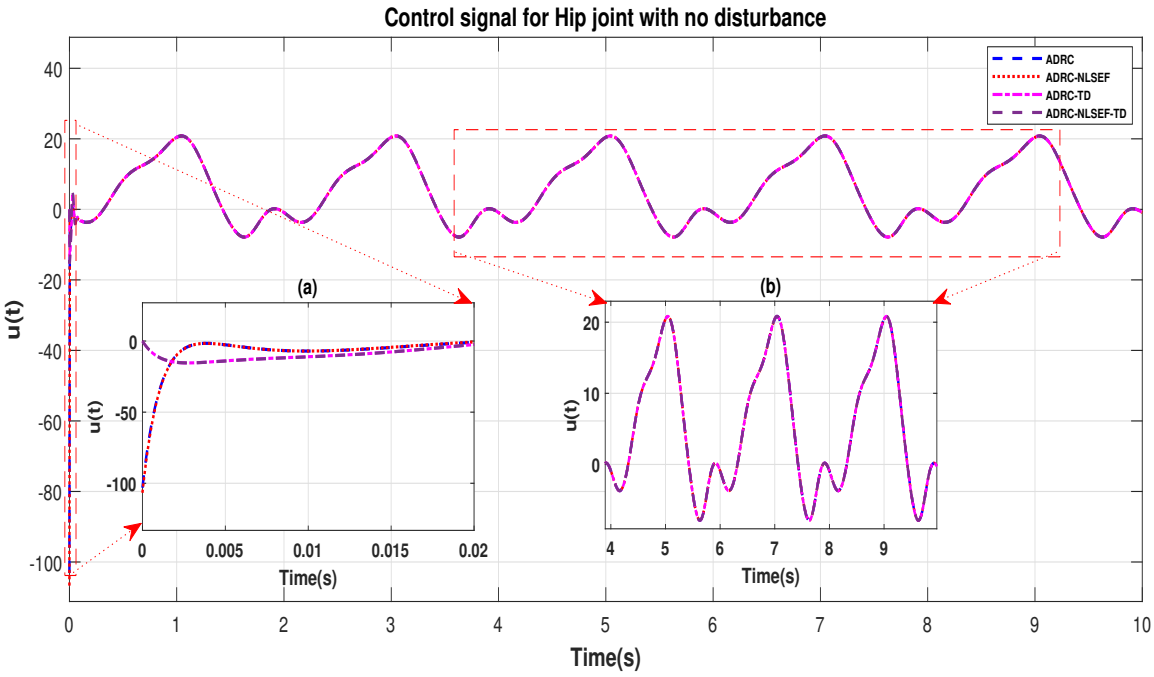

Figure 6. Control signal trajectory tracking comparison of ADRC, ADRC-NLSEF, ADRC-TD, and ADRC-NLSEF-TD for the hip joint with no disturbance. (**a**) initial response of the control signal; (**b**) control signal in blown up.

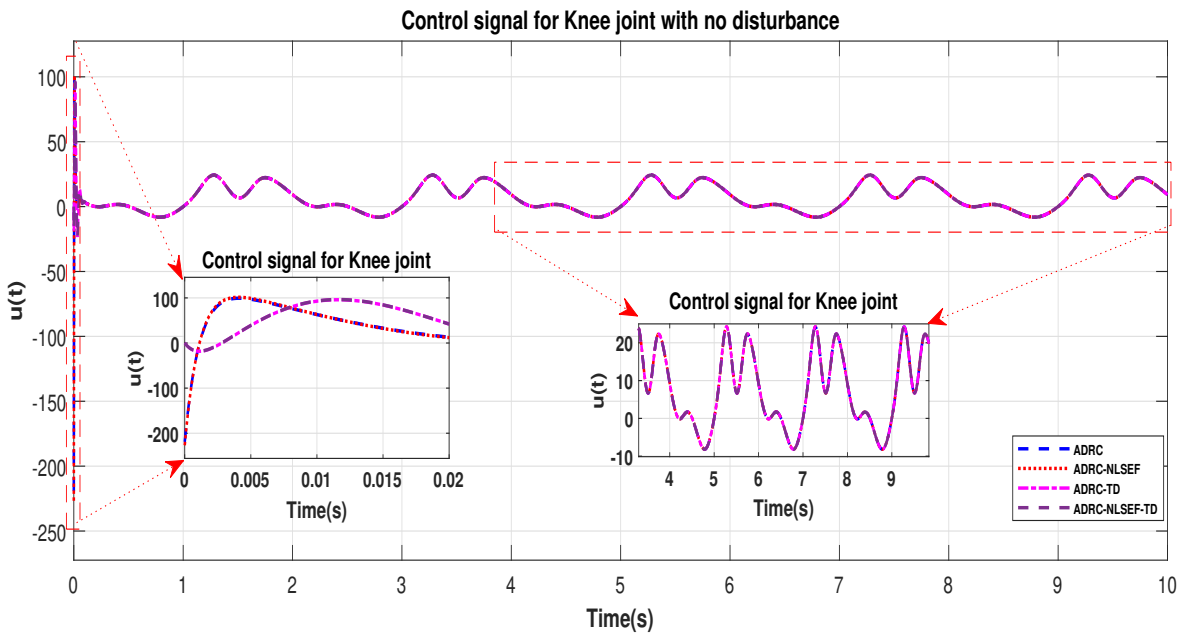

Figure 7. Control signal trajectory tracking comparison of ADRC, ADRC-NLSEF, ADRC-TD, and ADRC-NLSEF-TD for the knee joint with no disturbance.

Figures 8 and 9 show error while trajectory tracking in the minimized plot (a), in no disturbance case ADRC-NLSEF-TD outperforms all other controllers in terms of trajectory tracking followed by ADRC-TD, ADRC-NLSEF, and ADRC.

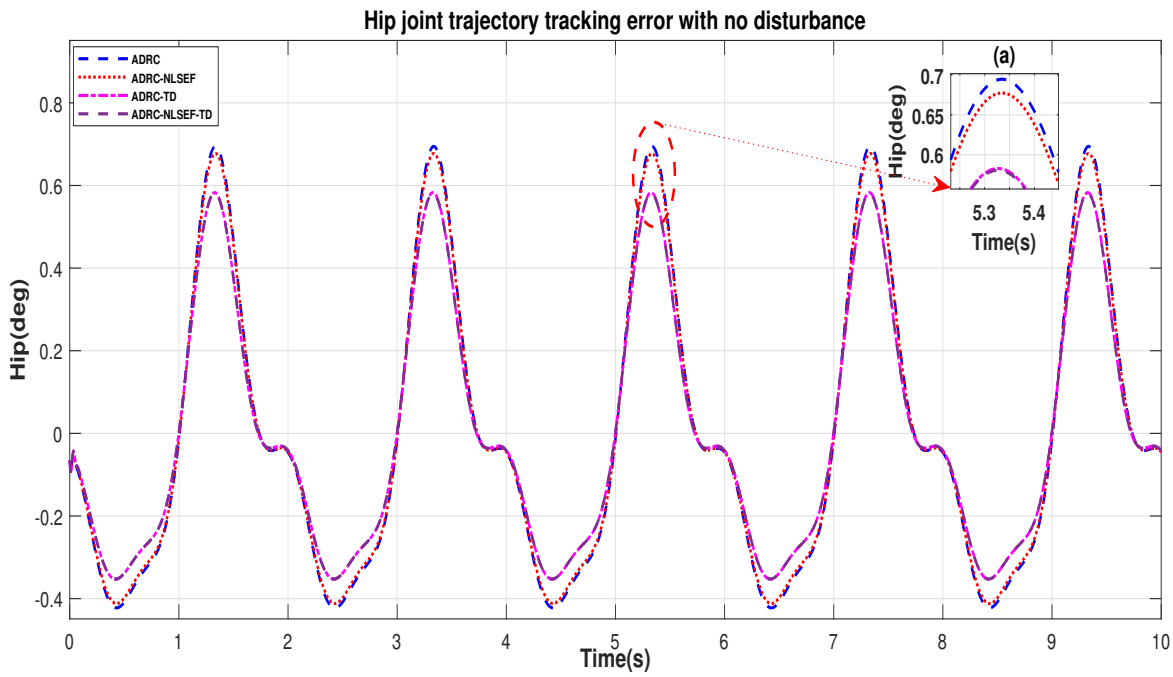

Figure 8. Gait trajectory tracking error comparison of ADRC, ADRC-NLSEF, ADRC-TD, and ADRC-NLSEF-TD for the hip joint with a reference without disturbance.

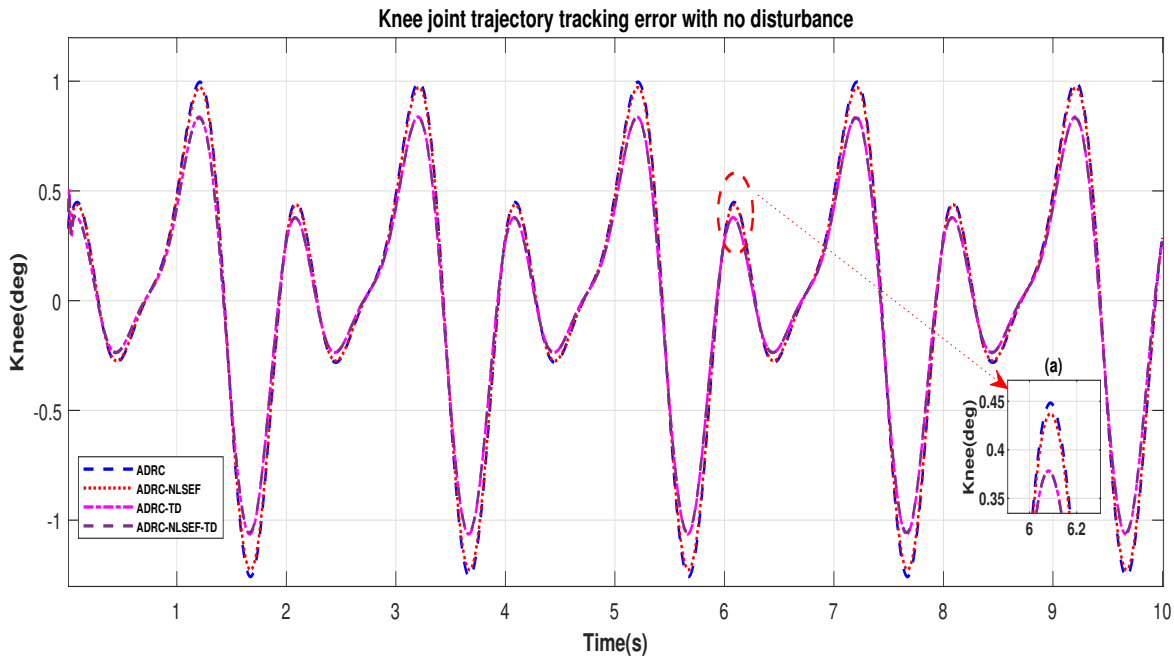

Figure 9. Gait trajectory tracking error comparison of ADRC, ADRC-NLSEF, ADRC-TD, and ADRC-NLSEF-TD for the knee joint with a reference without disturbance.

The Table 6 compares Performance indices for ADRC-NLSEF-TD, ADRC-TD, ADRC-NLSEF, and ADRC for the hip joint and the knee joint for no disturbance case.

Table 6. Performance indices for ADRC, ADRC-NLSEF, ADRC-TD, and ADRC-NLSEF-TD for the hip joint and the knee joint for the no disturbance case.

Control Method		**ADRC-NLSEF-TD**		**ADRC-TD**		**ADRC-NLSEF**		**ADRC**	
Joints		**Hip**	**Knee**	**Hip**	**Knee**	**Hip**	**Knee**	**Hip**	**Knee**
Performance indices	ITSE (Deg.)	4.241	13.2	4.253	13.32	5.793	17.95	6.083	18.87
	ISE (Deg.)	0.8447	2.454	0.8468	2.477	1.152	3.332	1.209	3.503
	ITAE (Deg.)	11.85	20.3	11.85	20.36	13.86	23.68	14.19	24.27
	IAE (Deg.)	2.397	3.883	2.397	3.895	2.8	4.526	2.866	4.638
	ISU N.m.)$\times 10^4$	0.1292	0.1739	0.1292	0.1738	0.1293	0.1724	0.1239	0.1722

ITSE, ISE, ITAE, IAE of ADRC-NLSEF-TD has values of 4.241, 0.8447, 11.85, and 2.397 for the hip joints and 13.2, 2.454, 20.3, and 3.883 for the knee joints, respectively which are minimum as compared ADRC-TD, ADRC-NLSEF, ADRC. This proves that In terms of trajectory tracking ADRC-NLSEF-TD has better performance. ADRC has ISU 1239 for the hip joint and 1722 for the knee joint which is almost the same or a slightly less than ADRC-TD, ADRC-NLSEF, and ADRC-NLSEF-TD.

Case 2: Random Disturbance

In Case 2, The performance of the ADRC is compared with the proposed controllers with addition of random control disturbance (between -1 and 1) $N.m$. The sampling time is 0.001 s. $N.m$. at t = 5 s. Figures 10 and 11 show the trajectory tracking performance of mentioned controllers for the hip and knee joints. Figures 12 and 13 show the control signal required and Figures 14 and 15 show the trajectory tracking error or ADRC, ADRC-NLSEF, ADRC-TD, and ADRC-NLSEF-TD for the hip and knee joints.

Figures 10 and 11 show the trajectory tracking performance for various controllers. The minimized plot (a), shows the trajectory tracking response of the controllers before the introduction of the random disturbance. Plot (b) shows the controller trajectory tracking performance after addition of random disturbance at t = 5 s. The trajectory tracked by ADRC-NLSEF-TD has best reference tracking followed by ADRC-TD, ADRC-NLSEF, and ADRC before and after inclusion of disturbance at t = 5 s, which proves its effectiveness against random disturbance.

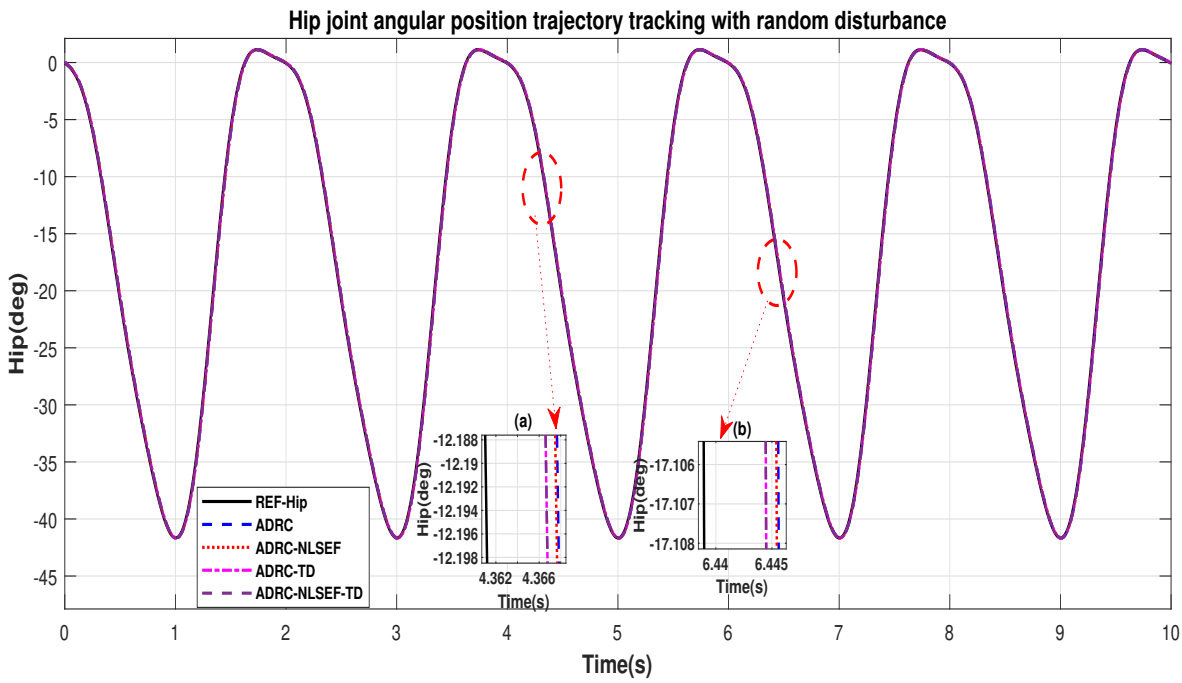

Figure 10. Gait trajectory tracking comparison of ADRC, ADRC-NLSEF, ADRC-TD, and ADRC-NLSEF-TD for the hip joint with a reference with random disturbance.

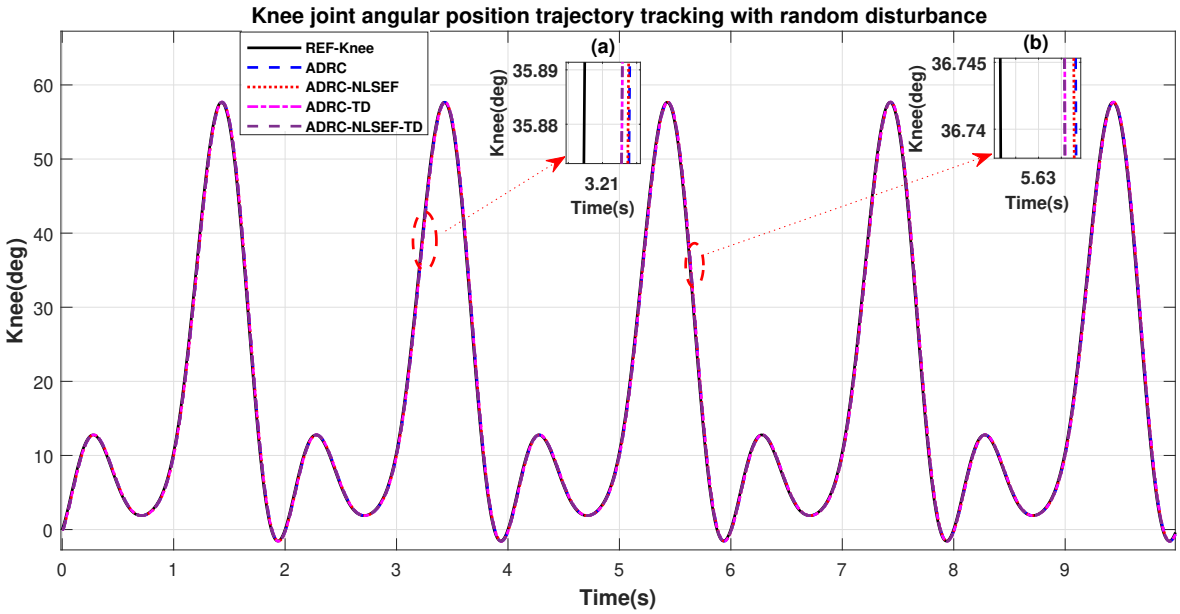

Figure 11. Gait trajectory tracking comparison of ADRC, ADRC-NLSEF, ADRC-TD, and ADRC-NLSEF-TD for the knee joint with a reference with random disturbance.

The initial response of the control signal is shown in the minimized plot (a) and control signal before inclusion of random disturbance in blown up in the minimized plot (b) shown in Figures 12 and 13. Plot (c) and plot (d) show the effect of random disturbance at t = 5 s and after 5 s.

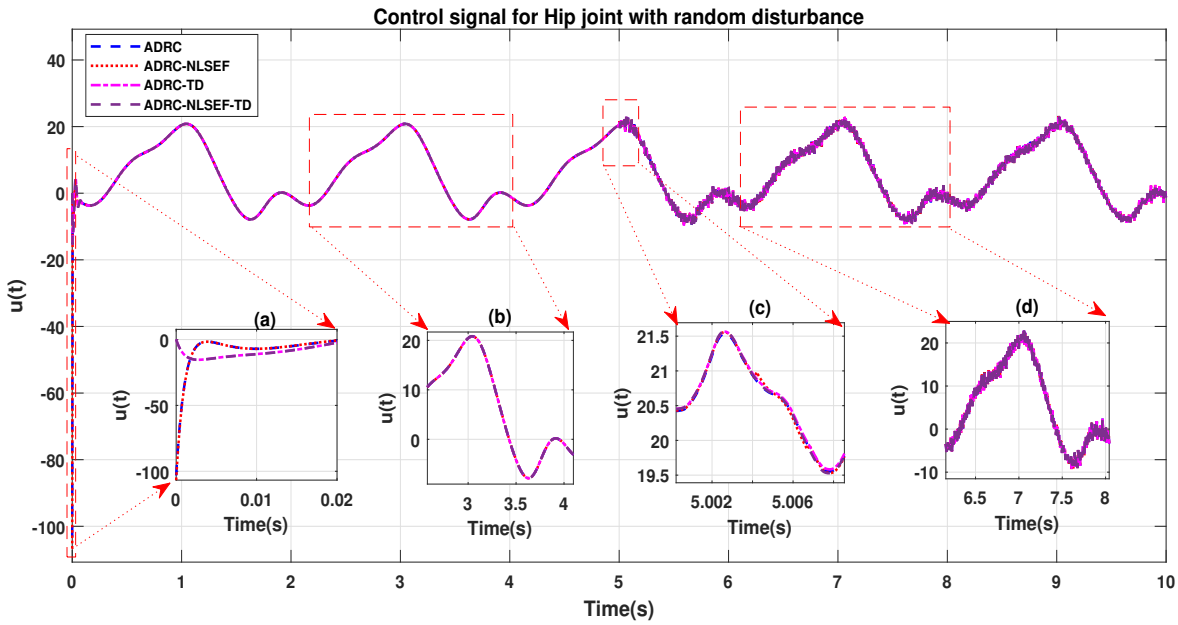

Figure 12. Control signal trajectory tracking comparison of ADRC, ADRC-NLSEF, ADRC-TD, and ADRC-NLSEF-TD for the hip joint with random disturbance.

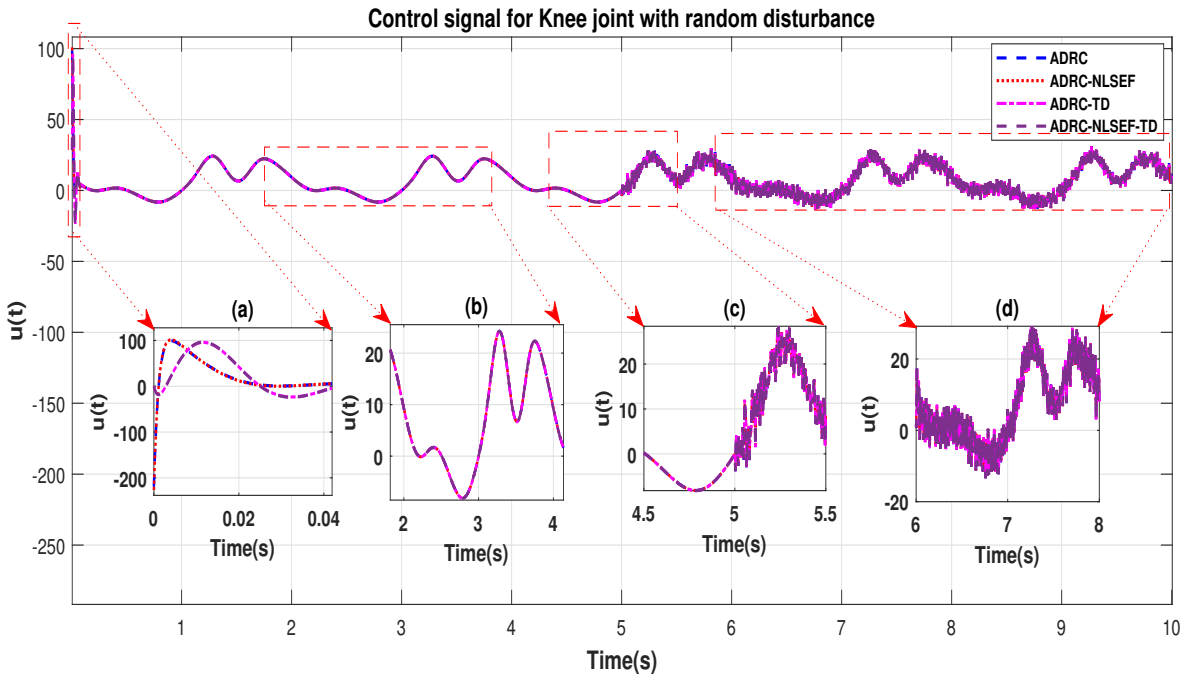

Figure 13. Control signal trajectory tracking comparison of ADRC, ADRC-NLSEF, ADRC-TD, and ADRC-NLSEF-TD for the knee joint with random disturbance.

Figures 14 and 15 show the error trajectory generated while reference tracking, the performance of the controller before and after addition of the random disturbance can be seen from the minimized plot (a) and plot (b), concludes the superiority of ADRC-NLSEF-TD over other controllers of trajectory tracking before and after addition of random disturbance.

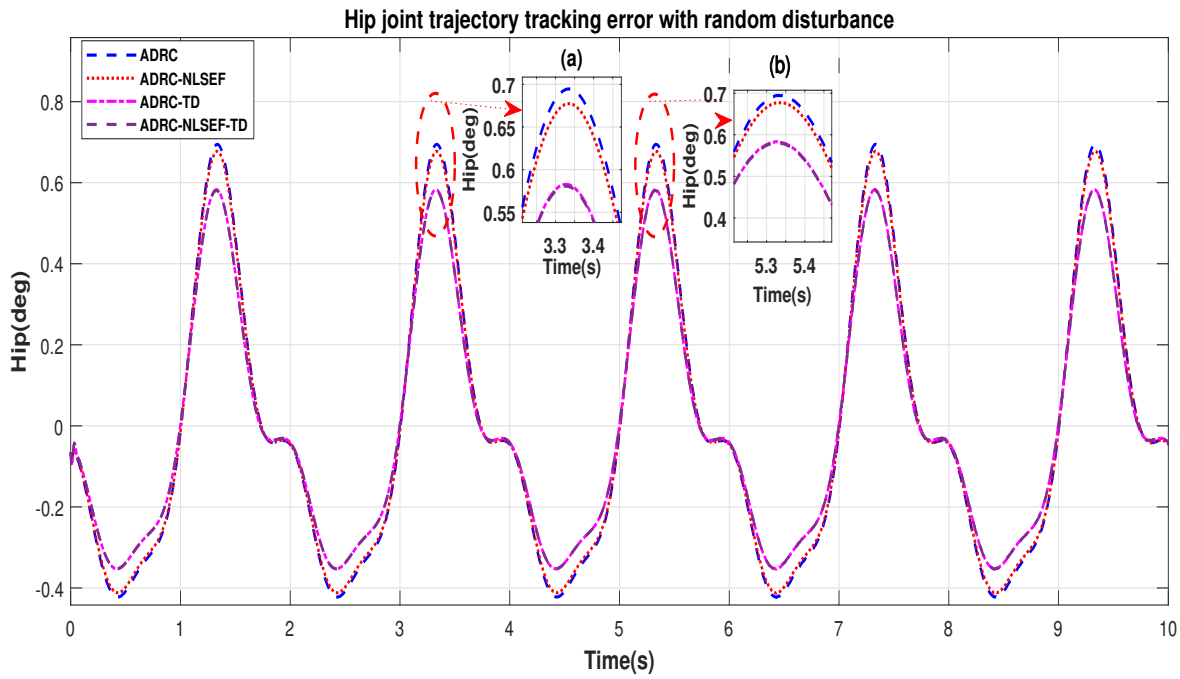

Figure 14. Gait trajectory tracking error comparison of ADRC, ADRC-NLSEF, ADRC-TD, and ADRC-NLSEF-TD for the hip joint for reference signal with random disturbance.

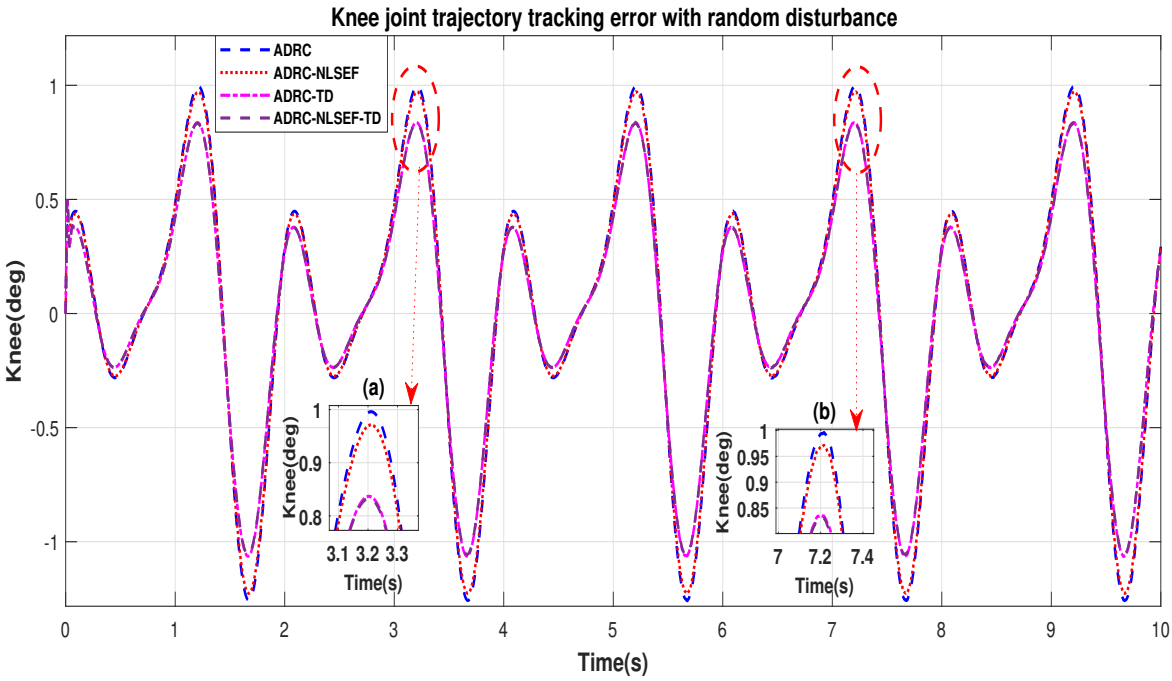

Figure 15. Gait trajectory tracking error comparison of ADRC, ADRC-NLSEF, ADRC-TD, and ADRC-NLSEF-TD for the knee joint for reference signal with random disturbance.

Table 7 compares performance indices for ADRC-NLSEF-TD, ADRC-TD, ADRC-NLSEF, and ADRC for the hip joint and the knee joint for random disturbance case.

Table 7. Performance indices for ADRC, ADRC-NLSEF, ADRC-TD, and ADRC-NLSEF-TD for the hip joint and the knee joint for random disturbance case.

Control Method		**ADRC-NLSEF-TD**		**ADRC-TD**		**ADRC-NLSEF**		**ADRC**	
Joints		**Hip**	**Knee**	**Hip**	**Knee**	**Hip**	**Knee**	**Hip**	**Knee**
Performance indices	ITSE (Deg.)	4.241	13.2	4.253	13.32	5.793	17.95	6.082	18.87
	ISE (Deg.)	0.8447	2.454	0.8468	2.477	1.152	3.332	1.209	3.503
	ITAE (Deg.)	11.85	20.3	11.85	20.36	13.86	23.68	14.19	24.27
	IAE (Deg.)	2.397	3.883	2.397	3.895	2.8	4.526	2.866	4.638
	ISU (N.m.)$\times 10^4$	0.1298	0.1817	0.1298	0.1817	0.1299	0.1803	0.1299	0.1801

ITSE, ISE, ITAE, IAE of ADRC-NLSEF-TD values are 4.241, 0.8447, 11.85, and 2.397 for the hip joints and 13.2, 2.454, 20.3, and 3.883 for the knee joints, respectively which are minimum as compared to ADRC-TD, ADRC-NLSEF, ADRC. This proves that In terms of trajectory tracking ADRC-NLSEF-TD has better performance compared to the rest of the controllers. ADRC has ISU 1299 for the hip joint and 1801 for the knee joint which is almost the same or a slightly less than ADRC-TD, ADRC-NLSEF, and ADRC-NLSEF-TD.

Case 3: Constant Disturbance

In Case 3, the performance of the ADRC is compared with the proposed controllers with addition of constant control disturbance of amplitude 5 N.m. at t = 5 s. Figures 16 and 17 shows the trajectory tracking performance for various controllers for the hip and knee joints. Figures 18 and 19 show the control signal required. Figures 20 and 21 show tracking error for ADRC, ADRC-NLSEF, ADRC-TD, and ADRC-NLSEF-TD for the hip and knee joints with constant disturbance.

Figures 16 and 17 show the trajectory tracking performance for various controllers. The minimized plot (a), show the trajectory tracking response of the controllers before the introduction of the constant disturbance. Plot (b) shows the controller trajectory tracking performance after addition of constant

disturbance at t = 5 s. The trajectory tracked by ADRC-NLSEF-TD has best reference tracking followed by ADRC-TD, ADRC-NLSEF, and ADRC before and after inclusion of disturbance at t = 5 s, which proves its effectiveness against constant disturbance.

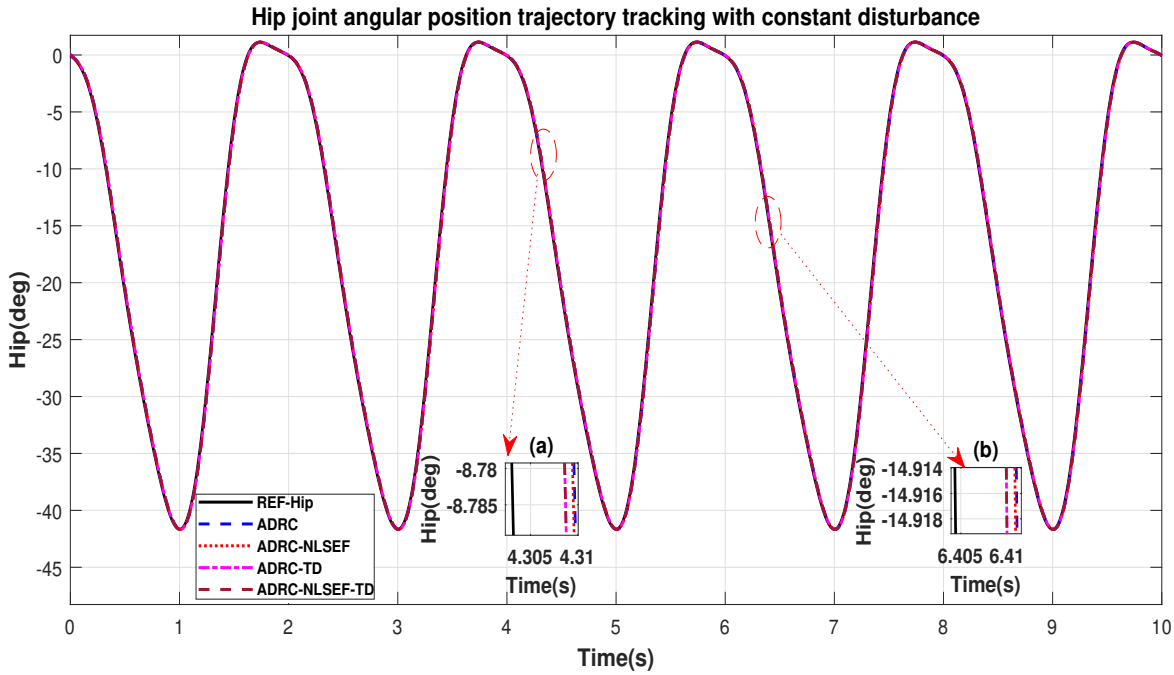

Figure 16. Gait trajectory tracking comparison of ADRC, ADRC-NLSEF, ADRC-TD, and ADRC-NLSEF-TD for the hip joint with a reference with constant disturbance.

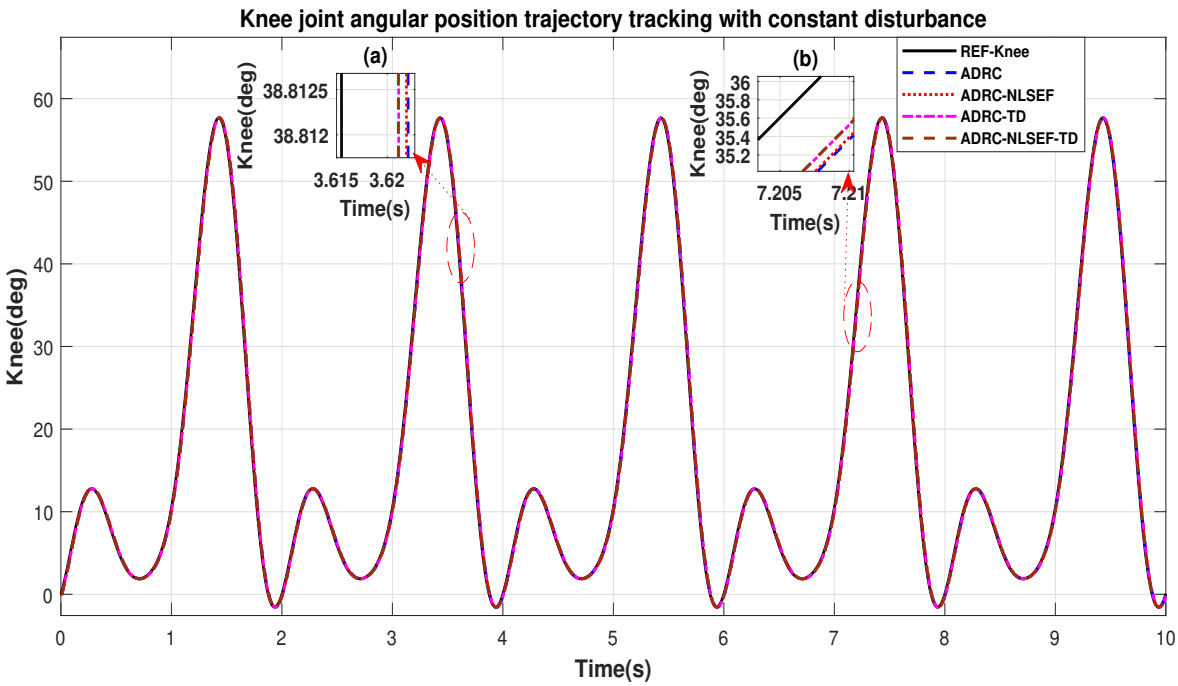

Figure 17. Gait trajectory tracking comparison of ADRC, ADRC-NLSEF, ADRC-TD, and ADRC-NLSEF-TD for the knee joint with a reference with constant disturbance.

The initial response of the control signal is shown in the minimized plot (a) and control signal before inclusion of random disturbance in blown up in the minimized plot (b) shown in Figures 18 and 19. Plot (c) and plot (d) show the effect of constant disturbance at t = 5 s and after 5 s.

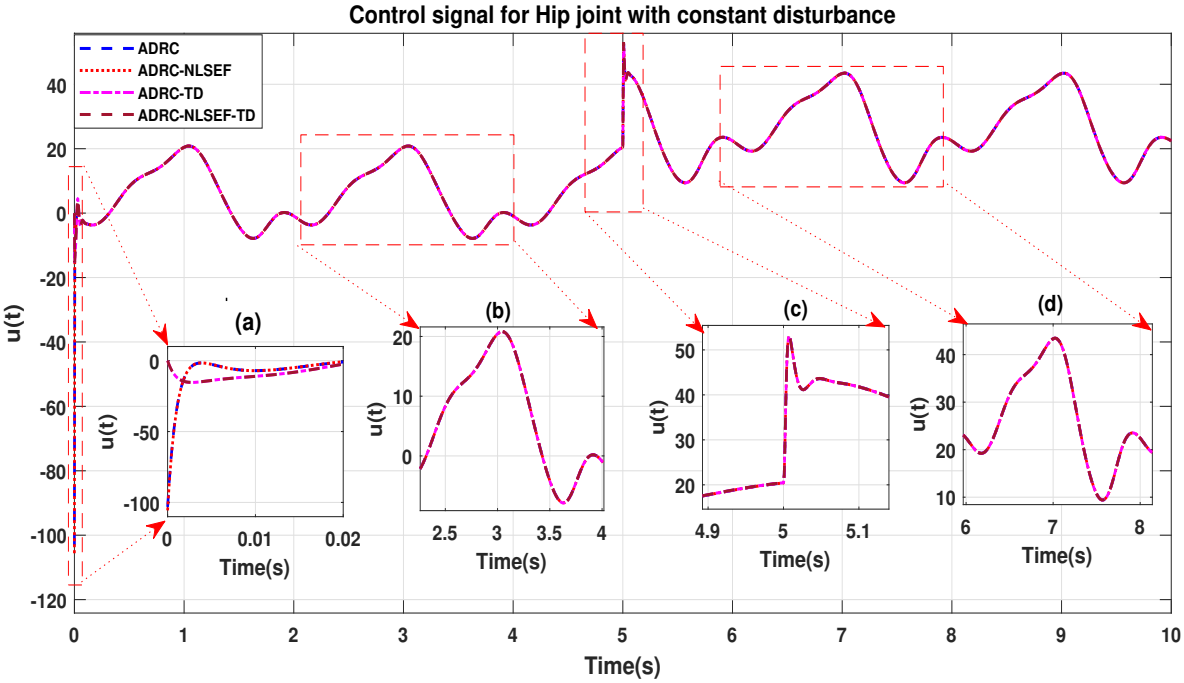

Figure 18. Control signal comparison of ADRC, ADRC-NLSEF, ADRC-TD, and ADRC-NLSEF-TD for the hip joint with constant disturbance.

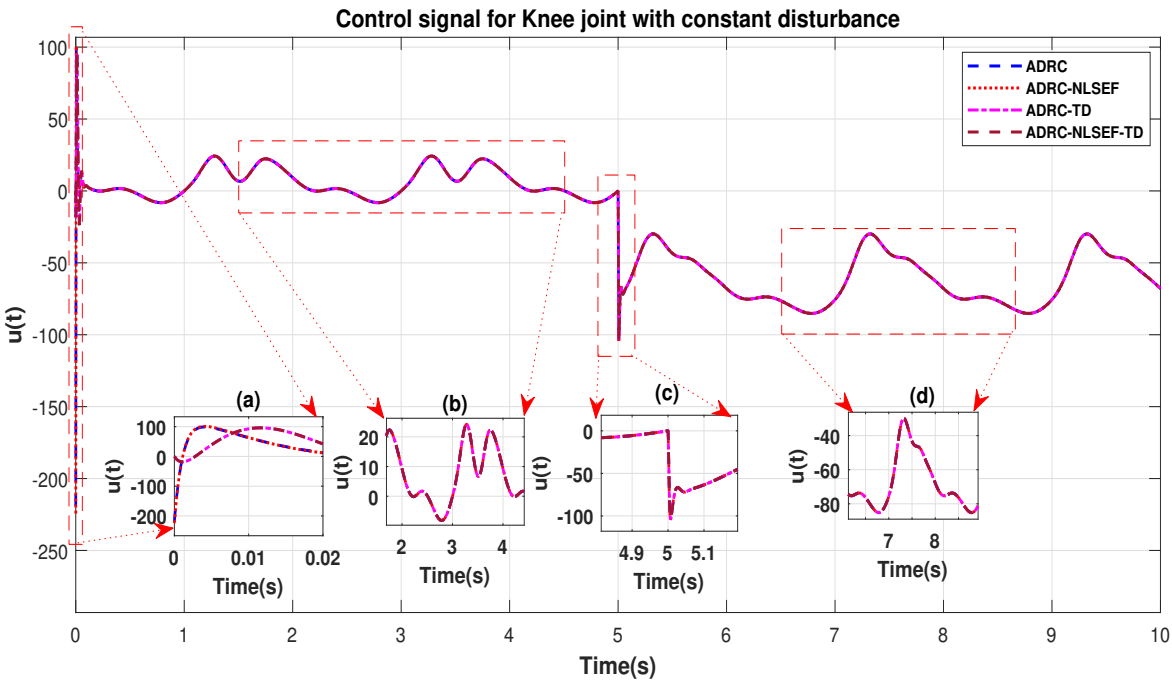

Figure 19. Control signal comparison of ADRC, ADRC-NLSEF, ADRC-TD, and ADRC-NLSEF-TD for knee Joint with constant disturbance.

Figures 20 and 21 show the error trajectory generated while reference tracking, the performance of the controller before and after addition of the constant disturbance can be seen from the minimized

plot (a) and plot (b), concluding the superiority of ADRC-NLSEF-TD over other controllers of trajectory tracking before and after addition of constant disturbance.

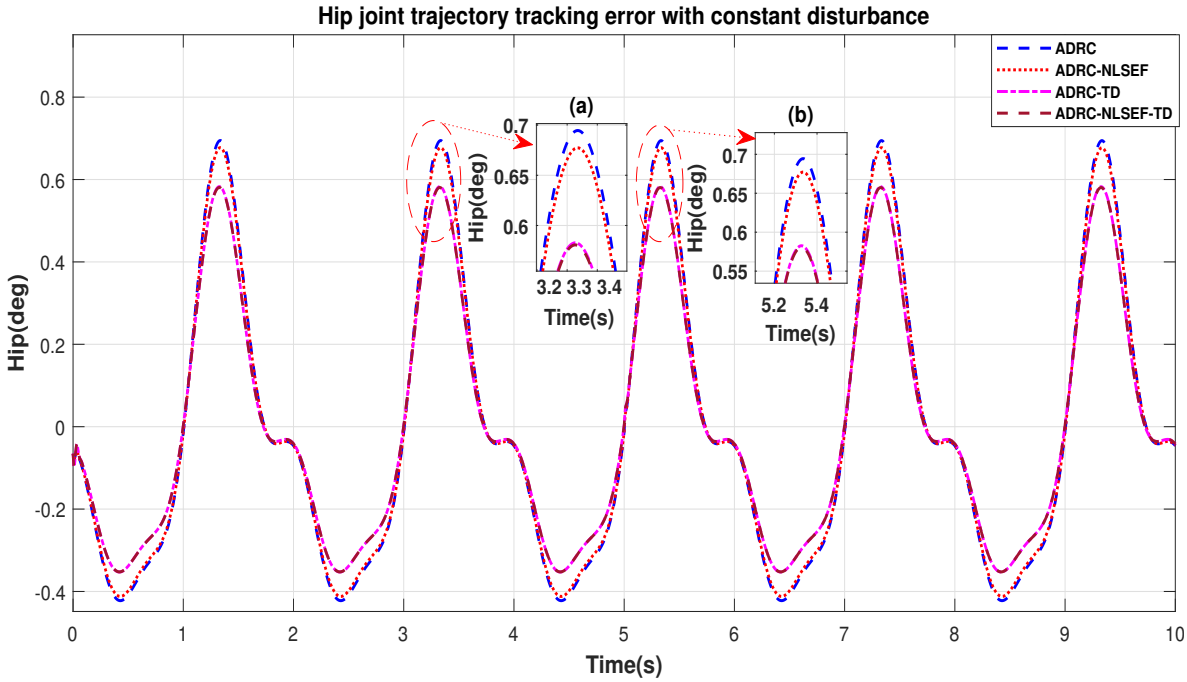

Figure 20. Gait trajectory tracking error comparison of ADRC, ADRC-NLSEF, ADRC-TD, and ADRC-NLSEF-TD for the hip joint with a reference with constant disturbance.

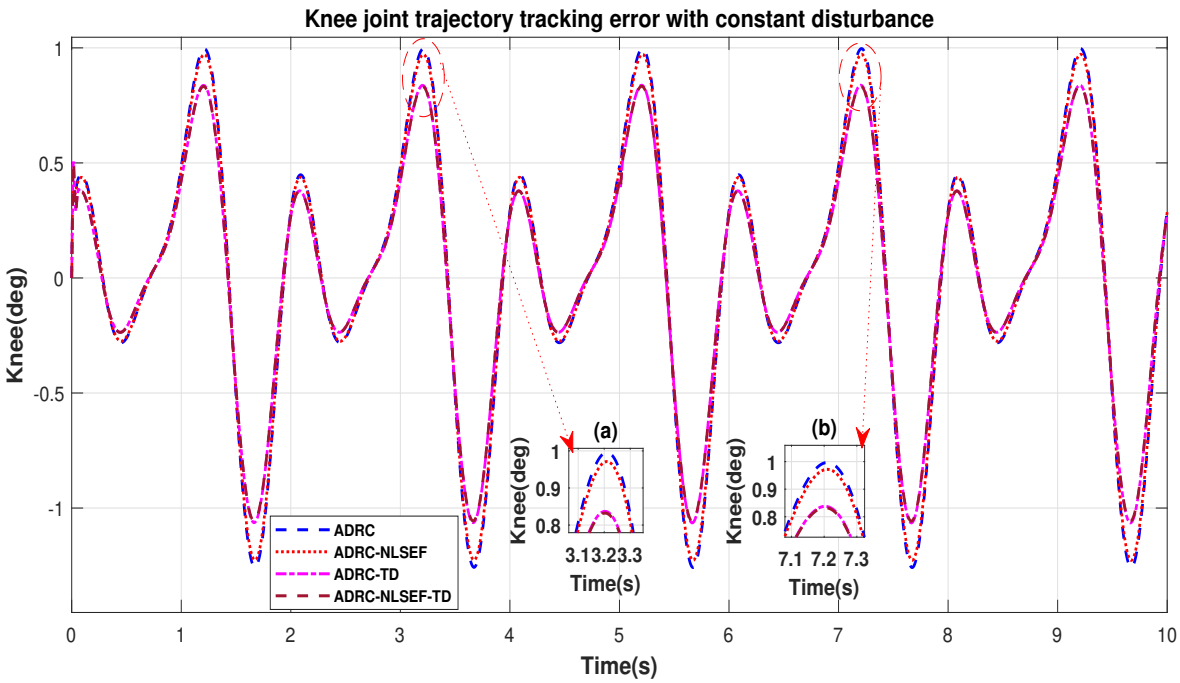

Figure 21. Gait trajectory tracking error comparison of ADRC, ADRC-NLSEF, ADRC-TD, and ADRC-NLSEF-TD for knee joint with a reference with constant disturbance.

Table 8 compares performance indices for ADRC-NLSEF-TD, ADRC-TD, ADRC-NLSEF, and ADRC for the hip joint and the knee joint for the constant disturbance case.

Table 8. Performance indices for ADRC, ADRC-NLSEF, ADRC-TD, and ADRC-NLSEF-TD for the hip joint and the knee joint for the constant disturbance case.

Control Method		**ADRC-NLSEF-TD**		**ADRC-TD**		**ADRC-NLSEF**		**ADRC**	
Joints		**Hip**	**Knee**	**Hip**	**Knee**	**Hip**	**Knee**	**Hip**	**Knee**
Performance indices	ITSE (Deg.)	4.241	13.21	4.252	13.34	5.792	17.96	6.081	18.89
	ISE (Deg.)	0.8446	2.456	0.8466	2.478	1.152	3.334	1.209	3.505
	ITAE (Deg.)	11.85	20.31	11.85	20.37	13.86	23.69	14.19	24.28
	IAE (Deg.)	2.397	3.884	2.398	3.896	2.8	4.527	2.866	4.639
	ISU (N.m.)$\times 10^4$	0.6217	3.167	0.6217	3.167	0.6214	3.166	0.6214	3.166

ITSE, ISE, ITAE, IAE of ADRC-NLSEF-TD had values of 4.241, 0.8446, 11.85, and 2.397 for hip joints and 13.21, 2.456, 20.31, and 3.884 for knee joints, respectively which are minimum as compared to ADRC-TD, ADRC-NLSEF, ADRC. This proves that in terms of trajectory tracking, ADRC-NLSEF-TD has better performance compared to the rest of the controllers. ADRC has ISU 6214 for the hip joint and 3.166×10^4 for the knee joint which is almost the same or a slightly less than ADRC-TD, ADRC-NLSEF, and ADRC-NLSEF-TD.

Case 4: Harmonic Disturbance

In Case 4, the performance of the ADRC is compared with the proposed controllers with addition of harmonic control disturbance of amplitude 5 *N.m. at* t = 5 s. Figures 22 and 23 shows the trajectory tracking performance for various controllers. Figures 24 and 25 show control signal required. Figures 26 and 27 show tracking error for ADRC, ADRC-NLSEF, ADRC-TD, and ADRC-NLSEF-TD for the hip and knee joints with harmonic disturbance.

Figures 22 and 23 show the trajectory tracking performance for various controllers. The minimized plot (a), show the trajectory tracking response of the controllers before the introduction of the harmonic disturbance. Plot (b) show the controller trajectory tracking performance after addition of harmonic disturbance at t = 5 s. The trajectory tracked by ADRC-NLSEF-TD has the best reference tracking followed by ADRC-TD, ADRC-NLSEF, and ADRC before and after inclusion of disturbance at t = 5 s, which proves its effectiveness against harmonic disturbance.

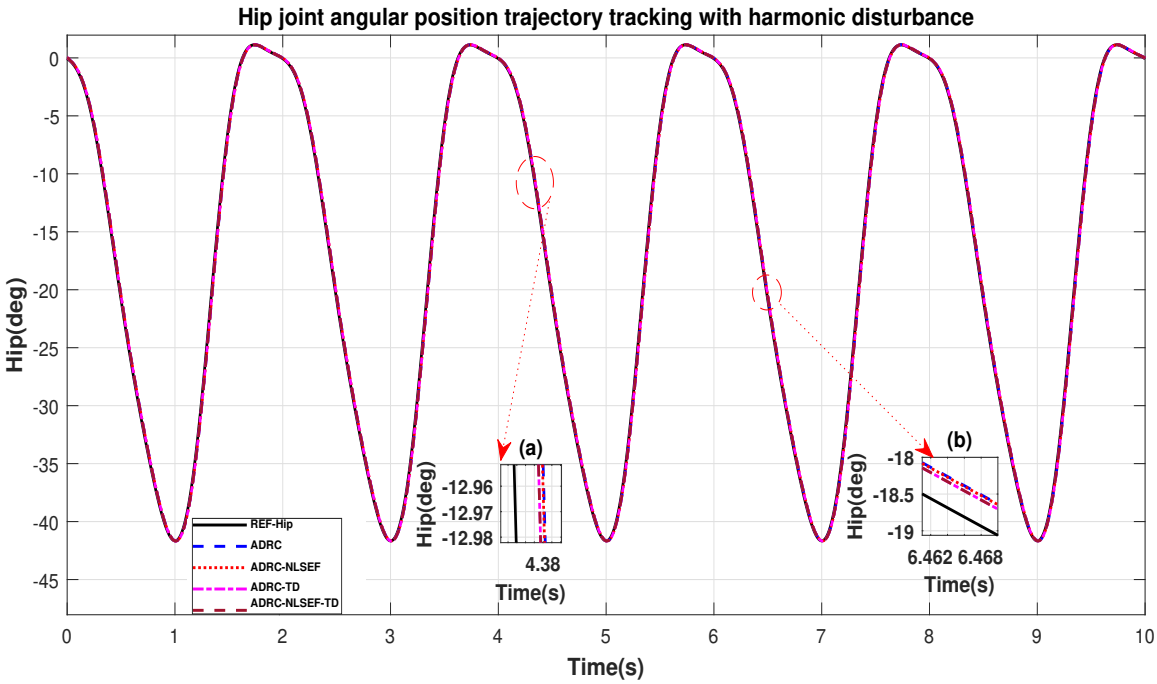

Figure 22. Gait trajectory tracking comparison of ADRC, ADRC-NLSEF, ADRC-TD, and ADRC-NLSEF-TD for the hip joint with a reference with harmonic disturbance.

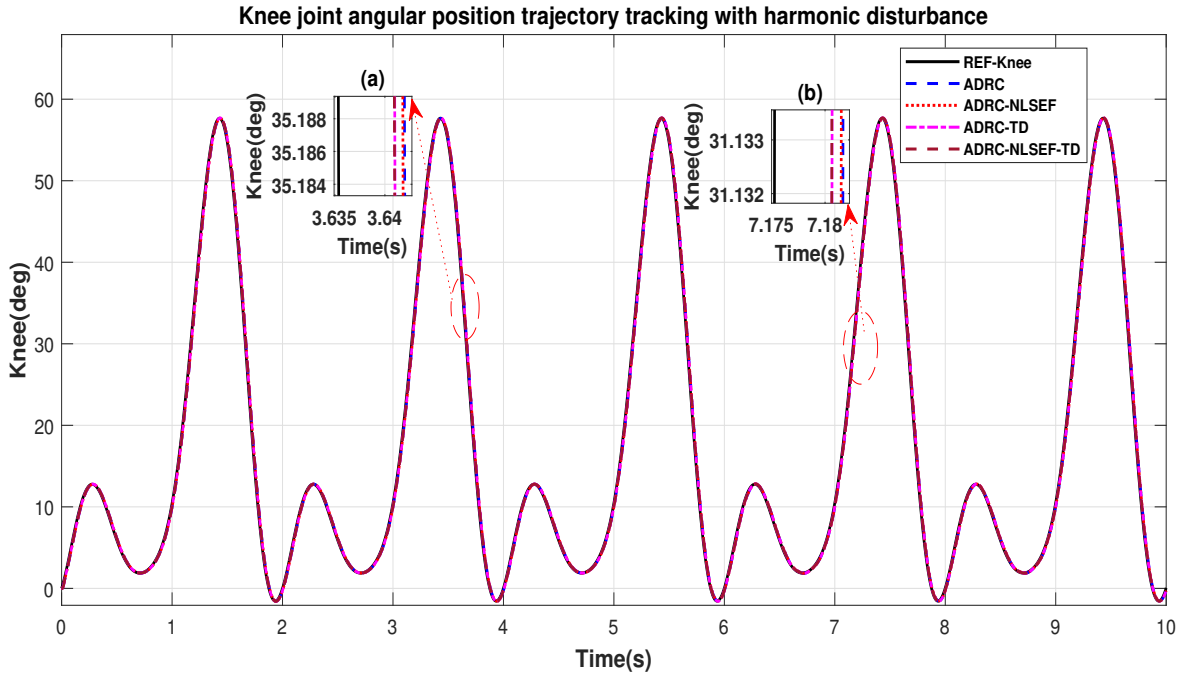

Figure 23. Gait trajectory tracking comparison of ADRC, ADRC-NLSEF, ADRC-TD, and ADRC-NLSEF-TD for the knee joint with a reference with harmonic disturbance.

The initial response of the control signal is shown in the minimized plot (a) and control signal before inclusion of harmonic disturbance in blown up in the minimized plot (b) shown in Figures 24 and 25. Plot (c) and plot (d) show the effect of harmonic disturbance at t = 5 s and after 5 s.

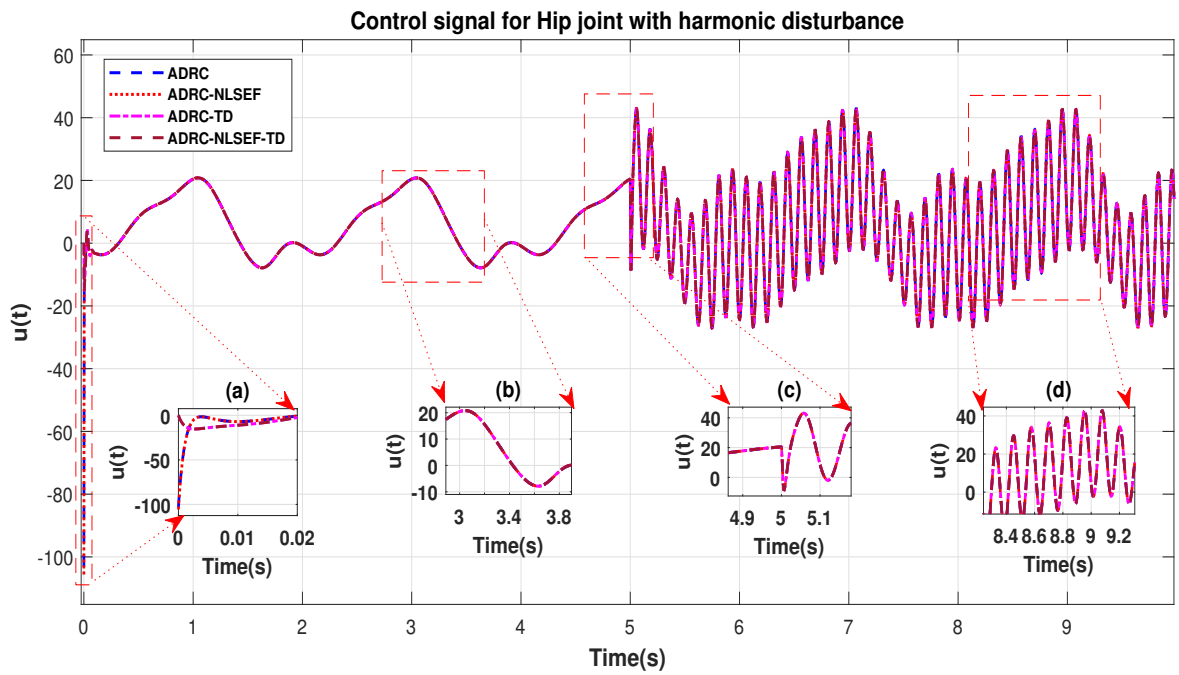

Figure 24. Control signal comparison of ADRC, ADRC-NLSEF, ADRC-TD, and ADRC-NLSEF-TD for the hip joint with harmonic disturbance.

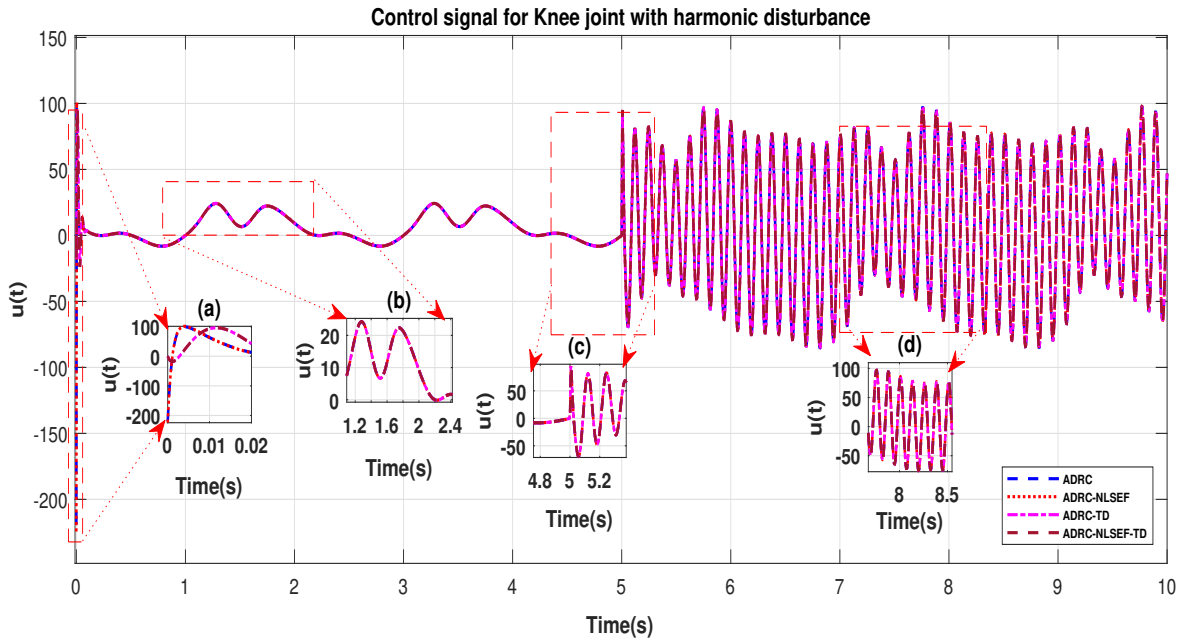

Figure 25. Control signal comparison of ADRC, ADRC-NLSEF, ADRC-TD, and ADRC-NLSEF-TD for the knee joint with harmonic disturbance.

Figures 26 and 27 show the error trajectory generated while reference tracking, the performance of the controller before and after addition of the harmonic disturbance can be seen from the minimized plot (a) and plot (b), concludes the superiority of ADRC-NLSEF-TD over other controllers of trajectory tracking before and after addition of harmonic disturbance.

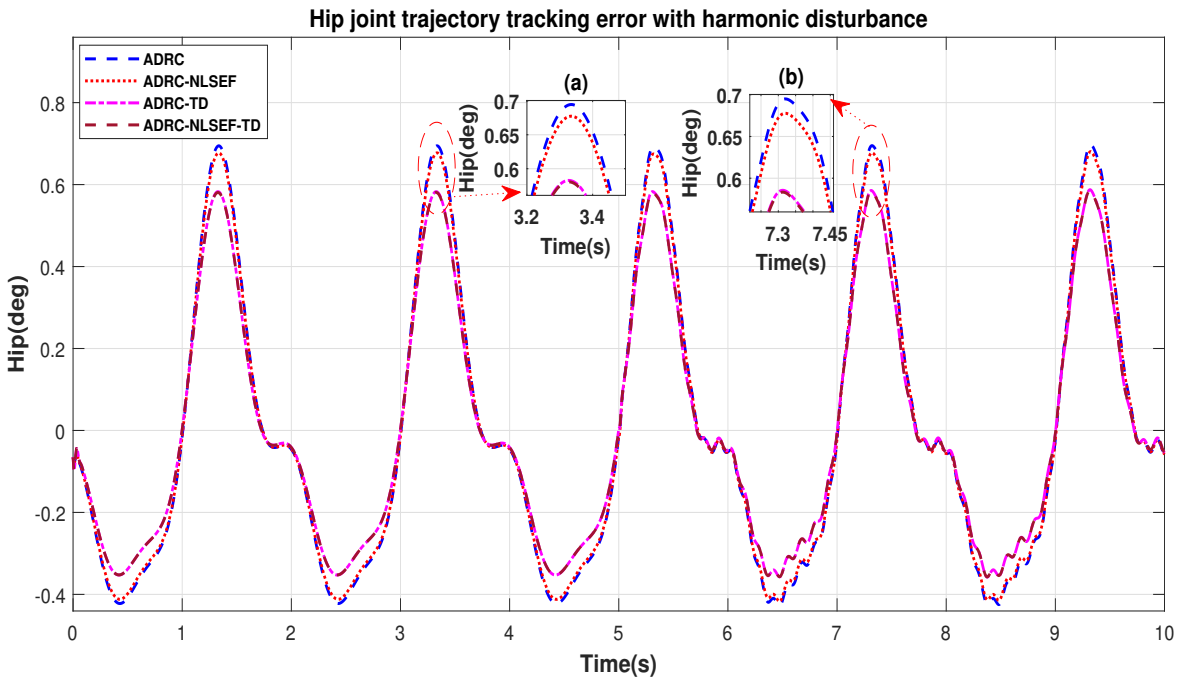

Figure 26. Gait trajectory tracking error comparison of ADRC, ADRC-NLSEF, ADRC-TD, and ADRC-NLSEF-TD for the hip joint with a reference with harmonic disturbance.

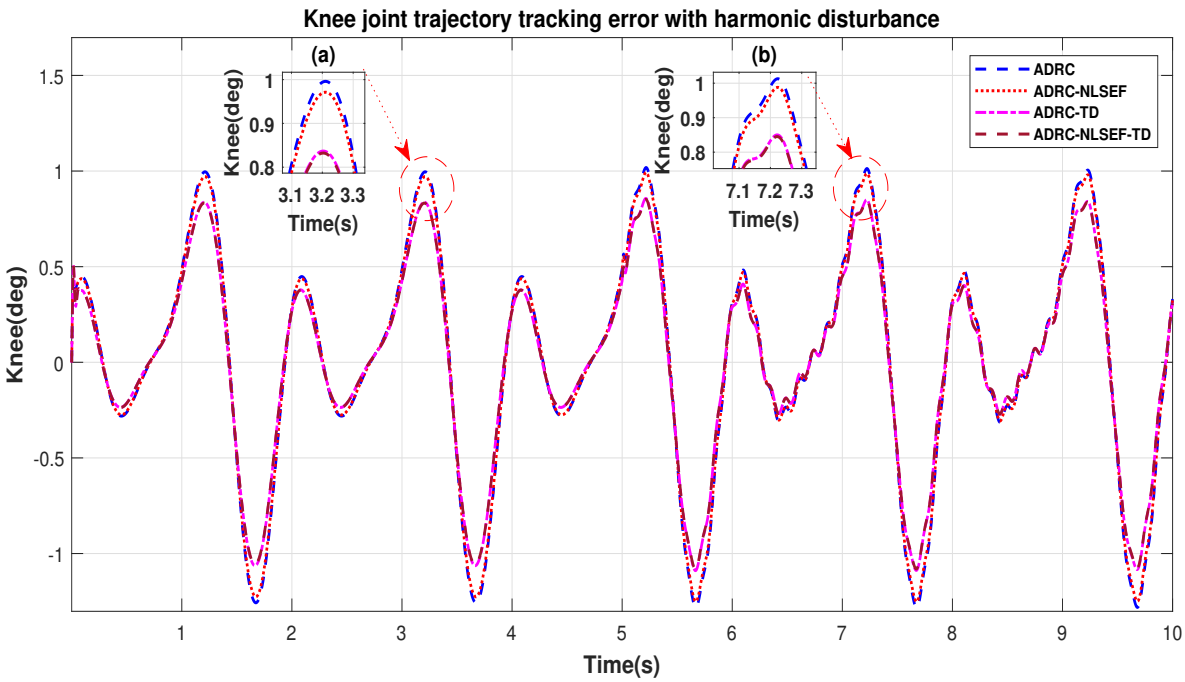

Figure 27. Gait trajectory tracking error comparison of ADRC, ADRC-NLSEF, ADRC-TD, and ADRC-NLSEF-TD for the knee joint with a reference with harmonic disturbance.

The Table 9 compares Performance indices for ADRC-NLSEF-TD, ADRC-TD, ADRC-NLSEF, and ADRC for the hip joint and the knee joint for no disturbance case.

Table 9. Performance indices for ADRC, ADRC-NLSEF, ADRC-TD, and ADRC-NLSEF-TD for the hip joint and the knee joint for harmonic disturbance case.

Control Method		**ADRC-NLSEF-TD**		**ADRC-TD**		**ADRC-NLSEF**		**ADRC**	
Joints		**Hip**	**Knee**	**Hip**	**Knee**	**Hip**	**Knee**	**Hip**	**Knee**
Performance indices	ITSE (Deg.)	4.243	13.22	4.255	13.34	5.795	17.97	6.085	18.89
	ISE (Deg.)	0.845	2.457	0.847	2.48	1.152	3.335	1.21	3.506
	ITAE (Deg.)	11.86	20.35	11.86	20.41	13.87	23.73	14.2	24.32
	IAE (Deg.)	2.399	3.89	2.399	3.902	2.801	4.533	2.867	4.645
	ISU (N.m.)$\times 10^4$	0.3034	2.039	0.3035	2.041	0.3035	2.038	0.3037	2.039

ITSE, ISE, ITAE, IAE of ADRC-NLSEF-TD had values of 4.243, 0.8450, 11.86, and 2.399 for the hip joints and 13.22, 2.457, 20.35, and 3.89 for the knee joints, respectively which are minimum as compared to ADRC-TD, ADRC-NLSEF, ADRC. This proves that In terms of trajectory tracking ADRC-NLSEF-TD has better performance compared to all other controllers. ADRC has ISU 3037 for the hip joint and 2.039×10^4 for the knee joint which is almost the same or a slightly less than ADRC-TD, ADRC-NLSEF, and ADRC-NLSEF-TD.

Overall Comparison of Four Disturbance Cases

Table 10 shows the overall performance of four cases for various combinations such as ADRC, ADRC-NLSEF, ADRC-TD, and ADRC-NLSEF-TD for the hip joint.

Table 10. Overall performance indices the hip joint.

Hip Joint						
Control Method	**Disturbance Case**	**ITSE (Deg.)**	**ISE (Deg.)**	**ITAE (Deg.)**	**IAE (Deg.)**	**ISU (N.m.)$\times 10^4$**
ADRC-NLSEF-TD	Case 1	4.241	0.8447	11.85	2.397	0.1292
	Case 2	4.241	0.8447	11.85	2.397	0.1298
	Case 3	4.241	0.8446	11.85	2.397	0.6217
	Case 4	4.243	0.8450	11.86	2.399	0.3034
ADRC-TD	Case 1	4.253	0.8468	11.85	2.397	0.1292
	Case 2	4.253	0.8468	11.85	2.397	0.1298
	Case 3	4.252	0.8466	11.85	2.398	0.6217
	Case 4	4.255	0.8470	11.86	2.399	0.3035
ADRC-NLSEF	Case 1	5.793	1.152	13.86	2.800	0.1293
	Case 2	5.793	1.152	13.86	2.800	0.1299
	Case 3	5.792	1.152	13.86	2.800	0.6214
	Case 4	5.795	1.152	13.87	2.801	0.3035
ADRC	Case 1	6.083	1.209	14.19	2.866	0.1293
	Case 2	6.082	1.209	14.19	2.866	0.1299
	Case 3	6.081	1.209	14.19	2.866	0.6214
	Case 4	6.085	1.21	14.20	2.867	0.3037

Case1: no disturbance, Case2: random disturbance, Case 3: constant disturbance, Case 4: harmonic disturbance.

Table 11 shows the overall performance of four cases for various combinations such as ADRC, ADRC-NLSEF, ADRC-TD, and ADRC-NLSEF-TD for the knee joint.

Table 11. Overall performance indices for the knee joint.

Knee Joint						
Control Method	**Disturbance Case**	**ITSE (Deg.)**	**ISE (Deg.)**	**ITAE (Deg.)**	**IAE (Deg.)**	**ISU (N.m.)$\times 10^4$**
ADRC-NLSEF-TD	Case 1	13.20	2.454	20.30	3.883	0.1739
	Case 2	13.20	2.454	20.30	3.883	0.1818
	Case 3	13.21	2.456	20.31	3.884	3.167
	Case 4	13.22	2.457	20.35	3.890	2.039
ADRC-TD	Case 1	13.32	2.477	20.36	3.895	0.1738
	Case 2	13.32	2.477	20.36	3.895	0.1817
	Case 3	13.34	2.478	20.37	3.896	3.167
	Case 4	13.34	2.48	20.41	3.902	2.041
ADRC-NLSEF	Case 1	17.95	3.332	23.68	4.526	0.1724
	Case 2	17.95	3.332	23.68	4.526	0.1803
	Case 3	17.96	3.334	22.69	4.527	3.166
	Case 4	17.97	3.335	22.73	4.533	2.038
ADRC	Case 1	18.87	3.503	24.27	4.638	0.1722
	Case 2	18.87	3.503	24.27	4.638	0.1801
	Case 3	18.89	3.505	24.28	4.639	3.166
	Case 4	18.89	3.506	27.32	4.645	2.039

Case1: no disturbance, Case 2: random disturbance, Case 3: constant disturbance, Case 4: harmonic disturbance.

It was observed that there is almost no change in any of the performance indices other than a slight change in ISU, which indicates the increase in control effort. This change is significant in case of constant disturbance when compared to other disturbance cases. Amongst all the controllers ADRC-NLSEF-TD proves a better selection because of its best tracking capabilities followed by ADRC-TD and ADRC-NLSEF, prove it as a promising strategy. The proposed controller ADRC-NLSEF-TD was found to provide a better performance in comparison to only LESO based ADRC i.e., ADRC.

6.2. Effect of Parameter Variation

To demonstrate the efficiency of proposed strategy over conventional LESO based ADRC, ±20% parameter variations are included in this subsection. The parameters are varied from actual values are given in Table 12, g is kept constant as 9.81 m/s^2 following observation are obtained are listed in Tables 13–16.

Table 12. Parameters of the exoskeleton.

Parameter	Symbol	Numerical Value (Actual)	−20% Varied Values	20% Varied Values
Thigh segment	m_h	5 kg	4 Kg	6 kg
length of thigh	l_h	435 mm	348 mm	522 mm
Length of shank	l_k	475 mm	380 mm	570 mm
Shank segment	m_k	2 kg	1.6 kg	2.4 kg

Table 13. Overall performance indices of the hip joint ±20% parameter variation.

Hip Joint											
		ITSE (Deg.)		ISE (Deg.)		ITAE (Deg.)		IAE (Deg.)		ISU (N.m.)×10^4	
Control Method	Disturbance Case	−20%	+20%	−20%	+20%	−20%	+20%	−20%	+20%	−20%	+20%
ADRC-TD-NLSEF	Case 1	4.240	4.242	0.8444	0.8448	11.85	11.85	2.397	2.397	0.1829	0.09875
	Case 2	4.240	4.242	0.8444	0.8448	11.85	11.85	2.397	2.397	0.1850	0.09897
	Case 3	4.238	4.241	0.8441	0.8447	11.85	11.85	2.397	2.398	1.848	0.2869
	Case 4	4.252	4.243	0.846	0.8449	11.88	11.86	2.401	2.398	0.8465	0.1572
ADRC-TD	Case 1	4.251	4.253	0.8464	0.8468	11.85	11.85	2.397	2.398	0.1829	0.09875
	Case 2	4.251	4.253	0.8464	0.8468	11.85	11.85	2.397	2.398	0.1850	0.09897
	Case 3	4.249	4.252	0.8461	0.8467	11.85	11.85	2.397	2.398	1.848	0.2869
	Case 4	4.264	4.254	0.8481	0.847	11.88	11.86	2.401	2.398	0.8470	0.1572
ADRC-NLSEF	Case 1	5.791	5.793	1.152	1.152	13.85	13.86	2.799	2.8	0.1830	0.09894
	Case 2	5.791	5.793	1.152	1.152	13.85	13.86	2.799	2.8	0.1851	0.09916
	Case 3	5.789	5.793	1.151	1.152	13.86	13.86	2.799	2.8	1.848	0.2871
	Case 4	5.803	5.794	1.153	1.152	13.88	13.86	2.803	2.8	0.8467	0.1574
ADRC	Case 1	6.081	6.083	1.209	1.21	14.19	14.19	2.866	2.866	0.1830	0.09892
	Case 2	6.081	6.083	1.209	1.21	14.19	14.19	2.866	2.866	0.1851	0.09914
	Case 3	6.078	6.082	1.209	1.209	14.19	14.19	2.866	2.866	1.848	0.2871
	Case 4	6.093	6.084	1.211	1.21	14.22	14.19	2.87	2.867	0.8472	0.1574

Case1: no disturbance, Case 2: random disturbance, Case 3: constant disturbance, Case 4: harmonic disturbance.

Table 14. Overall performance indices of the knee joint ±20% parameter variation.

Knee Joint											
		ITSE (Deg.)		ISE (Deg.)		ITAE (Deg.)		IAE (Deg.)		ISU (N.m.)×10^4	
Control Method	Distubance Case	−20%	+20%	−20%	+20%	−20%	+20%	−20%	+20%	−20%	+20%
ADRC-TD-NLSEF	Case 1	13.20	13.2	2.456	2.454	20.3	20.3	3.885	3.883	0.2489	0.1362
	Case 2	13.21	13.2	2.456	2.454	20.3	20.3	3.885	3.883	0.2759	0.1392
	Case 3	13.24	13.21	2.459	2.455	20.32	20.3	3.886	3.884	12.76	1.009
	Case 4	13.31	13.21	2.47	2.455	20.44	20.33	3.903	3.888	7.372	0.7600
ADRC-TD	Case 1	13.33	13.32	2.478	2.477	20.37	20.36	3.896	3.895	0.2489	0.1361
	Case 2	13.33	13.32	2.478	2.477	20.37	20.36	3.896	3.895	0.2757	0.1391
	Case 3	13.36	13.33	2.482	2.478	20.39	20.37	3.898	3.895	12.76	1.009
	Case 4	13.44	13.33	2.493	2.478	20.51	20.4	3.916	3.899	7.377	0.7604
ADRC-NLSEF	Case 1	17.96	17.95	3.333	3.332	23.69	23.68	4.527	4.526	0.2475	0.1347
	Case 2	17.96	17.95	3.333	3.332	23.69	23.68	4.527	4.526	0.2744	0.1377
	Case 3	17.99	17.96	3.338	3.333	23.71	23.69	4.529	4.526	12.76	1.008
	Case 4	18.07	17.96	3.348	3.333	23.83	23.72	4.546	4.531	7.372	0.7586
ADRC	Case 1	18.88	18.87	3.504	3.503	24.28	24.27	4.639	4.638	0.2473	0.1345
	Case 2	18.88	18.87	3.504	3.503	24.27	24.27	4.639	4.638	0.2741	0.1375
	Case 3	18.92	18.88	3.509	3.504	24.29	24.27	4.461	4.638	12.76	1.007
	Case 4	18.99	18.88	3.52	3.504	24.42	24.31	4.658	4.642	7.376	0.7588

Case1: no disturbance, Case 2: random disturbance, Case 3: constant disturbance, Case 4: harmonic disturbance.

Table 15. Overall performance indices of the hip joint +20% parameter variation and under influence of noise.

Hip Joint						
Control Method	**Disturbance Case**	**ITSE (Deg.)**	**ISE (Deg.)**	**ITAE (Deg.)**	**IAE (Deg.)**	**ISU (N.m) $\times 10^4$**
ADRC-TD-NLSEF	Case 1	4.244	0.8461	11.87	2.404	0.7248
	Case 2	4.244	0.8461	11.87	2.404	0.7277
	Case 3	4.243	0.8460	11.87	2.404	0.9132
	Case 4	4.245	0.8462	11.87	2.404	0.7802
ADRC-TD	Case 1	4.256	0.8482	11.87	2.404	0.7252
	Case 2	4.256	0.8482	11.87	2.404	0.7281
	Case 3	4.255	0.8481	11.87	2.404	0.9135
	Case 4	4.257	0.8483	11.87	2.405	0.7806
ADRC-NLSEF	Case 1	5.796	1.153	13.87	2.805	0.7239
	Case 2	5.796	1.153	13.87	2.805	0.7269
	Case 3	5..795	1.153	13.87	2.805	0.9123
	Case 4	5.797	1.153	13.88	2.805	0.7794
ADRC	Case 1	144	25.03	67.94	12.69	9.914
	Case 2	150.7	25.79	68.39	12.73	9.906
	Case 3	380.5	56.62	110.5	18.38	9.914
	Case 4	173.9	29.17	73.35	13.48	9.912

Case1: no disturbance, Case 2: random disturbance, Case 3: constant disturbance, Case 4: harmonic disturbance.

Table 16. Overall performance indices of the Knee joint +20% parameter variation and under influence of noise.

Knee Joint						
Control Method	**Disturbance Case**	**ITSE (Deg.)**	**ISE (Deg.)**	**ITAE (Deg.)**	**IAE (Deg.)**	**ISU (N.m) $\times 10^4$**
ADRC-TD-NLSEF	Case 1	13.20	2.464	20.31	3.894	0.8040
	Case 2	13.20	2.464	20.31	3.894	0.8240
	Case 3	13.21	2.465	20.32	3.894	1.659
	Case 4	13.21	2.465	20.34	3.898	1.44
ADRC-TD	Case 1	13.32	2.486	20.38	3.905	0.8031
	Case 2	13.33	2.486	20.38	3.905	0.8230
	Case 3	13.33	2.487	20.38	3.906	1.658
	Case 4	13.34	2.488	20.41	3.910	1.439
ADRC-NLSEF	Case 1	17.95	3.338	23.70	4.535	0.7989
	Case 2	17.95	3.338	23.70	4.535	0.8189
	Case 3	17.96	3.339	23.71	4.536	1.655
	Case 4	17.96	3.340	23.73	4.540	1.434
ADRC	Case 1	734.7	121.7	146.4	27.1	9.716
	Case 2	776.1	126.3	149.3	27.4	9.730
	Case 3	2149	308.7	253	41.37	9.742
	Case 4	873.6	140.7	157.2	28.78	9.742

Case1: no disturbance, Case 2: random disturbance, Case 3: constant disturbance, Case 4: harmonic disturbance.

The model parameters are varied with ±20% variations. The results are obtained for the gait trajectory tracking for the hip and knee joints, based on the performance indices. It can be concluded from the above results that the proposed control method performs superior and tracks the trajectory efficiently as compared to ADRC even with parameter variation the only change in the ISU occurs which defines the control effort, it is observed that the control effort with decreases with +20% variation and increases with −20% parametric variation.

6.3. Effect of Noise

The sinusoidal noise of -0.5° to 0.5° variance is incorporated with the +20% parameter variation and under the influence of various disturbance to demonstrate the efficacy of proposed controller with actuator saturation. Generally, the larger the observer bandwidth is, the more accurate the estimation

will be. However, a large observer bandwidth will increase noise sensitivity. Therefore, a proper observer bandwidth should be selected in a compromise between the tracking performance and noise tolerance. The performance under noise is tested with four disturbance cases and analyzed based on the performance indices.

Case 1: No Disturbance

In Case 1, the performance of the ADRC is compared with the proposed controllers with the only effect of noise and +20% parametric variation without the addition of external control disturbance. Figures 28 and 29 shows the trajectory tracking performance of mentioned controllers for the hip and knee joints. Figures 30 and 31 show control signal required, and Figures 32 and 33 show trajectory tracking error for ADRC, ADRC-NLSEF, ADRC-TD, and ADRC-NLSEF-TD for the hip and knee joints. Figures 28 and 29 show the trajectory tracking performance of the controllers in no disturbance case. The trajectory tracked by ADRC-NLSEF-TD has best reference tracking followed by ADRC-TD, ADRC-NLSEF, and ADRC in no disturbance case which can be seen from the minimized plot (a), (b), (c), and (d) in both the figures.

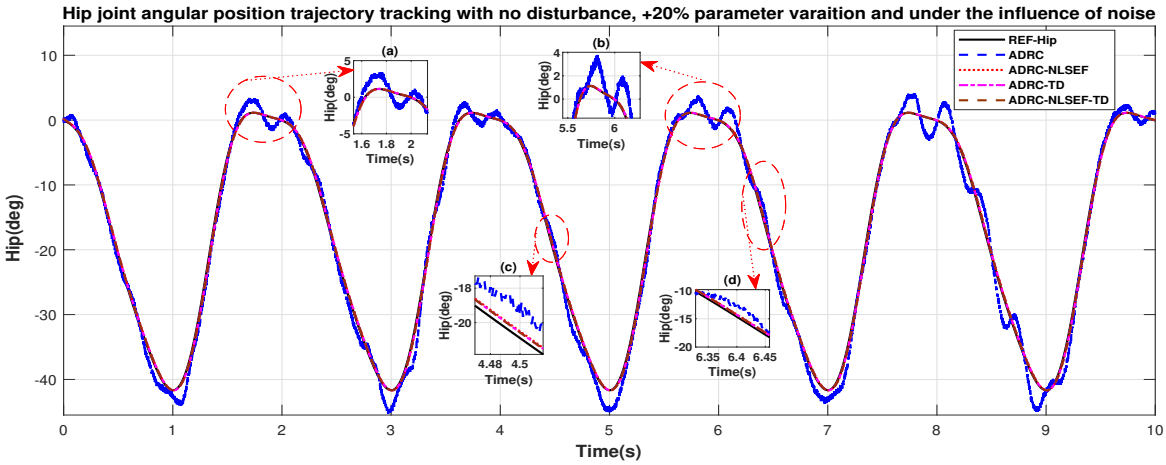

Figure 28. Gait trajectory tracking comparison of ADRC, ADRC-NLSEF, ADRC-TD, and ADRC-NLSEF-TD for the hip joint under the influence of noise, with parameter variation and without disturbance effect.

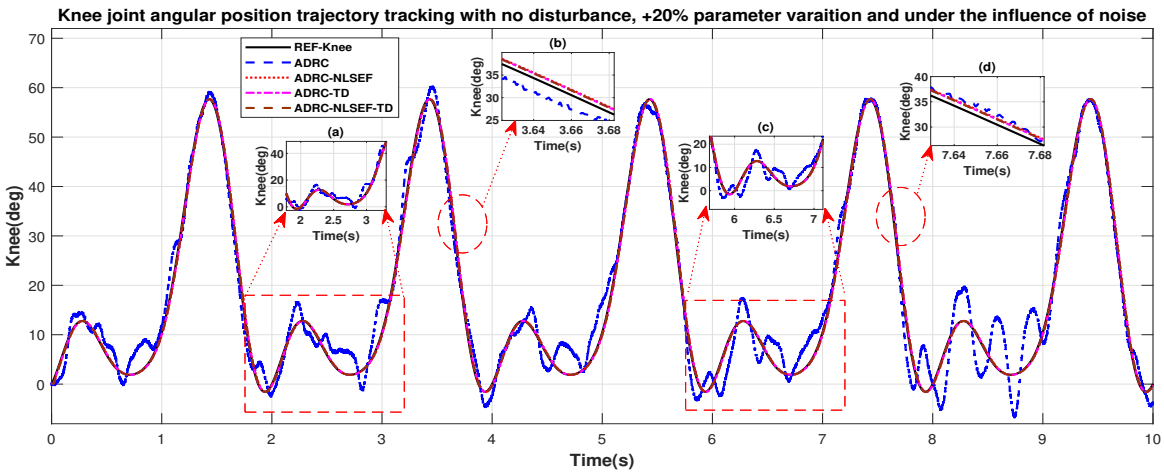

Figure 29. Gait trajectory tracking comparison of ADRC, ADRC-NLSEF, ADRC-TD, and ADRC-NLSEF-TD for the knee joint under the influence of noise, with parameter variation and without disturbance effect.

The initial response of the control signal is shown in the minimized plot (a) and control signal in blown up in the minimized plot (b) shown in Figures 30 and 31, gives us the idea of control signal required by the controllers. The control signal for ADRC completely saturates whereas in the proposed controlled methods it firstly saturates for a while and maintains its safe limit.

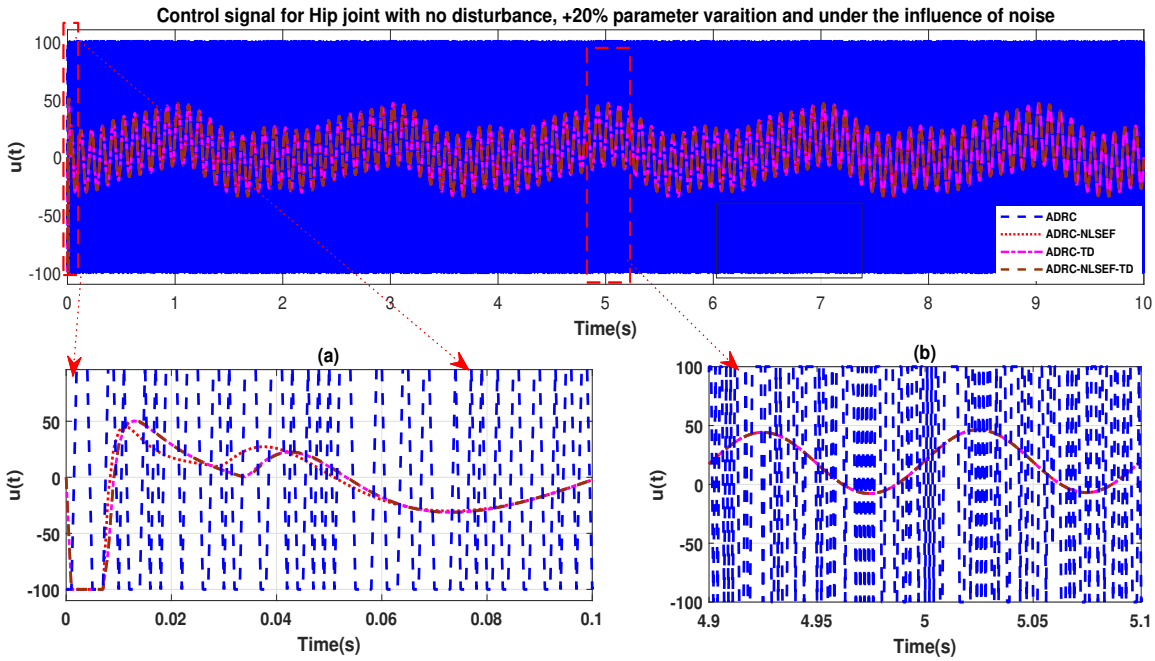

Figure 30. Control signal trajectory tracking comparison of ADRC, ADRC-NLSEF, ADRC-TD, and ADRC-NLSEF-TD for the hip joint under the influence of noise, with parameter variation and without disturbance effect.

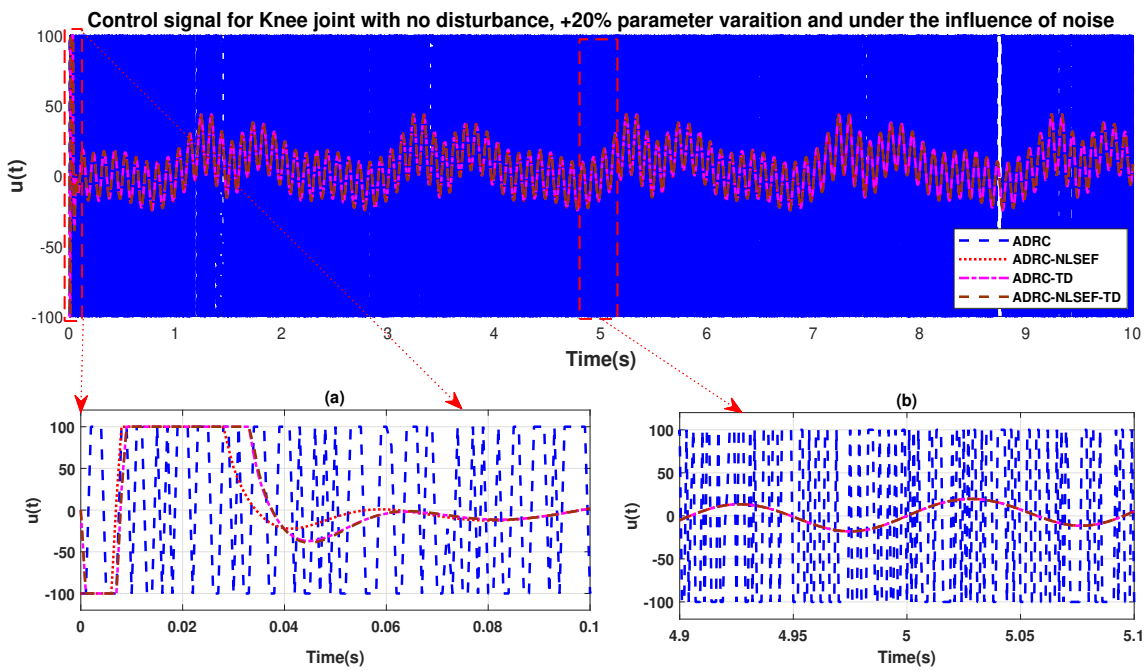

Figure 31. Control signal trajectory tracking comparison of ADRC, ADRC-NLSEF, ADRC-TD, and ADRC-NLSEF-TD for the knee joint under the influence of noise, with parameter variation and without disturbance effect.

Figures 32 and 33 show error while trajectory tracking under the influence of noise, with parameter variation and without disturbance effect. ADRC-NLSEF-TD outperforms all other controllers in terms of trajectory tracking followed by ADRC-TD, ADRC-NLSEF, and ADRC.

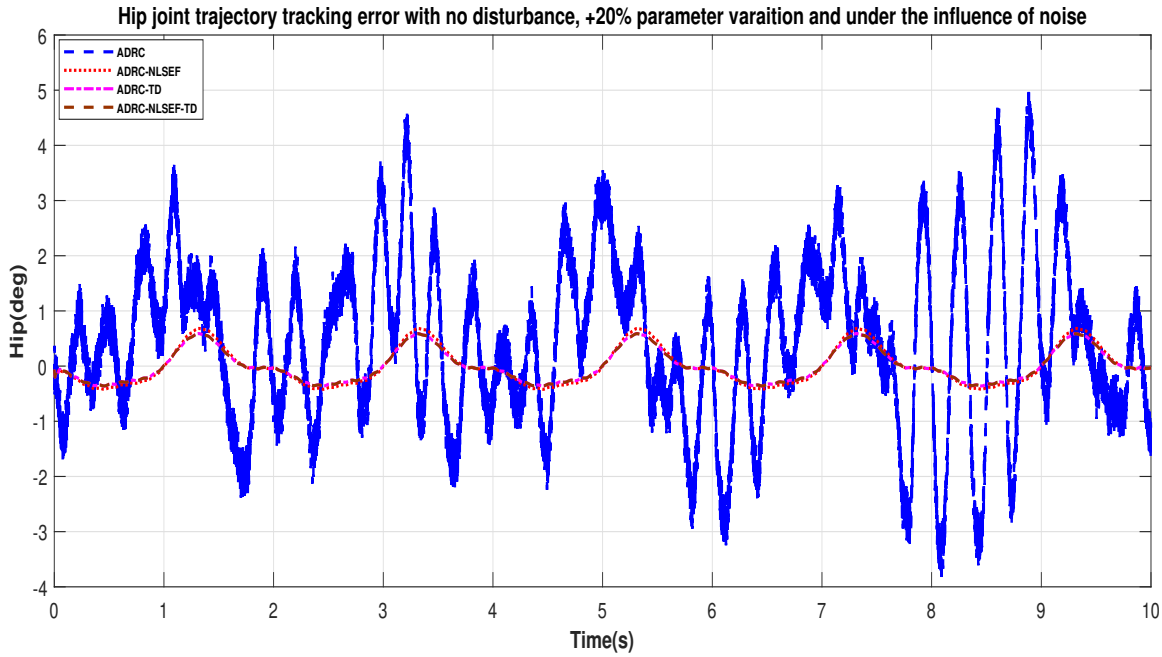

Figure 32. Gait trajectory tracking error comparison of ADRC, ADRC-NLSEF, ADRC-TD, and ADRC-NLSEF-TD for the hip joint under the influence of noise, with parameter variation and without disturbance effect.

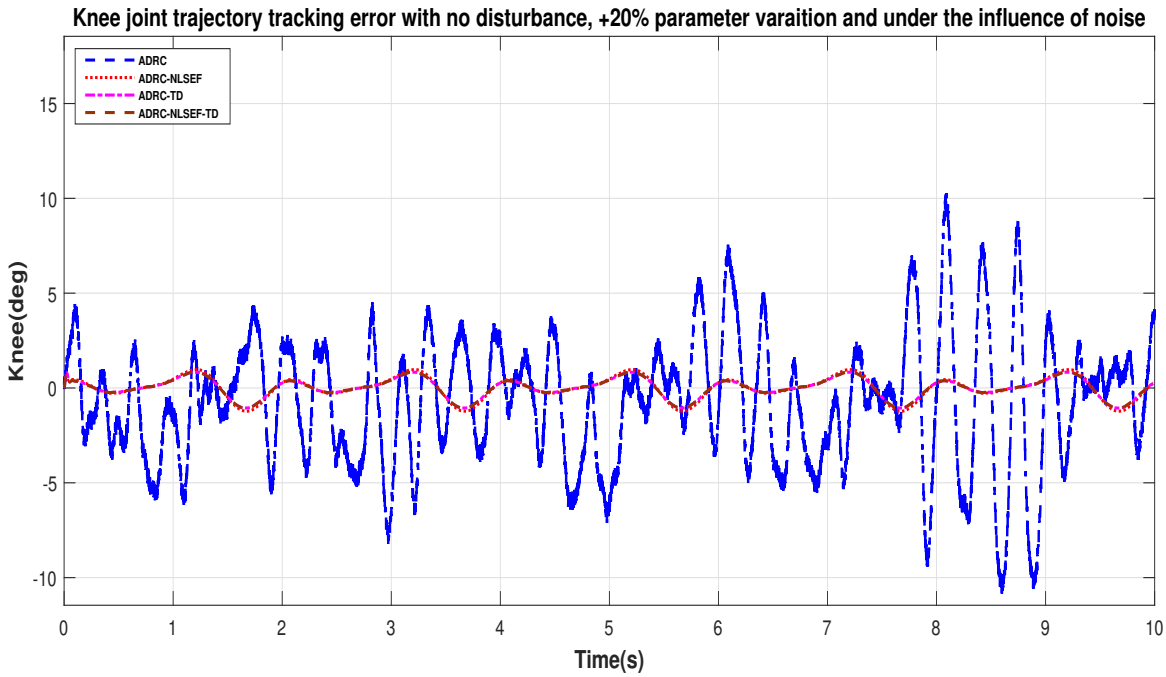

Figure 33. Gait trajectory tracking error comparison of ADRC, ADRC-NLSEF, ADRC-TD, and ADRC-NLSEF-TD for the knee joint under the influence of noise, with parameter variation and without disturbance effect.

Case 2: Random Disturbance

In Case 2, the performance of the ADRC is compared with the proposed controllers under the influence of noise, parametric variation of and with the addition of random control disturbance (between −1 and 1) *N.m.* The sampling time is 0.001 s. *N.m.* at t = 5 s. Figures 34 and 35 show the trajectory tracking performance of mentioned controllers for the hip and knee joints. Figures 36 and 37 show the control signal required and, Figures 38 and 39 show the trajectory tracking error or ADRC, ADRC-NLSEF, ADRC-TD, and ADRC-NLSEF-TD for the hip and knee joints.

Figures 34 and 35 show the trajectory tracking performance for various controllers. The minimized plot (a) and plot (b) show the trajectory tracking response of the controllers before the introduction of the random disturbance. Plot (c) and plot (d) show the controller trajectory tracking performance after addition of random disturbance at t = 5 s. The trajectory tracked by ADRC-NLSEF-TD has the best reference tracking followed by ADRC-TD, ADRC-NLSEF, and ADRC before and after inclusion of disturbance at t = 5 s, which prove its effectiveness under the influence of noise, parametric variation, and against random disturbance.

The initial response of the control signal is shown in the minimized plot (a) and control signal in blown up in the minimized plot (b) shown in Figures 36 and 37, gives us the idea of control signal required by the controllers. The control signal for ADRC completely saturates whereas in the proposed controlled methods it firstly saturates for a while and maintains its safe limit. Plot (b) show the effect of random disturbance at t = 5 s and after 5 s.

Figures 38 and 39 show the error trajectory generated while reference tracking, the performance of the controller before and after addition of the random disturbance, concludes the superiority of ADRC-NLSEF-TD over other controllers of trajectory tracking before and after addition of random disturbance, under the influence of noise and with parameter variation.

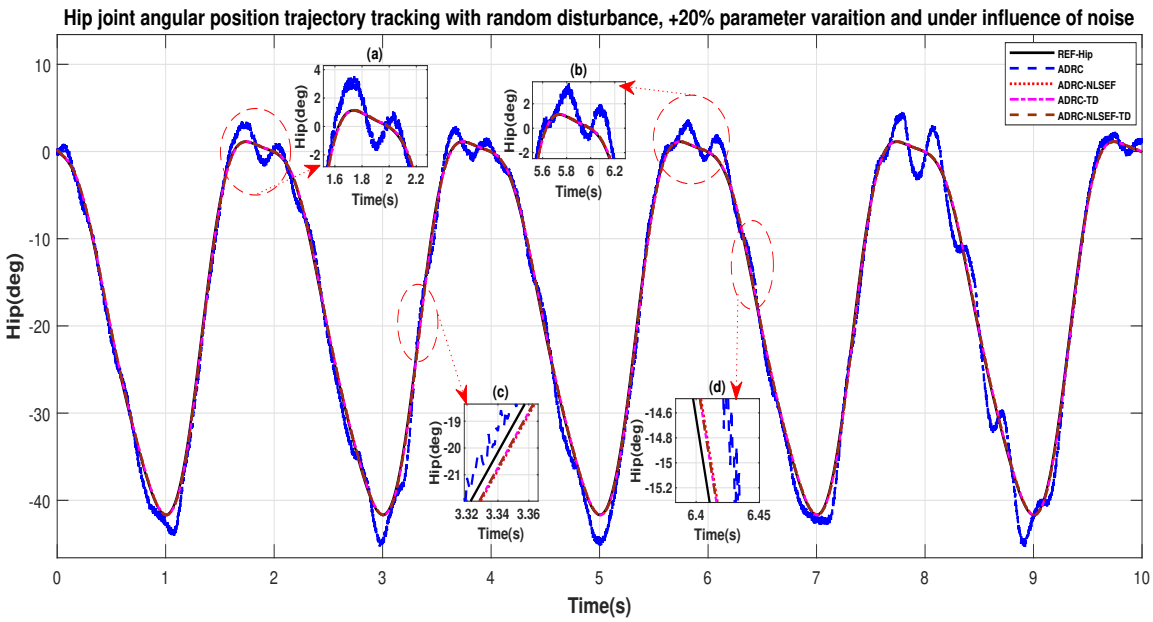

Figure 34. Gait trajectory tracking comparison of ADRC, ADRC-NLSEF, ADRC-TD, and ADRC-NLSEF-TD for the hip joint under the influence of noise, with parameter variation and with random disturbance effect.

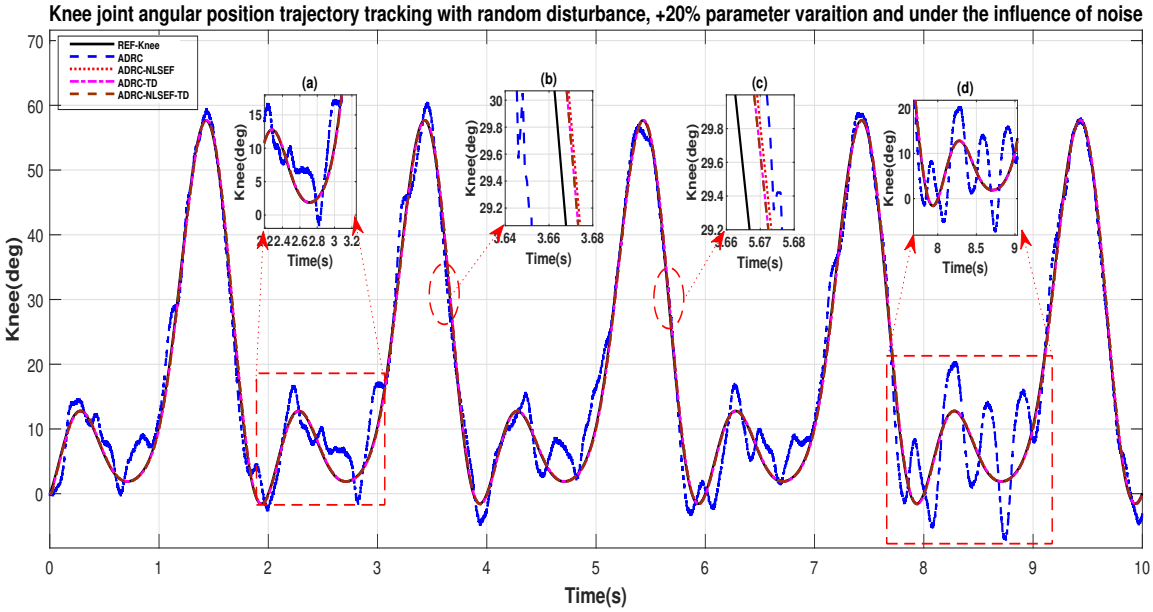

Figure 35. Gait trajectory tracking comparison of ADRC, ADRC-NLSEF, ADRC-TD, and ADRC-NLSEF-TD for the knee joint under the influence of noise, with parameter variation and with random disturbance effect.

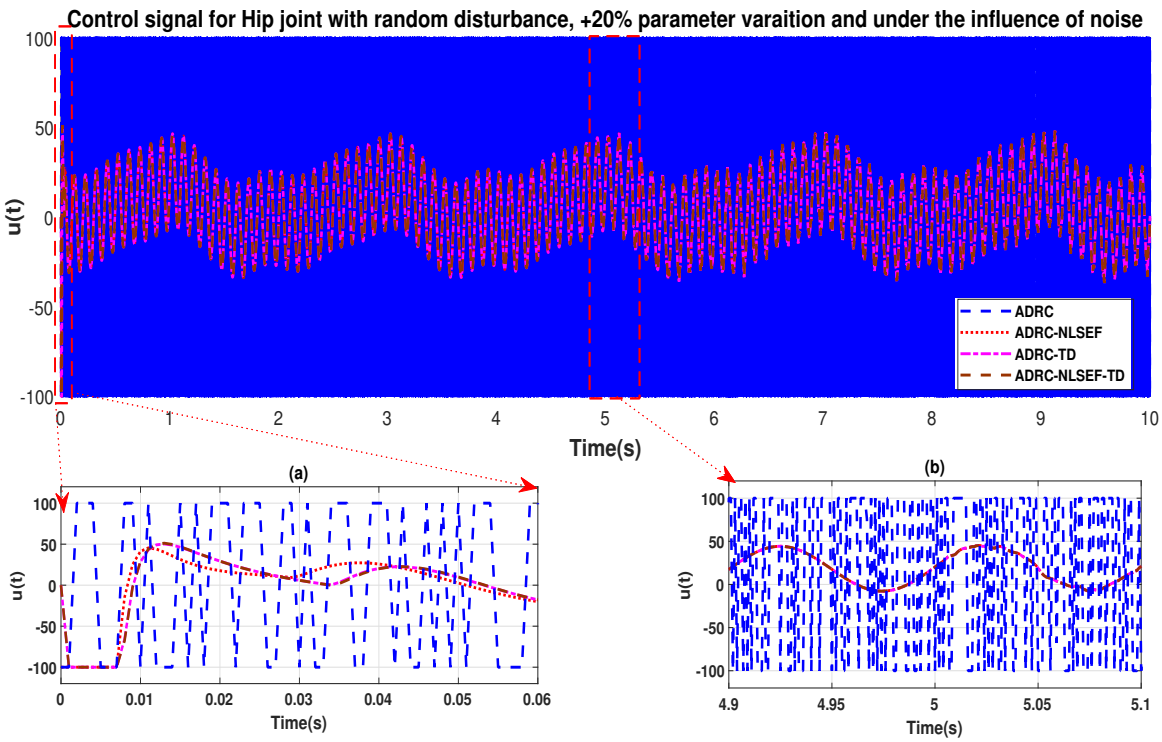

Figure 36. Control signal trajectory tracking comparison of ADRC, ADRC-NLSEF, ADRC-TD, and ADRC-NLSEF-TD for the knee joint under the influence of noise, with parameter variation and with random disturbance effect.

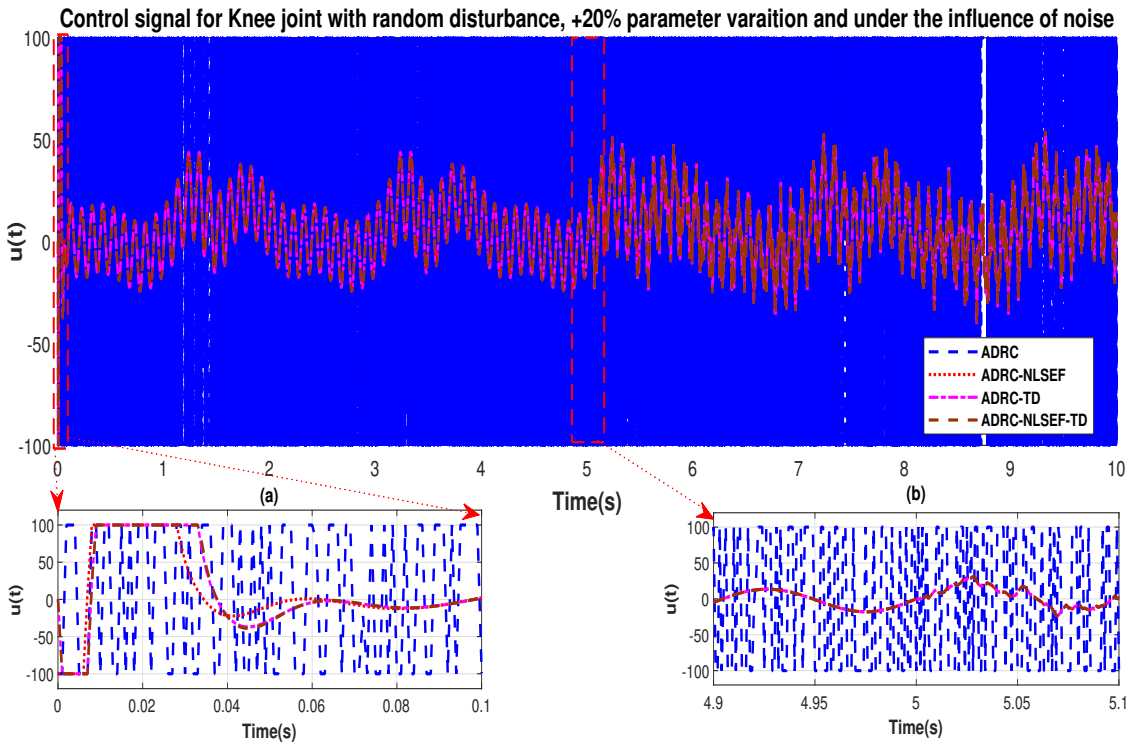

Figure 37. Control signal trajectory tracking comparison of ADRC, ADRC-NLSEF, ADRC-TD, and ADRC-NLSEF-TD for the knee joint under the influence of noise, with parameter variation and with random disturbance effect.

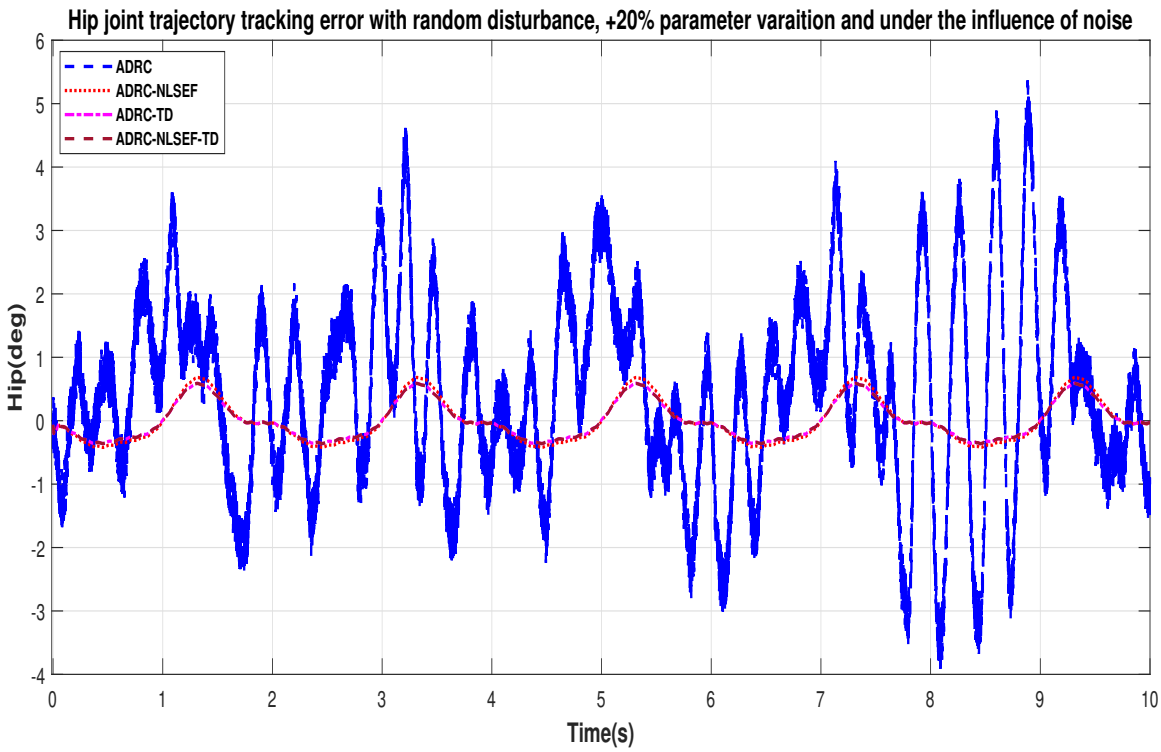

Figure 38. Gait trajectory tracking error comparison of ADRC, ADRC-NLSEF, ADRC-TD, and ADRC-NLSEF-TD for the hip joint under the influence of noise, with parameter variation and with random disturbance effect.

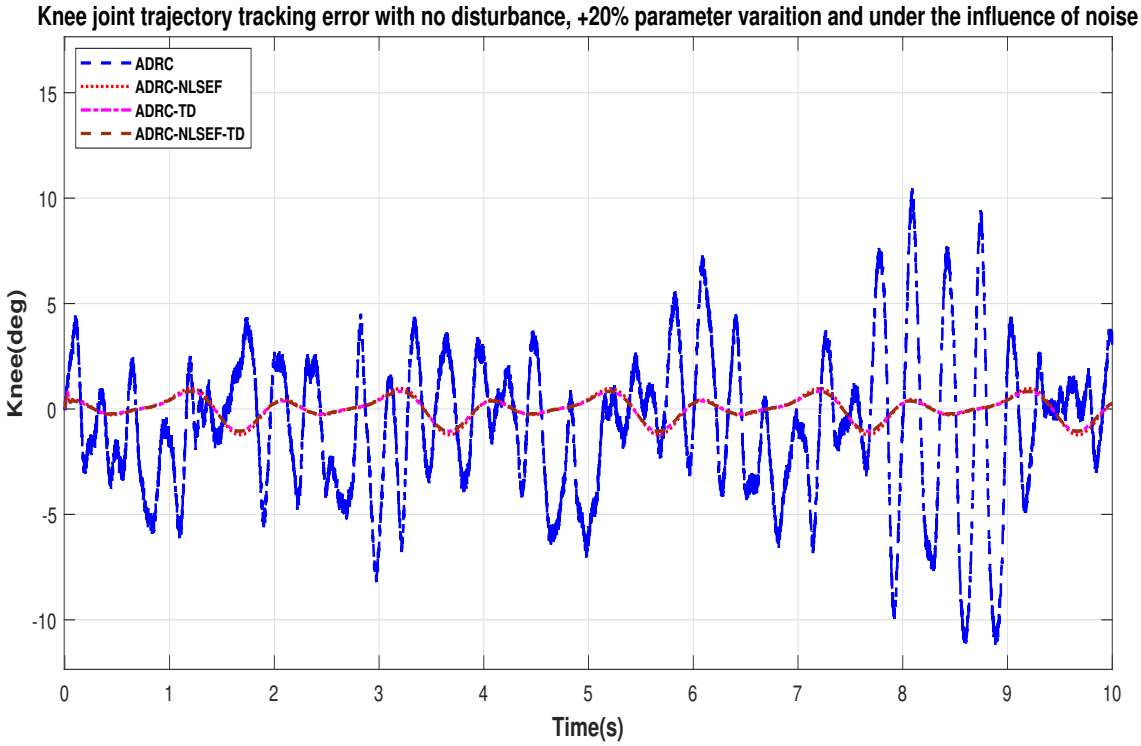

Figure 39. Gait trajectory tracking error comparison of ADRC, ADRC-NLSEF, ADRC-TD, and ADRC-NLSEF-TD for the hip joint under the influence of noise, with parameter variation and with random disturbance effect.

Case 3: Constant Disturbance

In Case 3, the performance of the ADRC is compared with the proposed controllers under the influence of noise, with parametric variation and with addition of constant control disturbance of amplitude *5 N.m.* at t = 5 s. Figures 40 and 41 show the trajectory tracking performance for various controllers for the hip and knee joints. Figures 42 and 43 show the control signal required. Figures 44 and 45 show tracking error for ADRC, ADRC-NLSEF, ADRC-TD, and ADRC-NLSEF-TD for the hip and knee joints with constant disturbance.

Figures 40 and 41 show the trajectory tracking performance for various controllers. The minimized plot (a) and plot (b), show the trajectory tracking response of the controllers before the introduction of the constant disturbance. Plot (c) and plot (d) show the controller trajectory tracking performance after addition of constant disturbance at t = 5 s. The trajectory tracked by ADRC-NLSEF-TD has best reference tracking followed by ADRC-TD, ADRC-NLSEF, and ADRC before and after inclusion of disturbance at t = 5 s, which proves its effectiveness under the influence of noise, parametric variation and against constant disturbance.

The initial response of the control signal is shown in the minimized plot (a) and control signal in blown up in the minimized plot (b) shown in Figures 42 and 43, gives us the idea of control signal required by the controllers. The control signal for ADRC completely saturates whereas in the proposed controlled methods it firstly saturates for a while and maintains its safe limit. Plot (b) show the effect of constant disturbance at t = 5 s and after 5 s.

Figures 44 and 45 show the error trajectory generated while reference tracking, the performance of the controller before and after addition of the constant disturbance, concludes the superiority of ADRC-NLSEF-TD over other controllers of trajectory tracking before and after addition of constant disturbance, under the influence of noise, with parameter variation.

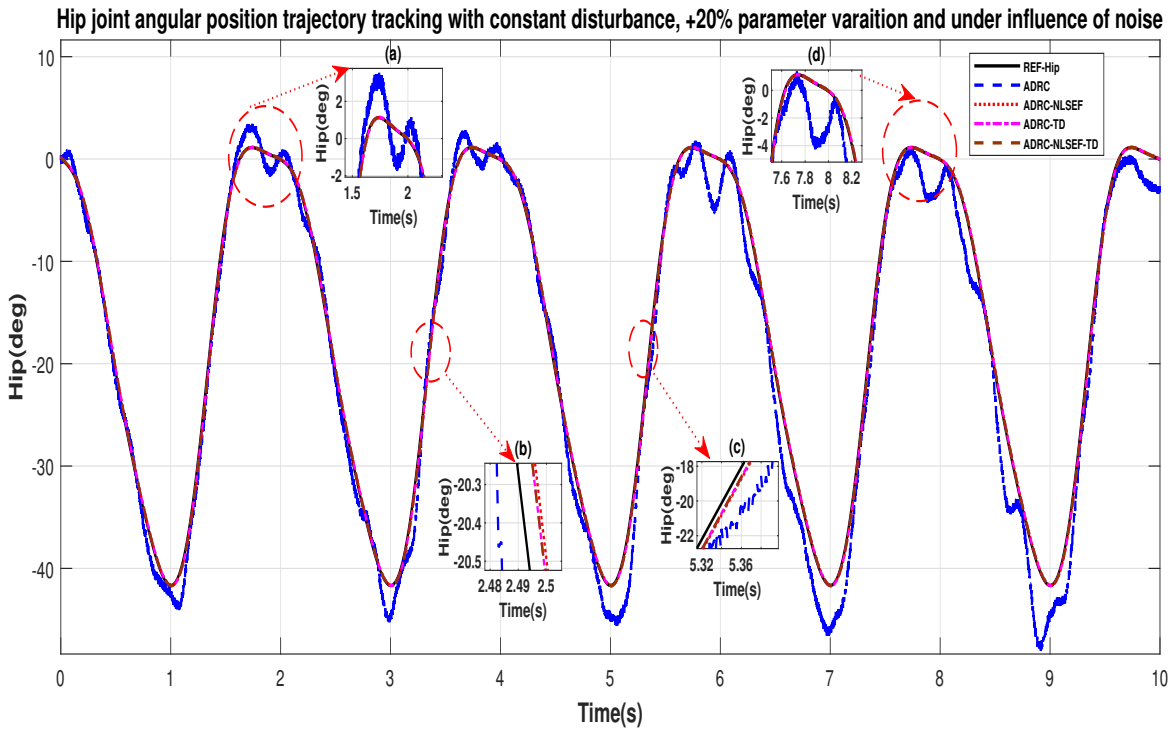

Figure 40. Gait trajectory tracking comparison of ADRC, ADRC-NLSEF, ADRC-TD, and ADRC-NLSEF-TD for knee joint under the influence of noise, with parameter variation and with constant disturbance effect.

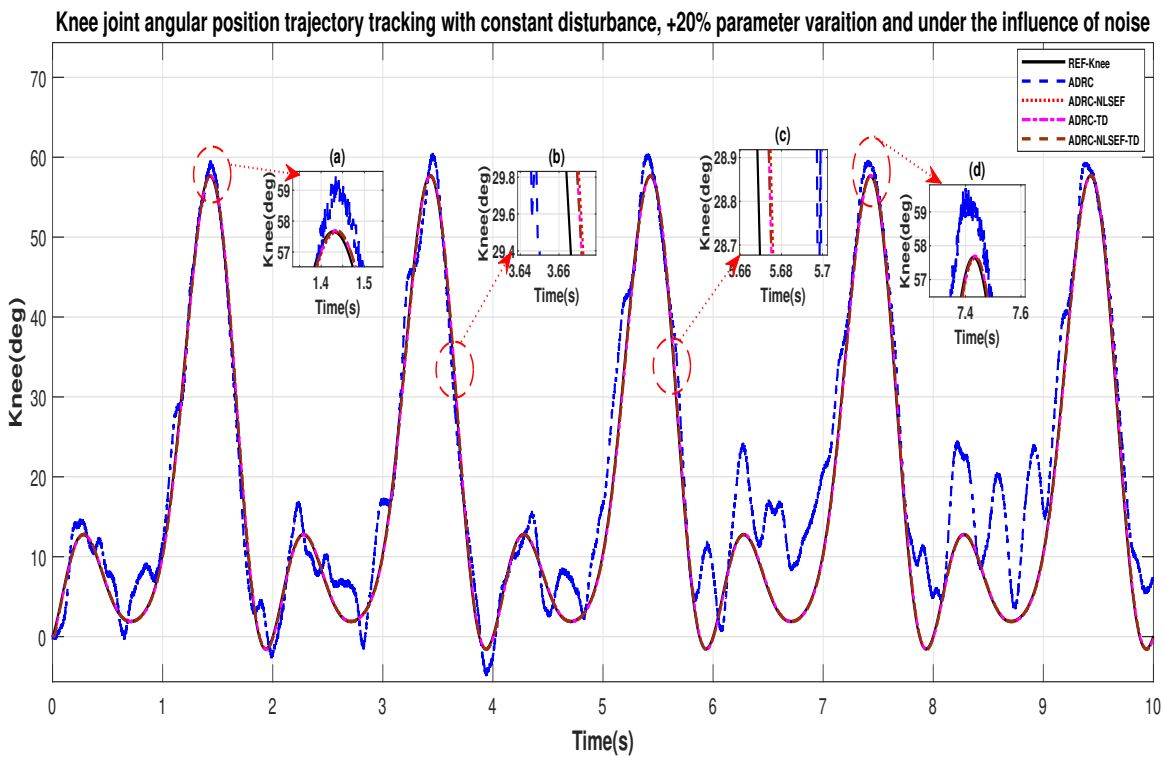

Figure 41. Gait trajectory tracking comparison of ADRC, ADRC-NLSEF, ADRC-TD, and ADRC-NLSEF-TD for the knee joint under the influence of noise, with parameter variation and with constant disturbance effect.

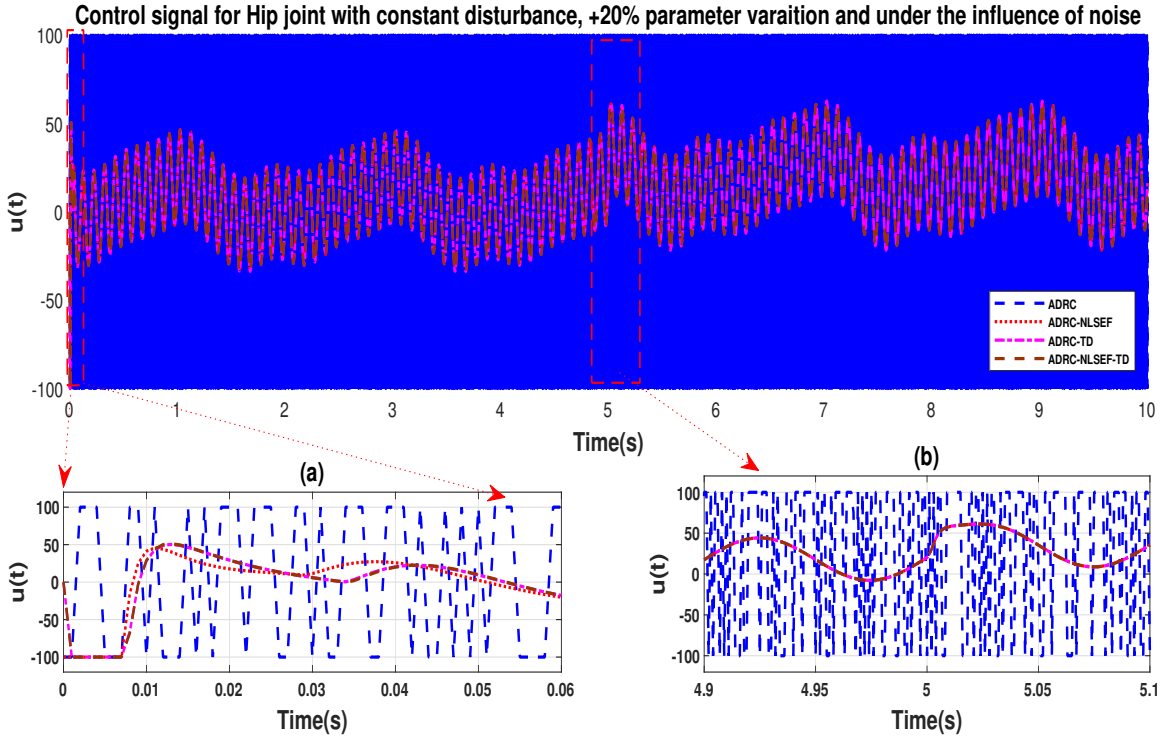

Figure 42. Control signal trajectory tracking comparison of ADRC, ADRC-NLSEF, ADRC-TD, and ADRC-NLSEF-TD for the knee joint under the influence of noise, with parameter variation and with constant disturbance effect.

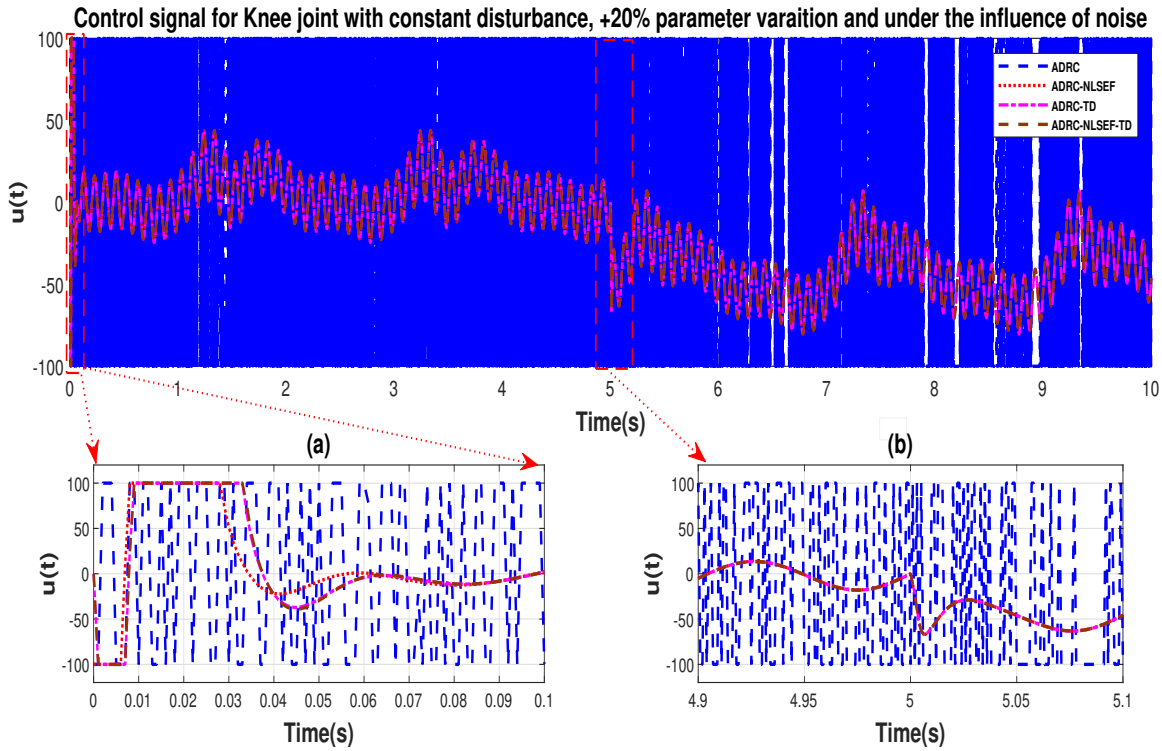

Figure 43. Control signal trajectory tracking comparison of ADRC, ADRC-NLSEF, ADRC-TD, and ADRC-NLSEF-TD for the knee joint under the influence of noise, with parameter variation and with constant disturbance effect.

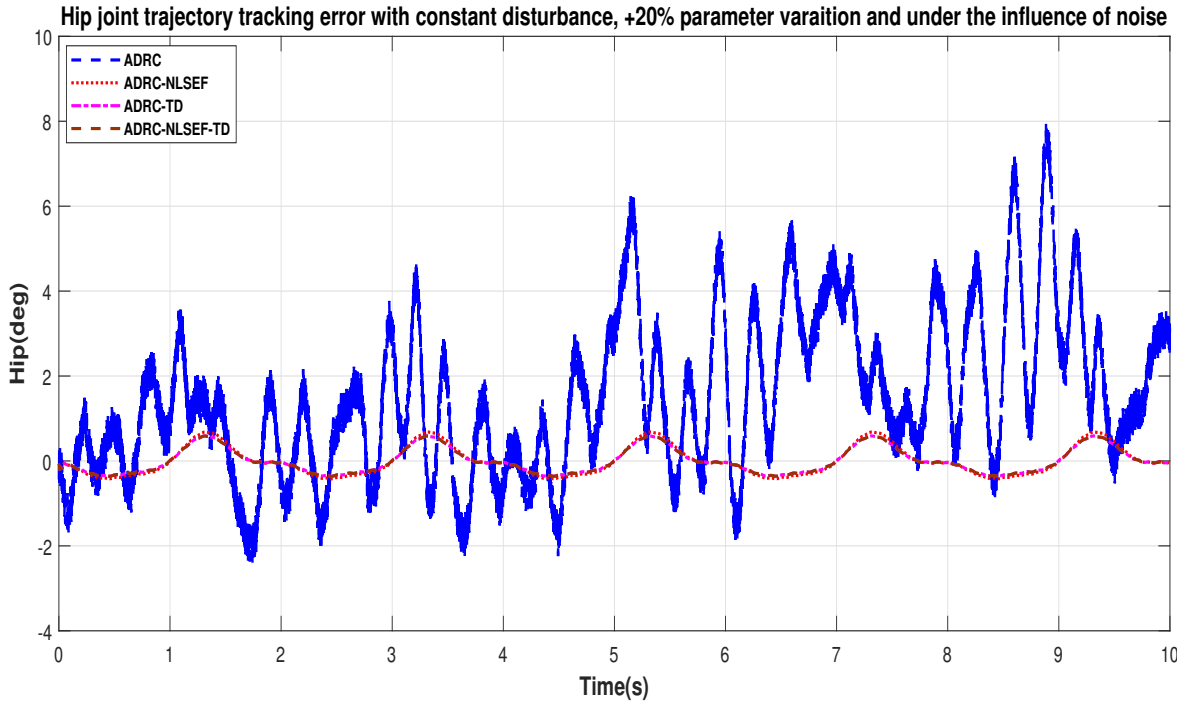

Figure 44. Gait trajectory tracking error comparison of ADRC, ADRC-NLSEF, ADRC-TD, and ADRC-NLSEF-TD for hip joint under the influence of noise, with parameter variation and with constant disturbance effect.

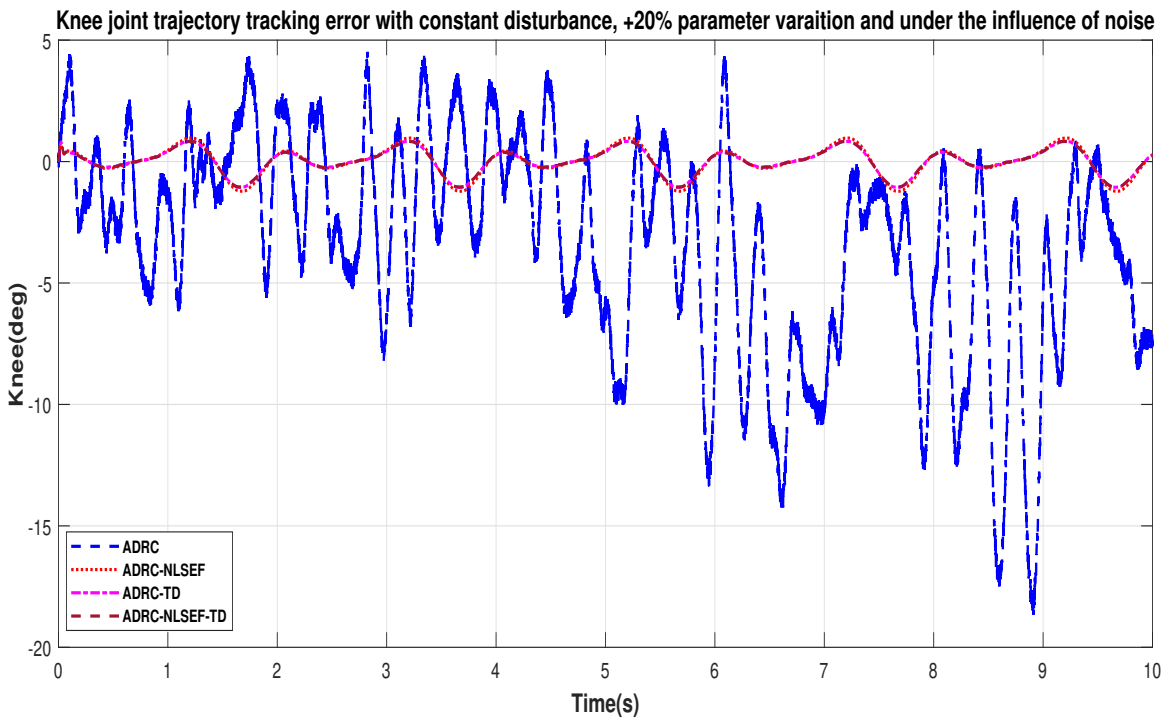

Figure 45. Gait trajectory tracking error comparison of ADRC, ADRC-NLSEF, ADRC-TD, and ADRC-NLSEF-TD for hip joint under the influence of noise, with parameter variation and with constant disturbance effect.

Case 4: Harmonic Disturbance

In case 4, the performance of the ADRC is compared with the proposed controllers, under the influence of noise, with parameter variation with addition of harmonic control disturbance of amplitude *5 N.m.* at t = 5 s. Figures 46 and 47 show the trajectory tracking performance for various controllers. Figures 48 and 49 show control signal required. Figures 50 and 51 show tracking error for ADRC, ADRC-NLSEF, ADRC-TD, and ADRC-NLSEF-TD for the hip and knee joints with harmonic disturbance.

In Figures 46 and 47 show the trajectory tracking performance for various controllers. The minimized plot (a) and plot (b) show the trajectory tracking response of the controllers before the introduction of the harmonic disturbance. Plot (c) and plot (d) show the controller trajectory tracking performance after addition of harmonic disturbance at t = 5 s. The trajectory tracked by ADRC-NLSEF-TD has the best reference tracking followed by ADRC-TD, ADRC-NLSEF, and ADRC before and after inclusion of disturbance at$t$ = 5 s, which proves its effectiveness under the influence of noise, with parameter variation and against harmonic disturbance.

The initial response of the control signal is shown in the minimized plot (a) and control signal in blown up in the minimized plot (b) shown in Figures 48 and 49, gives us the idea of control signal required by the controllers. The control signal for ADRC completely saturates whereas in the proposed controlled methods it firstly saturates for a while and maintains its safe limit. Plot (b) shows the effect of harmonic disturbance at t = 5 s and after 5 s.

Figures 50 and 51 show the error trajectory generated while reference tracking, the performance of the controller before and after addition of the constant disturbance, concludes the superiority of ADRC-NLSEF-TD over other controllers of trajectory tracking before and after addition of harmonic disturbance, under the influence of noise, with parameter variation.

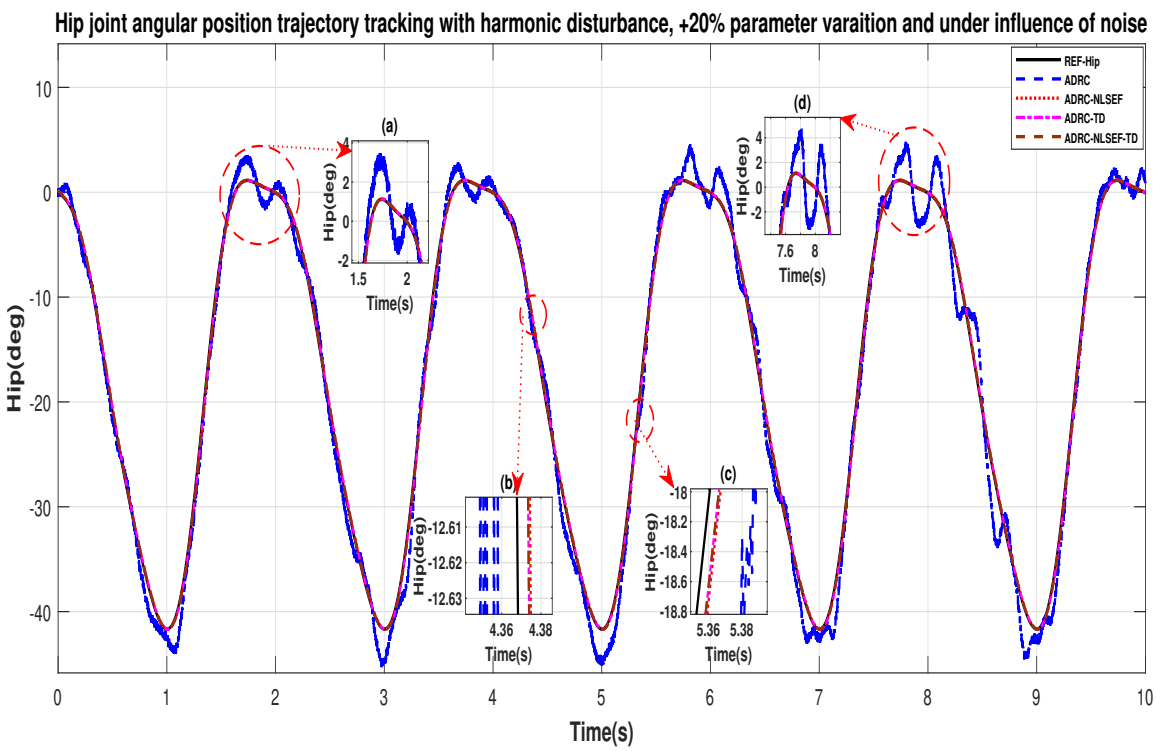

Figure 46. Gait trajectory tracking comparison of ADRC, ADRC-NLSEF, ADRC-TD, and ADRC-NLSEF-TD for the knee joint under the influence of noise, with parameter variation and with harmonic disturbance effect.

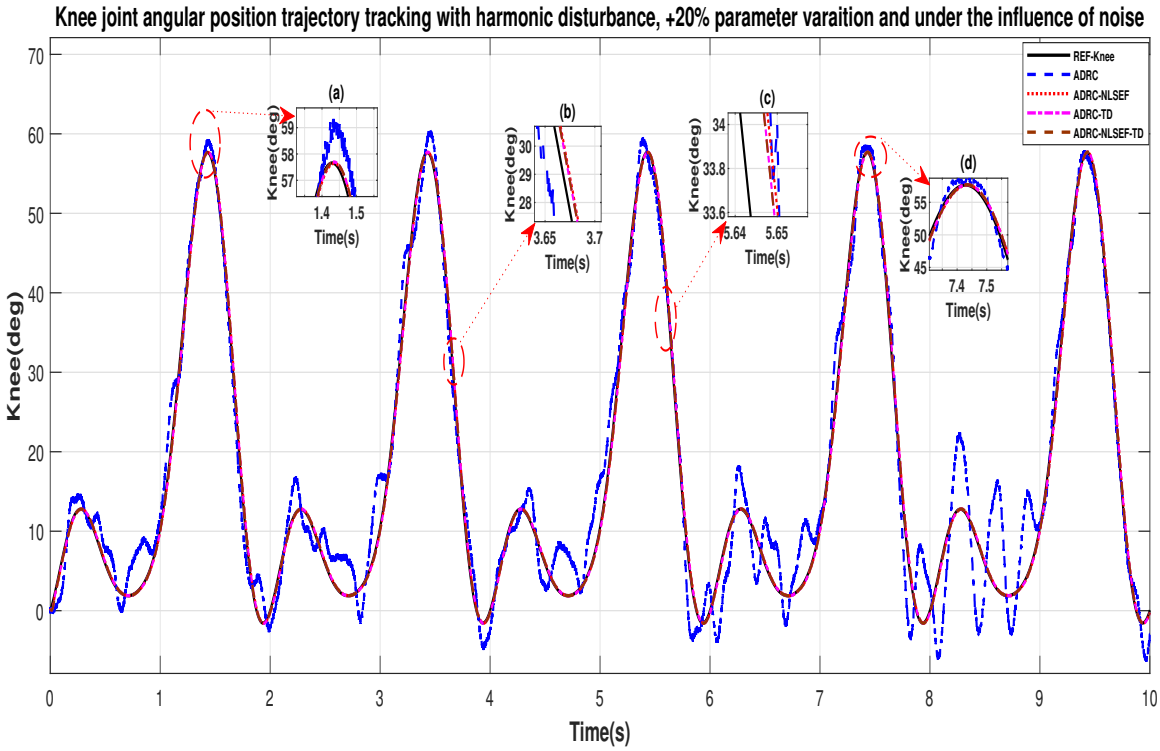

Figure 47. Gait trajectory tracking comparison of ADRC, ADRC-NLSEF, ADRC-TD, and ADRC-NLSEF-TD for the knee joint under the influence of noise, with parameter variation and with harmonic disturbance effect.

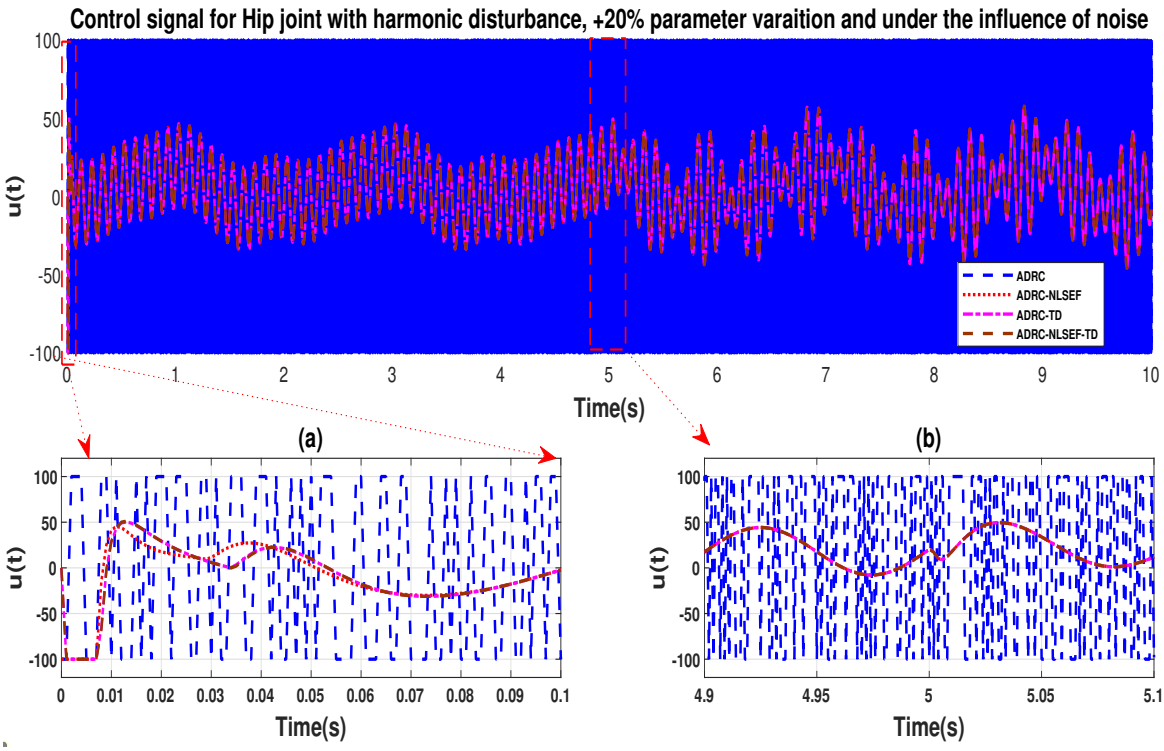

Figure 48. Control signal trajectory tracking comparison of ADRC, ADRC-NLSEF, ADRC-TD, and ADRC-NLSEF-TD for the knee joint under the influence of noise, with parameter variation and with harmonic disturbance effect.

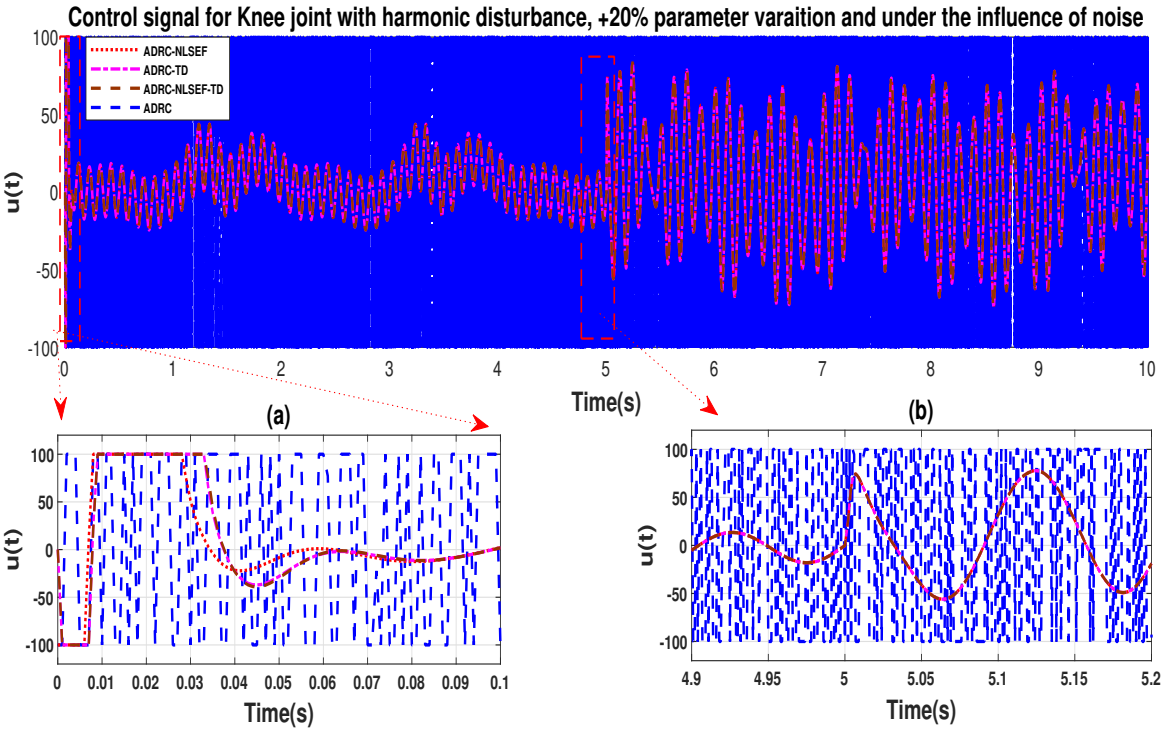

Figure 49. Control signal trajectory tracking comparison of ADRC, ADRC-NLSEF, ADRC-TD, and ADRC-NLSEF-TD for the knee joint under the influence of noise, with parameter variation and with harmonic disturbance effect.

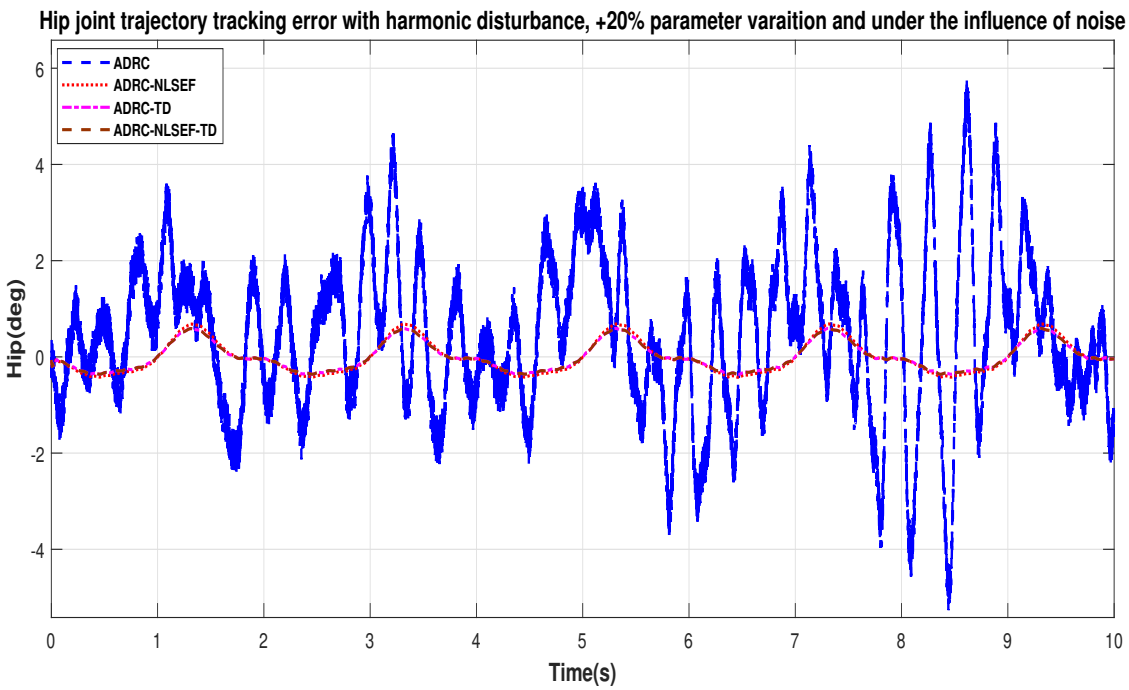

Figure 50. Gait trajectory tracking error comparison of ADRC, ADRC-NLSEF, ADRC-TD, and ADRC-NLSEF-TD for the hip joint under the influence of noise, with parameter variation and with harmonic disturbance effect.

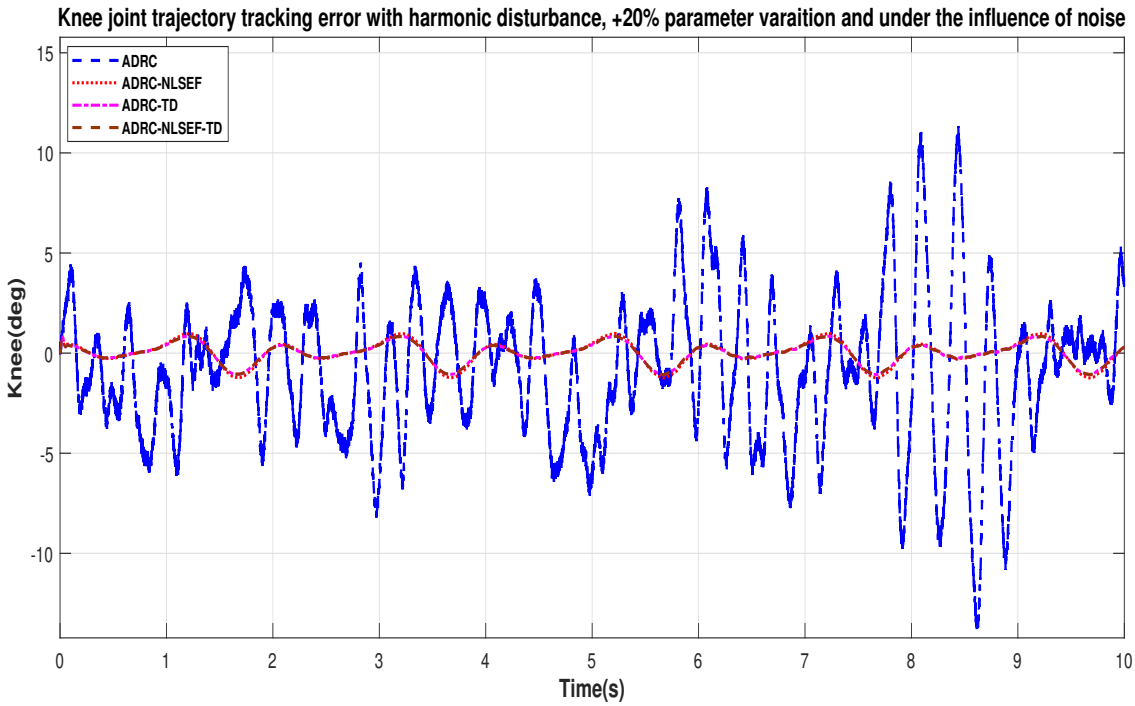

Figure 51. Gait trajectory tracking error comparison of ADRC, ADRC-NLSEF, ADRC-TD, and ADRC-NLSEF-TD for the hip joint under the influence of noise, with parameter variation and with harmonic disturbance effect.

The parametric variations of +20%, under the influence of noise and inclusion of disturbances over the ADRC, ADRC-NLSEF, ADRC-TD, and ADRC-NLSEF-TD controller resulted in the superior performance of ADRC-NLSEF-TD amongst all, for the gait trajectory tracking for the hip and knee joints, based on the performance indices. LESO based ADRC fails to track the trajectory and is severely affected by noise which can be clearly visible through the trajectory tracking, control signal, and large tracking error. Performance shown in the figures and based on performance indices, the proposed control method performs superior and tracks the trajectory efficiently as compared to ADRC even with parameter variation, under the effect of noise and disturbance and with actuator saturation it keeps the control signal in safe operation limits.

7. Discussion

The use of exoskeleton has various potential applications in the medical and non-medical fields. A medical exoskeleton is utilized for rehabilitation over conventional methods for better treatment, again it is useful for the persons suffering from the loss of limbs (amputees) to provide mobility. In non-medical, it can be utilized to support human workers in industries for physically demanding tasks such as heavy load lifting, for the soldiers in wartime or medical emergencies exoskeleton is helpful for strength augmentation, and elderly persons to perform the daily chores by providing reduced physical effort, its application has already started in some countries.

This paper is more focused on designing the control based on the passive rehabilitation aspect of given exoskeleton for gait tracking. The use of exoskeletons for rehabilitation requires special care as the motion trajectories for joints can not be provided through the wearer, the affected person cannot make the required actions. The international safety regulatory requirements (published by the International Organization for Standardization (ISO; www.iso.org) and International Electro-technical Commission (IEC; www.iec.ch)) for medical exoskeletons, such regulations are still underdeveloped by the joint working group IEC SC62D and ISO TC299 JWG36 (medical robots for rehabilitation). The design and development of the algorithm for the lower limb rehabilitation robotic devices was the preliminary task. The experimental work for the proposed system includes testing of all combinations

of ADRC algorithm presented in this paper with LESO based ADRC. In future experimentation, the protocol and set up will be undertaken in a controlled laboratory environment. Each volunteer performs two trials of a 5 gait cycle for each controller. During trials the exoskeleton wearer will walk forward. The exoskeleton will be connected to the wearer's lower limb through the connection cuff, the walking cycle is tested on flat terrain. The control enclosure will have an embedded computer, the actuators, encoders, and power modules. The embedded pc will send the desired command signals to the actuators and then generates the control signal to drive the exoskeleton to follow the predefined gait. The encoder will capture the angular position of the joints and send back to the embedded pc.

In this paper, an I-ADRC method is proposed which is an extension to the work [39]. The paper compares various combinations of ADRC with the LESO based ADRC [39], it can be concluded from the results that I-ADRC has improved trajectory tracking response, better performance is obtained under the influence of noise and disturbance, again it gives an improved performance with parameter variation, although the proposed method has some disadvantages over ADRC that the design becomes complex and number of tuning parameters increases. The proposed method is found to be more accurate for the given modeled system but its scope is not limited. The proposed method developed in this paper specifically addresses the rehabilitation issue, the proposed algorithm is the generalized method and can be utilized for the areas of interest.

8. Conclusions

In this paper an improved active disturbance rejection control (I-ADRC) method encompasses of linear extended state observer (LESO), tracking differentiator (TD) and nonlinear state error feedback (NLSEF) is effectively applied for sagittal plane gait trajectory tracking on a 2 DoF LLRRE with the hip and the knee joints in the simulation study. The performance indices ITSE, ITAE, IAE, ISE, and ISU reflects the potential of proposed ADRC combinations over ADRC in terms of trajectory tracking, control signal requirement, and disturbance rejection, under the influence of noise and parametric variation. Amongst all the controllers, ADRC-NLSEF-TD proves a better selection because of its best tracking capabilities followed by ADRC-TD and ADRC-NLSEF, which proves it as a promising strategy. Proposed ADRC in the future can be used for various assistive devices/exoskeletons and orthoses for improvement in tracking. This article presented the overall results of the controller with emphasis on simulation. In the next phase of research in the coming months, it would be validated through experimental work.

Author Contributions: S.A. and I.E. participated in drafting the manuscript. L.W., B.P., and F.M. gave critical revision of the manuscript. All authors read and approved the final manuscript.

Funding: Funds for this research was provided by Universiti Teknologi PETRONAS (UTP) Malaysia, Shri Guru Gobind Singhji Institute of Engineering and Technology, Nanded, India and University of Burgundy, Dijon, France, under YUTP Grant No. 015LC0-243.

Acknowledgment: The authors would like to thank Universiti Teknologi PETRONAS (UTP) Malaysia, Shri Guru Gobind Singhji Institute of Engineering and Technology, Nanded, India, and University of Burgundy, Dijon, France for their support.

Conflicts of Interest: The authors declare no conflict of interest.

References

1. Riener, R.; Lunenburger, L.; Jezernik, S.; Anderschitz, M.; Colombo, G.; Dietz, V. Patient-cooperative strategies for robot-aided treadmill training: first experimental results. *IEEE Trans. Neural Syst. Rehabilitation Eng.* **2005**, *13*, 380–394. [CrossRef] [PubMed]
2. Díaz, I.; Gil, J.J.; Sánchez, E. Lower-limb robotic rehabilitation: literature review and challenges. *J. Robot.* **2011**, *2011*, 1–11 [CrossRef]
3. Chen, B.; Ma, H.; Qin, L.Y.; Gao, F.; Chan, K.M.; Law, S.W.; Qin, L.; Liao, W.H. Recent developments and challenges of lower extremity exoskeletons. *J. Orthop. Transl.* **2016**, *5*, 26–37. [CrossRef]

4. Guo, Z.; Yu, H.; Yin, Y.H. Developing a mobile lower limb robotic exoskeleton for gait rehabilitation. *J. Med Devices* **2014**, *8*, 044503. [CrossRef]
5. Vinodh, K.E.; Jovitha, J.; Ayyappan, S. Comparison of four state observer design algorithms for MIMO system. *Arch. Control Sci.* **2013**, *23*, 243–256. [CrossRef]
6. Emken, J.L.; Harkema, S.J.; Beres-Jones, J.A.; Ferreira, C.K.; Reinkensmeyer, D.J. Feasibility of manual teach-and-replay and continuous impedance shaping for robotic locomotor training following spinal cord injury. *IEEE Trans. Biomed. Eng.* **2007**, *55*, 322–334. [CrossRef]
7. Su, Y.; Sun, D.; Ren, L.; Mills, J.K. Integration of saturated PI synchronous control and PD feedback for control of parallel manipulators. *IEEE Trans. on Robot.* **2006**, *22*, 202–207.
8. Taha, Z.; Majeed, A.P.A.; Abidin, A.F.Z.; Ali, M.A.H.; Khairuddin, I.M.; Deboucha, A.; Tze, M.Y.W.P. A hybrid active force control of a lower limb exoskeleton for gait rehabilitation. *Biomed. Tech. Eng.* **2018**, *63*, 491–500. [CrossRef] [PubMed]
9. Saglia, J.A.; Tsagarakis, N.G.; Dai, J.S.; Caldwell, D.G. Control strategies for patient-assisted training using the ankle rehabilitation robot (ARBOT). *IEEE/ASME Trans. Mechatronics* **2012**, *18*, 1799–1808. [CrossRef]
10. Lu, R.; Li, Z.; Su, C.Y.; Xue, A. Development and learning control of a human limb with a rehabilitation exoskeleton. *IEEE Trans. Ind. Electron.* **2013**, *61*, 3776–3785. [CrossRef]
11. Jamwal, P.K.; Xie, S.Q.; Hussain, S.; Parsons, J.G. An adaptive wearable parallel robot for the treatment of ankle injuries. *IEEE/ASME Trans. Mechatronics* **2012**, *19*, 64–75. [CrossRef]
12. Kazerooni, H.; Racine, J.L.; Huang, L.; Steger, R. On the control of the berkeley lower extremity exoskeleton (BLEEX). In Proceedings of the 2005 IEEE international conference on robotics and automation, Barcelona, Spain, 18–22 April 2005; pp. 4353–4360.
13. Kazerooni, H.; Chu, A.; Steger, R. That which does not stabilize, will only make us stronger. *Int. J. Robot. Res.* **2007**, *26*, 75–89. [CrossRef]
14. Yang, Z.; Zhu, Y.; Yang, X.; Zhang, Y. Impedance control of exoskeleton suit based on adaptive RBF neural network. In Proceedings of the 2009 International Conference on Intelligent Human-Machine Systems and Cybernetics, Hangzhou, Zhejiang, China, 26–27 August 2009; Volume 1, pp. 182–187.
15. Li, S.; Yang, J.; Chen, W.H.; Chen, X. Disturbance observer-based control: methods and applications. In Proceedings of the 2016 International Conference on Unmanned Aircraft Systems (ICUAS), Arlington, VA, USA, 7–10 June 2016.
16. Gao, Z.; Huang, Y.; Han, J. An alternative paradigm for control system design. In Proceedings of the 40th IEEE Conference on Decision and Control, Orlando, FL, USA, 4–7 December 2001; Volume 5, pp. 4578–4585.
17. Gao, Z.; Hu, S.; Jiang, F. A novel motion control design approach based on active disturbance rejection. In Proceedings of the 40th IEEE Conference on Decision and Control, Orlando, FL, USA, 4–7 December 2001, Volume 5, pp. 4877–4882.
18. Tian, G.; Gao, Z. Benchmark tests of active disturbance rejection control on an industrial motion control platform. In Proceedings of the 2009 American Control Conference, St. Louis, MO, USA, 10–12 June 2009; pp. 5552–5557.
19. Su, Y.X.; Duan, B.Y.; Zheng, C.H.; Zhang, Y.F.; Chen, G.D.; Mi, J.W. Disturbance-rejection high-precision motion control of a Stewart platform. *IEEE Trans. Control. Syst. Technol.* **2004**, *12*, 364–374. [CrossRef]
20. Ginhoux, R.; Gangloff, J.; de Mathelin, M.; Soler, L.; Sanchez, M.M.A.; Marescaux, J. Active filtering of physiological motion in robotized surgery using predictive control. *IEEE Trans. Robot.* **2005**, *21*, 67–79. [CrossRef]
21. Zhu, E.; Pang, J.; Sun, N.; Gao, H.; Sun, Q.; Chen, Z. Airship horizontal trajectory tracking control based on Active Disturbance Rejection Control (ADRC). *Nonlinear Dyn.* **2013**, *75*, 725–734. [CrossRef]
22. Changmao, Q.; Naiming, Q.; Rui, L.; Kai, Z. ADRC fractional order PID controller design of hypersonic flight vehicle. *Trans. Nanjing Univ. Aeronaut. Astronaut.* **2011**, *28*, 240–244.
23. Desai, R.; Patre, B.M.; Pawar, S.N. Active disturbance rejection control with adaptive rate limitation for process control application. In Porceedings of the 2018 Indian Control Conference (ICC), Kanpur, India, 4–6 January 2018; pp. 131–136.
24. Huang, Y.; Xue, W. Active disturbance rejection control: Methodology and theoretical analysis. *ISA Trans.* **2014**, *53*, 963–976. [CrossRef] [PubMed]

25. Yu, T.; Chan, K.W.; Tong, J.P.; Zhou, B.; Li, D.H. Coordinated robust nonlinear boiler-turbine-generator control systems via approximate dynamic feedback linearization. *J. Process. Control.* **2010**, *20*, 365–374. [CrossRef]
26. Huang, C.E.; Li, D.; Xue, Y. Active disturbance rejection control for the ALSTOM gasifier benchmark problem. *Control. Eng. Pr.* **2013**, *21*, 556–564. [CrossRef]
27. Dulf, E.H.; Both, R.; Muresan, C.I. Active disturbance rejection controller for a separation column. In Porceedings of the 2014 IEEE International Conference on Automation, Quality and Testing, Robotics, Cluj-Napoca, Romania, 22–24 May 2014; pp. 1–6.
28. Tan, W.; Fu, C. Linear active disturbance-rejection control: Analysis and tuning via IMC. *IEEE Trans. Ind. Electron.* **2016**, *63*, 2350–2359. [CrossRef]
29. Garran, P.T.; Garcia, G. Design of an optimal PID controller for a coupled tanks system employing ADRC. *IEEE Lat. Am. Trans.* **2017**, *15*, 189–196. [CrossRef]
30. Pawar, S.N.; Chile, R.H.; Patre, B.M. Modified reduced order observer based linear active disturbance rejection control for TITO systems. *ISA Trans.* **2017**, *71*, 480–494. [CrossRef] [PubMed]
31. Madonski, R.; Nowicki, M.; Przemys, l.H. Application of active disturbance rejection controller to water supply system. In Proceedings of the 33rd Chinese Control Conference, Nanjing, China, 28–30 July 2014; pp. 4401–4405.
32. Zheng, Q.; Gao, Z. An energy saving, factory-validated disturbance decoupling control design for extrusion processes. In Proceedings of the 10th World congress on intelligent control and automation, Beijing, China, 6–8 July 2012; pp. 2891–2896.
33. Zeng, D.; Yu, Z.; Xiong, L.; Fu, Z.; Li, Z.; Zhang, P.; Leng, B.; Shan, F. HFO-LADRC lateral motion controller for autonomous road sweeper. *Sensors* **2020**, *20*, 2274. [CrossRef]
34. Li, D.; Ding, P.; Gao, Z. Fractional active disturbance rejection control. *ISA Trans.* **2016**, *62*, 109–119. [CrossRef] [PubMed]
35. Han, J. From PID to active disturbance rejection control. *IEEE Trans. Ind. Electron.* **2009**, *56*, 900–906. [CrossRef]
36. Han, J. Auto-disturbances-rejection controller and its applications. *Control Decis.* **1998**, *13*, 19–23. (In Chinese)
37. Gao, Z. Active disturbance rejection control: A paradigm shift in feedback control system design. In Proceedings of the American Control Conference, 2006, Minneapolis, MN, USA, 14–16 June 2006; pp. 7–pp.
38. Viteckova, S.; Kutilek, P.; Jirina, M. Wearable lower limb robotics: A review. *Biocybern. Biomed. Eng.* **2013**, *33*, 96–105. [CrossRef]
39. Long, Y.; Du, Z.; Cong, L.; Wang, W.; Zhang, Z.; Dong, W. Active disturbance rejection control based human gait tracking for lower extremity rehabilitation exoskeleton. *ISA Trans.* **2017**, *67*, 389–397. [CrossRef]
40. Guerrero-Castellanos, J.F.; Rifa, H.; Arnez-Paniagua, V.; Linares-Flores, J.; Saynes-Torres, L.; Mohammed, S. Robust Active Disturbance Rejection Control via Control Lyapunov Functions: Application to Actuated-Ankle-Foot-Orthosis. *Control. Eng. Pr.* **2018**, *80*, 49–60. [CrossRef]
41. Xun, W.Q.; Yu, Z.K. An exoskeleton joint output force control technology based on improved ADRC. In Proceedings of the 2017 2nd International Conference on Robotics and Automation Engineering (ICRAE), Shanghai, China, 29–31 December 2017; pp. 146–150.
42. Meng, W.; Liu, Q.; Zhou, Z.; Ai, Q.; Sheng, B.; Xie, S.S. Recent development of mechanisms and control strategies for robot-assisted lower limb rehabilitation. *Mechatronics* **2015**, *31*, 132–145. [CrossRef]
43. Roman, R.C.; Precup, R.E.; Bojan-Dragos, C.A.; Szedlak-Stinean, A.I. Combined Model-Free Adaptive Control with Fuzzy Component by Virtual Reference Feedback Tuning for Tower Crane Systems. *Procedia Comput. Sci.* **2019**, *162*, 267–274. [CrossRef]
44. Zhang, H.; Liu, X.; Ji, H.; Hou, Z.; Fan, L. Multi-Agent-Based Data-Driven Distributed Adaptive Cooperative Control in Urban Traffic Signal Timing. *Energies* **2019**, *12*, 1402. [CrossRef]
45. Joe, H.M.; Oh, J.H. A Robust Balance-Control Framework for the Terrain-Blind Bipedal Walking of a Humanoid Robot on Unknown and Uneven Terrain. *Sensors* **2019**, *19*, 4194. [CrossRef] [PubMed]
46. Hassan, M.; Kadone, H.; Suzuki, K.; Sankai, Y. Wearable gait measurement system with an instrumented cane for exoskeleton control. *Sensors* **2014**, *14*, 1705–1722. [CrossRef] [PubMed]
47. Del-Ama, A.J.; Moreno, J.C.; Gil-Agudo, A.; De-los Reyes, A.; Pons, J.L. Online assessment of human-robot interaction for hybrid control of walking. *Sensors* **2012**, *12*, 215–225. [CrossRef] [PubMed]

48. Long, Y.; Du, Z.J.; Wang, W.D.; Dong, W. Robust sliding mode control based on GA optimization and CMAC compensation for lower limb exoskeleton. *Appl. Bionics Biomech.* **2016**, *2016*. [CrossRef] [PubMed]
49. Chen, G.; Chan, C.K.; Guo, Z.; Yu, H. A review of lower extremity assistive robotic exoskeletons in rehabilitation therapy. *Crit. Rev. Biomed. Eng.* **2013**, *41*, 4–5. [CrossRef] [PubMed]
50. Bortole, M.; Venkatakrishnan, A.; Zhu, F.; Moreno, J.C.; Francisco, G.E.; Pons, J.L.; Contreras-Vidal, J.L. The H2 robotic exoskeleton for gait rehabilitation after stroke: early findings from a clinical study. *J. Neuroeng. Rehabilitation* **2015**, *12*, 54. [CrossRef]
51. Bovi, G.; Rabuffetti, M.; Mazzoleni, P.; Ferrarin, M. A multiple-task gait analysis approach: Kinematic, kinetic and EMG reference data for healthy young and adult subjects. *Gait Posture* **2011**, *33*, 6–13. [CrossRef]
52. Chen, W.H.; Yang, J.; Guo, L.; Li, S. Disturbance-observer-based control and related methods : An overview. *IEEE Trans. Ind. Electron.* **2015**, *63*, 1083–1095. [CrossRef]
53. Radke, A.; Gao, Z. A survey of state and disturbance observers for practitioners. In Proceedings of the 2006 American Control Conference, Minneapolis, MN, USA, 14–16 June 2006.
54. Zheng, Q.; Dong, L.; Lee, D.H.; Gao, Z. Active disturbance rejection control for MEMS gyroscopes. In Proceedings of 2008 American Control Conference, Seattle, WA, USA, 11–13 June 2008; pp. 4425–4430.
55. Zheng, Q. On Active Disturbance Rejection Control; Stability Analysis and Applications in Disturbance Decoupling Control. Ph.D. Thesis, Cleveland State University, Cleveland, OH, USA, July 2009.
56. Gao, Z. Scaling and bandwidth-parameterization based controller tuning. In Proceedings of the American Control Conference, Minneapolis, MN, USA, 14–16 June 2006; Volume 6, pp. 4989–4996.
57. Zhao, L.; Liu, X.; Wang, T.; Liu, B. A reduced-order extended state observer-based trajectory tracking control for one-degree-of-freedom pneumatic manipulator. *Adv. Mech. Eng.* **2018**, *10*, 1687814018767289. [CrossRef]
58. Liu, Z.; Jiang, Y. Design of a Modified Tracking Differentiator. *World J. Eng. Technol.* **2017**, *5*, 668. [CrossRef]
59. Liu, B.; Zhu, C.; Guo, X. Current-Loop Control for the Pitching Axis of Aerial Cameras via an Improved ADRC. *Math. Probl. Eng.* **2017**, *2017*. [CrossRef]
60. MATLAB/Simulink (2018a, The Mathworks, Inc., Natick, Massachusetts). Available online: https://www.mathworks.com/products/matlab.html (accessed on 26 November 2019).
61. Tavazoei, M.S. Notes on integral performance indices in fractional-order control systems. *J. Process. Control.* **2010**, *20*, 285–291. [CrossRef]
62. Dorf, R.C.; Bishop, R.H. *Modern Control Systems*; Pearson: London, UK, 2011.
63. Ibraheem, I.K.; Abdul-Adheem, W.R. On the Improved Nonlinear Tracking Differentiator Based Nonlinear PID Controller Design. *arXiv* **2018**, arXiv:1803.02908.

© 2020 by the authors. Licensee MDPI, Basel, Switzerland. This article is an open access article distributed under the terms and conditions of the Creative Commons Attribution (CC BY) license (http://creativecommons.org/licenses/by/4.0/).